TRAP PARAMETER EXTRACTION OF DEEP DEFECTS IN SEMICONDUCTORS USING NOISE MEASUREMENTS

By

SHENG-LYANG JANG

A DISSERTATION PRESENTED TO THE GRADUATE SCHOOL
OF THE UNIVERSITY OF FLORIDA IN
PARTIAL FULFILLMENT OF THE REQUIREMENTS
FOR THE DEGREE OF DOCTOR OF PHILOSOPHY

UNIVERSITY OF FLORIDA

1989

TO MY PARENTS

ACKNOWLEDGEMENTS

The author wishes to express his sincere appreciation to Dr. Gijs Bosman for his guidance and encouragement during the course of this study and to Professor F. A. Lindholm for his encouragement and support.

The author wishes to thank Dr. T. Nishida for fabricating the devices used in this work and the other members of the supervisory committee--Drs. A. Neugroschel, S. S. Li and U. H. Kurzweg for their valuable academic counseling and their participation on my supervisory committee.

The author is grateful to his fellow students in the Noise Research Laboratory, Young-June Yu, Min-Yih Luo and Horng-Jye Luo, for their help and for many interesting discussions. Special thanks go to his host families, Samuel F. Evans and Sandra Lyons, who have encouraged him over the years.

TABLE OF CONTENTS

		Page
ACKNOWLEDGEMENTS		iii
ABSTRACT		vii
CHAPTER		
I	INTRODUCTION	1
	1.1 Basic Concepts of Defects and Impurities in Solids	2
	1.2 Noise as a Tool for Measuring Defect Properties	5
	1.3 Comparison of Noise Measurements with Other Trap Characterization Techniques	8
	1.4 Field-Dependent Noise and Generation-Recombination Processes	10
	1.5 Microscopic Description of Generation-Recombination Processes	10
	1.6 Thesis Outline	11
II	LOW-FIELD INVESTIGATION OF THE GOLD DONOR LEVEL IN SILICON	13
	2.1 Introduction	13
	2.2 Theory	14
	2.2.1 Overcompensated Devices	18
	2.2.2 Lightly Doped Devices	20
	2.2.3 Arbitrary Doping Levels	22
	2.3 Experimental Results and Discussion	23
III	EXPERIMENTAL EVIDENCE FOR A SECOND-DONOR LEVEL OF GOLD IN SILICON	29
	3.1 Introduction	29
	3.2 Theory	31
	3.2.1 Deep Double-Donor Defects in Nearly Compensated Material	40
	3.2.2 Simplified Double-Donor Noise Theory	43

3.3 Device Description, Experimental Results and Discussion 44
3.4 Summary 50
3.5 Comparison of Experimental Results for the Single- and Double-Donor Model 52

IV THE EFFECT OF FIELD-DEPENDENT EMISSION ON THE CURRENT-VOLTAGE CHARACTERISTICS OF A P^+-P^--P^+ Si:Au:B DEVICE 55

4.1 Introduction 55
4.2 Theory 57
4.3 Experimental Details and Discussion 60
4.4 High Field Effects 68

V LOW-FREQUENCY GENERATION-RECOMBINATION NOISE AS A TOOL FOR INVESTIGATING DEEP DEFECTS, DEVICE DESIGN CONSIDERATIONS 72

5.1 Introduction 72
5.2 Theory 74
5.2.1 Single-Level Noise Model 77
5.2.1.1 Deep Defects in Overcompensated Devices . 77
5.2.1.2 Deep Defects in Uncompensated Devices 79
5.2.1.3 Device Design Consideration 80
5.2.1.4 Single-Acceptor Noise Model 81
5.2.2 Double-Donor Noise Model 82
5.2.2.1 Deep Defects with Closely Spaced Energy Levels in Nearly-Compensated Material 84
5.2.2.2 Deep Defects with Closely Spaced Energy Levels in Uncompensated Material 87
5.2.2.3 Deep Defects with Energy Levels Far Apart from Each Other in Overcompensated Material 88
5.2.2.4 Deep Defects with Energy Levels Far Apart from Each Other in Uncompensated Material 90
5.2.3 Acceptor-Donor Noise Model 92
5.2.3.1 Deep Defects with Energy Levels Close to Each Other in Overcompensated Devices 95
5.2.3.2 Deep Defects with Energy Levels Far Away from Each Other in Overcompensated Material 97
5.2.3.3 Deep Defects with Energy Levels Closely Spaced to Each Other in Uncompensated Material 98
5.2.3.4 Deep Defects with Energy Levels Separated by More than a Few KT from Each Other in Uncompensated Material 99

5.3 Conclusions 101

VI CARRIER CAPTURE, EMISSION AND RECOMBINATION 104

6.1 Carrier Capture and Emission 104
6.2 Microscopic Capture Model 105
6.2.1 Introduction 105
6.2.2 Theory 108
6.2.2.1 Transition Probability 109
6.2.2.2 Density of States of Delocalized Optical Phonons 116
6.2.2.3 Evaluation of Electronic Matrix Elements .. 118
6.2.2.4 Calculation of the Capture Coefficient 120

VII DEFECT PARAMETER EXTRACTION FROM FIELD-EFFECT TRANSISTORS 124

7.1 Fluctuations in the Charge States of Shockley-Hall-Read Centers Located in the Space Charge Region 125
7.2 Generation-Recombination Noise in Metal-Oxide-Semiconductor Field-Effect Transistors 128
7.2.1 Low-Field Noise Theory 128
7.2.2 Field Dependent Noise Theory 130
7.3 Generation-Recombination Noise in Junction-gate Field-Effect Transistors 131
7.3.1 Low-Field Junction Generation-Recombination Noise 131
7.3.2 Generation-Recombination Noise in the Channel of Junction Field-Effect Transistors 133

VIII GENERATION-RECOMBINATION NOISE IN POLYSILICON RESISTORS 135

8.1 Introduction 135
8.2 Theory 136

IX CONCLUSIONS AND SUGGESTIONS FOR FURTHER RESEARCH 146

9.1 Conclusions 146
9.2 Suggestions for Further Research 149

REFERENCES 151

BIOGRAPHICAL SKETCH 155

Abstract of Dissertation Presented to the Graduate School of the University of Florida in Partial Fulfillment of the Requirements for the degree of Doctor of Philosophy

TRAP PARAMETER EXTRACTION OF DEEP DEFECTS IN SEMICONDUCTORS USING NOISE MEASUREMENTS

By

Sheng-Lyang Jang

December 1989

Chairman: Gijs Bosman
Major Department: Electrical Engineering

In this dissertation, generation-recombination (G-R) noise is used as a tool for investigating the properties of deep defects. The first experiment we describe deals with low-field noise measurements, which were done on p^+-p^--p^+ silicon devices doped with a boron concentration of 10^{15} cm^{-3} and an unknown gold concentration. The resistance and the G-R noise spectral density of the device were measured as a function of temperature and used to extract the trap energy, hole capture cross section, degeneracy factor, and trap density. The resistance and the noise data show the same activation energy of 0.336 eV, which stems from the generally accepted gold donor level, hereafter referred to as the gold first-donor level. The values of trap parameters so obtained are in good agreement with the

published data in the literature, indicating that this method is accurate for investigating deep-defect properties.

The second experiment described in this thesis was done on p^+-p^--p^+ silicon devices doped with a boron concentration of 2.7 $x10^{15}$ cm^{-3}. The resistance and low frequency voltage noise of the devices were measured as a function of temperature. The resistance data indicate that gold produces an activation energy of 0.267 eV, and the noise data indicate that gold produces an activation energy of 0.336 eV. This observation is explained in terms of double donor centers interacting with the valence band.

Then the current-voltage (I-V) characteristics of the devices used in the first experiment were measured. They showed sublinear behavior at moderately high fields. With the use of low frequency voltage noise data measured as a function of electric field, we determined that the sublinear I-V behavior was caused by a decrease in the hole concentration with increasing electric field. This decrease is caused by a field-induced decrease in the hole emission coefficient, which is larger than the associated field-induced decrease in the hole capture coefficient.

Device design schemes for investigating deep defects by noise measurements are presented. We analyzed the noise of several multi-level trap centers and derived the conditions for which the noise of a multi-level trap center reduces to the noise of a single-level trap center. We also devised a method by which G-R noise measurements

can be used to discriminate between donor-like and acceptor-like trap behavior.

In addition to the above described macroscopic G-R noise models, a microscopic model for carrier capture in deep traps is derived. Finally, theories for G-R noise generated in field-effect devices and polysilicon resistors are presented.

CHAPTER I
INTRODUCTION

All solids in equilibrium and at finite temperatures contain intrinsic point defects. In addition, all solids inevitably contain chemical impurities. The presence of defects can affect the usefulness of materials and performance of solid-state devices in both desirable and undesirable ways. Defect study in semiconductor engineering started originally with seeking methods to suppress generation of harmful defects during device processing in order to achieve a high yield of device fabrication. Then a new trend developed in which crystal defects are utilized to improve the device performance and reliability. A typical example is using a deep level impurity to control the lifetime of carriers. The latter trend accounts, to a considerable extent, for the intensive and continuing research activity in the defect solid state area.

Defect engineering becomes increasingly important for two reasons: (1) Undesirable defects cause nothing but trouble; they make devices inoperable or accelerate the degradation of device performance. The trend towards VLSI submicron semiconductor circuitry has increased the vulnerability of devices for unwanted process-induced defects. (2) Defects regulate many optical and electrical properties of interest. The device performance can be improved by controlling doping profiles and impurity concentrations. Isovalent impurities [1] can be used to make radiative recombination

possible in an indirect band gap semiconductor, which thus becomes a material suitable for light emitting diode applications. In fast switching applications, efficient recombination mechanisms are necessary to remove mobile carriers quickly. Deep level defects with large hole and electron capture coefficient are good candidates for this application.

Gold has been used as a desirable impurity in silicon device technology to reduce carrier lifetime. Despite the fact that it has received much attention, its behavior, once incorporated, is not always predictable. Since different techniques measure defect properties under different conditions, applying various techniques to characterize gold in silicon will provide a complete picture of this defect.

In this thesis, the term noise is used to describe fluctuations in an electronic signal measured on an electronic device. Noise arises from the statistical nature of the electron and/or phonon processes which affect charge transport. Since it is associated with the microscopic motion of carriers in a crystal, noise measurements can be used to investigate for example the properties of defects in a semiconductor host as we will show in this thesis.

1.1. Basic Concepts of Defects and Impurities in Solids

A perfect crystal consists of a three-dimensional array of atoms arranged on a periodic lattice. The intentional or unintentional introduction of native defects and impurities in such a crystal disrupts this periodic structure and may alter the properties of the material in a significant way. The term "flaw" or "imperfection," hereinafter referred to as defect, refers to foreign atoms, vacancies, interstitials or combinations of any of these. By measuring the changes in the

properties of a bulk semiconductor after defect introduction, we are able to determine the characteristics of defects. Defects can be classified based on their physical location in the lattice or on their electronic structure.

There are three main categories of defects. The first one comprises lattice defects, i.e., intrinsic defects, which can be point defects, line defects, or planar defects [1]. The second category deals with impurities, i.e., extrinsic defects. And the third category consists of any combination of lattice defects and impurities. There are two possible point defects: the vacancy (Fig. 1.(b)), i.e., a vacant atomic site, and the interstitial (Fig. 1.(c)), i.e., an extra atom occupying an interstitial site. An impurity may replace one of the host atoms, in which case it is known as a substitutional impurity. Alternatively, it may occupy an interstitial site, in which case it may be either a simple interstitial, or what is known as an interstitialcy [1].

When a defect is incorporated into a crystal, the defect can give rise to various localized, charge states in the band gap of a semiconductor. Positively charged states of a defect are defined as donor states, and negatively charged states are defined as acceptor states. Neutral states bear no other distinctive name. Some defects can behave either as donors or acceptors depending on the position of the local Fermi level. This characteristic is referred to as amphoteric.

Gold is widely used in silicon device technology to reduce the minority carrier lifetime. In spite of being a subject of interest and investigation for many years, much has still to be learned concerning this system. The values quoted in the literature for energy levels and

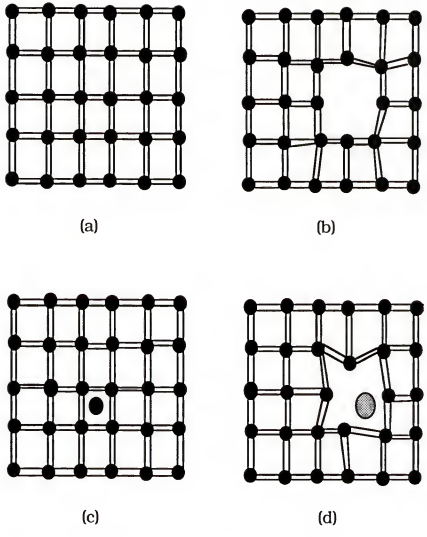

Figure 1.1. Schematic illustration of various flaws: (a) perfect crystal, (b) ideal vacancy, (c) self-interstitial, (d) vacancy-interstial pair.

capture cross sections show discrepancies. For example, gold donor energy values reported in the literature vary from E_v +0.33 eV to E_v +0.37 eV and reported hole capture cross sections range from 1.1×10^{-14} cm^2 to 1.5×10^{-15} cm^2.

However, the consensus is that the main energy levels attributed to gold in silicon are an acceptor level at E_c -0.54 eV and a donor level at about E_v +0.35 eV. Recently, L. S. Lu et al. [2] drew the conclusion that the donor and the acceptor levels belong to the same center; the magnitude of the hole capture cross section and its temperature independent data support a neutral potential for hole capture by the gold donor. As for the atomic configuration of the gold center, the published results seem to favor the gold-vacancy structure (Fig. 1.(d)) of Watkins, in which the gold is predicted to behave like closed d shells inside a vacancy.

1.2. Noise as a Tool for Measuring Defect Properties

Electronic devices and systems exhibit random fluctuations in voltage (or current) at their terminals, and these fluctuations are usually referred to as noise. As a result, noise imposes a practical limit on the performance of a circuit; noise can also be exploited as a means for investigating the electrical characteristics of a circuit. Physically, noise is due to the statistical nature of the charge transport process; it may arise both from electronic transitions between discrete energy levels and from scattering during transport [3].

Generation-recombination (G-R) noise is due to carrier transitions between traps and the associated conduction or valence band of a semiconductor. Generally, the noise spectrum from a single

trap has a Lorentzian form as shown in Fig. 1.2., which can be well described by a plateau part and a roll-off time constant. In the past, low-frequency (L.F.) G-R noise spectra have been used to determine dopant parameters [4,5,6] in samples with impurity concentrations low compared to the intended shallow doping in uniformly doped material. The trap energy is then extracted from the roll-off time constants of the spectral components. Experimentally, G-R noise data measured on uncompensated devices can not be used to determine whether a defect is a donor or an acceptor center, and this information should be inferred from the magnitude of the extracted carrier capture coefficient. Since noise may exist in various forms, for example: thermal noise, 1/f noise, the proper evaluation of the G-R noise magnitude from an overall noise spectrum is essential for trap parameter extraction.

The G-R noise characteristics from junction devices, such as junction field-effect transistors (JFET), metal-oxide-semiconductor (MOS) field-effect transistors, have also been investigated for decades. The activation energy of the gold acceptor level of 0.55 eV was extracted from G-R noise characteristics measured on a JFET by P. O. Lauritzen [7] and measured on a MOSFET by L. D. Yau and C. T. Sah [8]. The latter also measured the thermal emission rates as a function of electric field normal to the silicon-silicon dioxide surface. Recently, F. Scholz et al. [9] used L.F. noise data measured as a function of temperature as a MOS device characterization tool in a manner analogous to Deep Level Transient Spectroscopy (DLTS), and found that it is a powerful diagnostic technique for investigating deep

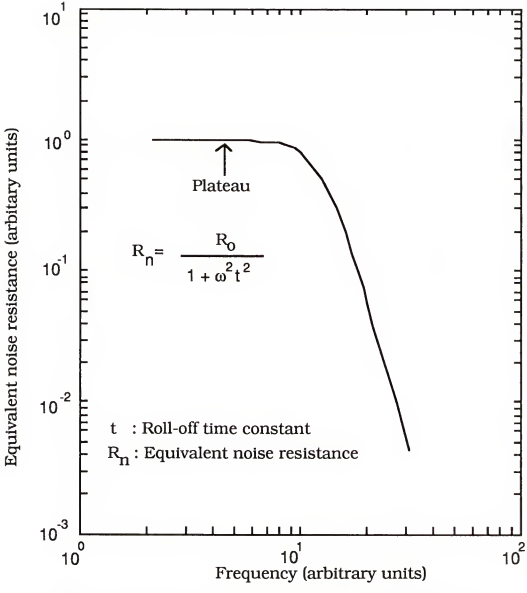
Equivalent noise resistance (arbitary units)
Frequency (arbitrary units)
Plateau
$R_n = \frac{R_0}{1 + \omega^2 t^2}$
t : Roll-off time constant
R_n : Equivalent noise resistance

Figure 1.2. Generation-recombination noise spectrum

defects. In general, it is difficult to extract information about the field dependence of G-R processes from noise measurements on device structures. In order to do this, G-R noise from a simple bulk semiconductor resistor should be analyzed.

In this dissertation, we address G-R noise measurements on samples with overcompensated, deep impurity concentrations. As we will indicate, the low-field noise data combined with the resistance data of the device can be used to determine trap parameters also under overcompensated conditions. Under these conditions, the G-R noise is dominant over other noise components in the low frequency range we investigated because of the large impurity concentration present in these devices. As we will show later, in an overcompensated p-type device, it is difficult to measure the G-R noise of a deep acceptor, while with suitable doping conditions one can measure the defect properties of a deep donor. Consequently, we are able to determine whether a deep center forms a donor or an acceptor center.

1.3. Comparison of Noise Measurements with Other Trap Characterization Techniques

Defects may be identified using parameters related to the thermodynamics of defect formation, such as diffusion, or using electronic macroscopic parameters. The phenomenological electronic parameters, i.e., thermal-emission rates, capture cross sections, optical cross sections and activation energies, can be measured by changing the carrier population in defects either thermally, optically, or electrically. In order to obtain electronic characteristics of a defect, one relies on the sensitivity of experimental techniques to changes in

defect characteristics when subjected to external disturbances. The experimental methods for characterization of electronic properties of defects can be divided into three groups namely into electrical techniques, optical techniques and techniques employing electron paramagnetic resonance [10].

The most widely used electrical techniques are the transient methods [11] among which are DLTS, junction capacitance transient methods [12], and pulsed junction capacitance methods [13]. Most of the above techniques probe the thermal emission or thermal capture of free carriers by traps located in the depletion region of a diode by measuring the transient response of the centers. The field in the junction is very large and nonhomogeneous. In the case that field-dependent emission or capture occurs, the observed activation energies will show some variation with the applied electric field. In addition, it is difficult to use these techniques to characterize low field effects in defects. However, we can use transient methods to identify acceptor or donor trap behavior by applying either a minority or majority carrier pulse to junction devices [11].

Generation-recombination noise is caused by fluctuations in electron capture and emission rates. In G-R noise measurements, the magnitude of the homogeneous electric field is determined from the externally applied bias voltage and the device length and the noise data are collected under steady state conditions. Measured activation energies are thermal activation energies.

The response of deep centers to these different experimental situations and techniques should help us to unravel some of the

problems associated with carrier capture and emission from deep centers.

1.4. Field Dependent Noise and Generation-Recombination Processes

G-R noise is proportional in most cases to the square of the d.c. current flowing through a device, and it sets therefore a limit to device sensitivity under high field operation. Consequently, it is important to investigate high-field noise spectra. Recently, Gasquet et al. [5] measured the field-dependent noise of shallow dopants to extract trap parameters. However, high field noise data from deep centers are unavailable at present. Since G-R noise can be measured simultaneously with current-voltage (I-V) characteristics, it allows us to determine the effects of G-R processes on the I-V curves of devices.

Gold is a deep center in silicon and is widely investigated. Its high field capture and emission coefficient data obtained by techniques such as DLTS can be found in the literature. Thus a comparison of the results obtained by G-R noise and DLTS experiments should give us insight in the dynamics of carriers in the presence of this deep center and external disturbances. In addition, since data for medium electric field strengths have not been reported in the literature, it is also one of our goals to investigate the exact field-dependence of emission and capture coefficients going from near equilibrium to the hot carrier regime.

1.5. Microscopic Description of Generation-Recombination Processes

The presence of nonlinear effects in the high field operation of a device makes a rigorous analytical approach to any high-field problem

very difficult. Alternatively, the Monte Carlo method [14] has proved to be a very powerful technique for the study of high field phenomena. In order to use this technique, a microscopic probability formula for the trapping and detrapping of carriers in traps should be developed. Although several macroscopic approaches to G-R problems can be found in the literature [15], microscopic theories are very scarce and microscopic probability formulae for G-R processes related to gold centers in silicon are unavailable. Therefore, an attempt is being made to derive such formulae using a multiphonon carrier capture model.

1.6. Thesis Outline

The organization of this thesis is as follows. In Chapter II, a macroscopic single-donor G-R noise model for trap parameter extraction is developed. A parameter extraction example is then illustrated. The resistance and the low frequency voltage noise are measured as a function of temperature on an overcompensated device made of Si:Au:B, and used to extract device parameters. The normalized, low-frequency noise spectral density and the resistance of the device versus 1000/T show an activation energy of 0.336 eV, which is in agreement with the well-established gold donor energy level. The other extracted trap parameters are also consistent with published data.

Chapter III discusses a double-donor G-R noise and resistance model. With this model we are able to explain why different activation energies were observed for the resistance and the low frequency voltage noise measured as a function of temperature on a p^+-p^--p^+ device made of Si:Au:B with a boron concentration of 2.7 x10^{15} cm^{-3}.

The normalized, low-frequency noise spectral density versus 1000/T shows an activation energy of 0.336 eV, which is in agreement with the well-established gold donor energy level. The plot of the resistance versus 1000/T reveals an activation energy of 0.267 eV, which we associate with a second donor level of gold. The double-donor model reduces to the single-donor model discussed in Chapter II under certain conditions.

In Chapter IV, the current-voltage characteristics of a silicon p^+-p^--p^+ device doped with boron and gold were measured and showed sublinear behavior at moderately high fields. With the use of low frequency voltage noise data measured as a function of electric field, we found that the sublinear current-voltage characteristics are caused by a decrease in the hole concentration with increasing electric field. This decrease is caused by a field-induced decrease in the hole emission coefficient, which is larger than the simultaneously observed, field-induced decrease in the hole capture coefficient.

Chapter V discusses how to design a device to investigate deep defects by G-R noise measurement techniques. Under certain conditions, a multi-level G-R noise model reduces to a single-level G-R noise model. We address the problem of using G-R noise measurements to discriminate between a donor center and an acceptor center. In Chapter VI, a microscopic nonradiative carrier capture model is proposed. Chapter VII discusses how to use G-R noise data from field-effect transistors to extract trap parameters and compares these techniques with G-R noise measurements on bulk devices. In Chapter VIII, a G-R noise model for polysilicon resistors is proposed. Finally, suggestions for further research are made.

CHAPTER II
LOW-FIELD INVESTIGATION OF THE GOLD DONOR LEVEL IN SILICON

2.1. Introduction

Gold is one of the widely studied deep-level elements in silicon due to its lifetime killer effect. It is believed that gold introduces an acceptor and a donor level in the bandgap of silicon. Recently, Lu et al. [2] drew the conclusion that the donor and the acceptor levels belong to the same center; the magnitude of the electron capture cross section data supports a neutral potential model for electron capture by the gold acceptor; the magnitude of the hole capture cross section and its temperature independent data support a neutral potential for hole capture by the gold donor. As for the atomic configuration of the gold center, the published results seem to favor the gold-vacancy structure of Watkins [16], in which the gold is predicted to behave like closed d shells inside a vacancy.

The experimental methods, by which the above information was obtained, are generally based on transient capacitance related techniques such as DLTS and probe the thermal emission and capture of carriers from traps located in the depletion region of a diode. The emission and capture coefficient are measured as two independent parameters. The trap activation energy is obtained from an Arrhenius plot of emission coefficient versus temperature assuming that the internal electric field has no influence on the results. However, depending on the doping level and bias voltage, this electric field can

be very large and field effects on the capture as well as the emission processes should be expected. One must be cautioned against wrong information being extracted from the emission data if the field effect is not properly accounted for. Since the electric field will affect the carrier velocity distribution and the trap potential configuration, and the field is not homogeneous and transient conditions prevail, i.e., transient rather than steady state carrier velocity distribution are generated, it is difficult to study and unravel these effects from experimental data measured with the DLTS technique. To overcome these problems, the G-R noise spectra of a homogeneous doped semiconductor resistor are measured. The electric field in such a resistor operating in the space-charge free domain is independent of position and its value is determined by the applied bias voltage and the device length. In addition, G-R noise measurements are done under steady state conditions so that transient carrier distributions are avoided.

In the following section, we derive the expressions for the G-R noise spectral density and device resistance in terms of the shallow and deep impurity concentrations. Then we present detailed descriptions of the experiment and the parameter extraction procedures.

2.2. Theory

In this section, we develop and use a G-R noise theory to extract trap parameters from a defect with a single-donor level. The device structure is a p^+-p^--p^+ Si:Au:B resistor shown in figure 2.1. Figure 2.2 is the schematic energy band diagram of this device. The gold donor

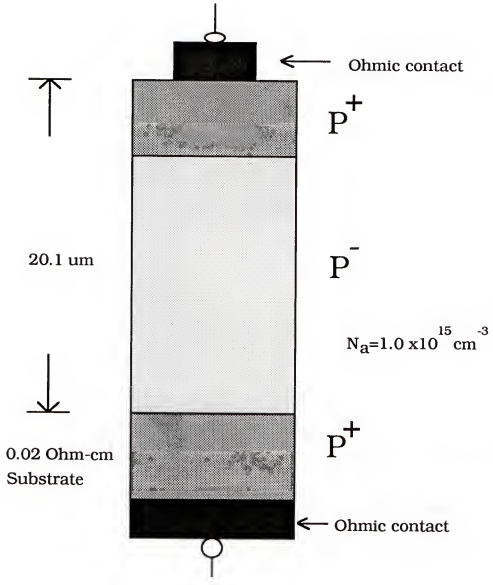

Figure 2.1. Device structure

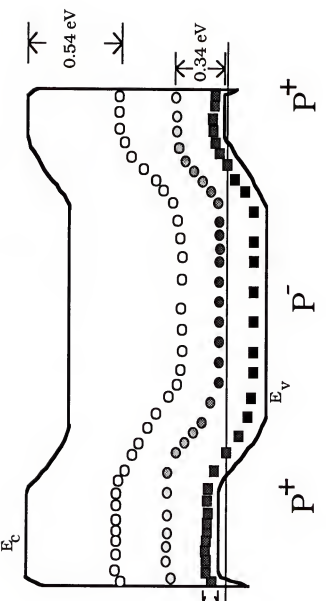

Figure 2.2. Schematic energy band diagram in equilibrium

energy level is 0.336 eV above the valence band edge, the gold acceptor energy level is 0.54 eV below the conduction band edge. The shallow acceptor energy level is 0.045 eV above the valence band edge.

For simplicity, the following assumptions are made: (1) only gold donors interact with the valence band, (2) the electron density is neglected, (3) space charge neutrality and space uniformity prevail.

The carrier densities can be written as

$$P = P_o + \Delta P, \tag{2.1}$$

$$Nau^+ = Nauo^+ + \Delta Nau^+, \tag{2.2}$$

where P, Nau^+ are the hole concentration in the valence band and the charged gold donor concentration, respectively; ΔP, ΔNau^+ are the corresponding fluctuations in P and Nau^+ and P_o and $Nauo^+$ are the corresponding densities in steady state.

The condition of charge neutrality gives the following equation for the fluctuations in P, and Nau^+

$$\Delta Nau^+ + \Delta P = 0. \tag{2.3}$$

The rate equation takes the form

$$\frac{dP}{dt} = e_p\ Nau^+ - c_p P\ (Nau - Nau^+), \tag{2.4}$$

where c_p is the hole capture coefficient and e_p is the hole emission coefficient.

In steady state, eq. (2.4) gives

$$e_p = c_p\ (Nau - Nauo^+)\left(\frac{P_o}{Nau^+}\right), \tag{2.5}$$

Using eqs. (2.1) through (2.5), we get after linearization

$$\frac{d\Delta P}{dt} = -\left[e_p + c_p P_o + c_p\ (Nau - Nauo^+)\right]\Delta P. \tag{2.6}$$

This equation can be further simplified as we will show in the following section.

2.2.1. Overcompensated Devices

If the gold concentration is larger than the boron concentration, i.e., the device is overcompensated, the Fermi level will be located between the gold donor energy level and the valence band edge at temperatures between 150 and 250 K. Then P is very small, more precisely $P << (Nau^- - Nau^+), Nau^+, Nau$.

With the aid of eq. (2.5), we can assume that

$$[e_p + c_p P_o] << [c_p (Nau^- - Nauo^+)]. \tag{2.7}$$

Then eq. (2.6) simplifies to

$$\frac{d\Delta P}{dt} = - c_p (Nau^- - Nauo^+) \Delta P = - \frac{\Delta P}{t_p}, \tag{2.8}$$

with

$$\frac{1}{t_p} = c_p (Nau - Nauo^+). \tag{2.9}$$

Assuming $Na = Na^- = Nauo^+$, where Na is the concentration of boron, eq. (2.9) becomes

$$\frac{1}{t_p} = c_p (Nau - Na). \tag{2.10}$$

The normalized, spectral density of G-R noise has the form [17]

$$\frac{S_{vv}(\omega)}{V_o^2} = \frac{S_{PP}(\omega)}{P_o^2} = \frac{4\, g_o\, t_p^2}{L\, w\, d\, P_o^2\, (1+\omega^2 t_p^2)}, \tag{2.11a}$$

where g_o is the free carrier generation rate given by

$$g_o = Nauo^+ e_p. \tag{2.11b}$$

The normalized plateau value of the G-R noise can then be written as

$$\frac{S_{vv}(0)}{V^2} = \frac{4\, Nauo^+ e_p\, t_p^2}{L\, w\, d\, P_o^2}. \tag{2.12}$$

The density $Nauo^+$ can be expressed in terms of Nau using Fermi-Dirac statistics

$$Nauo^+ = \frac{Nau}{1 + g_{au}\, e^{\frac{E_f - E_{au}}{KT}}}, \qquad (2.13)$$

where E_{au} is the gold donor energy level, E_f is the Fermi level, K is the Boltzmann constant, T is the temperature, and g_{au} is the degeneracy factor of the gold donor.

Combining eqs. (2.5) and (2.13), we get

$$e_p = c_p\, N_v\, g_{au}\, e^{\frac{E_v - E_{au}}{KT}}. \qquad (2.14)$$

Using the charge neutrality equation

$$Na^- = P + Nau^+, \qquad (2.15a)$$

and assuming that the shallow acceptors are fully ionized, P can be written as

$$P = \frac{g_{au}\,(Na - P)\, N_v\, e^{\frac{E_v - E_{au}}{KT}}}{Nau - Na + P}. \qquad (2.15b)$$

Using eqs. (2.10), (2.12), (2.14) and (2.15b), and assuming that the hole density is small, we get

$$\frac{S_{vv}(0)}{V^2} = \frac{4\, e^{\frac{E_{au} - E_v}{KT}}}{L\, w\, d\, N_v\, c_p\, Na\, g_{au}}, \qquad (2.16)$$

where L, w, d are the length, width, and thickness of the device, E_v is the valence band edge, and N_v is the density of states of the valence band.

The resistance of the device is given by

$$R = \frac{L}{e\, w\, d\, \mu_p\, P}. \qquad (2.17)$$

Using eqs. (2.15b) and (2.17), we get

$$R = \frac{L\,(N_{au} - N_a)\,e^{\frac{E_{au}-E_v}{KT}}}{e\,w\,d\,\mu_p N_a\,N_v\,g_{au}} \quad , \tag{2.18}$$

where μ_p is the hole mobility, and -e is the charge of an electron.

Equations (2.16) and (2.18) show that the activation energies extracted from these equations should have the same value.

With the use of a low field mobility formula, eqs. (2.16) and (2.18), and an optimization procedure [18], we are able to extract trap parameters from the previous equations. The semi-empirical mobility formula that we use is [19]

$$\mu_p = 54.3\left(\frac{T}{300}\right)^{-0.57} + \frac{1.36 \times 10^8\,(T)^{-2.23}}{1+[Nf/(2.35 \times 10^{17}(\frac{T}{300})^{2.4})]0.88\,(\frac{T}{300})^{-0.146}} \quad , \tag{2.19}$$

where Nf is the effective charged impurity concentration, and all quantities are in c.g.s. units.

2.2.2. Lightly Doped Devices

If the gold concentration is smaller than the boron concentration, we may assume that

$$P >> Nau^{+}, Nau. \tag{2.20}$$

With this condition eq. (2.6) simplifies to

$$\frac{d\Delta P}{dt} = -\,[e_p + c_p P_o]\Delta P = -\,\frac{\Delta P}{t_p}, \tag{2.21}$$

with

$$\frac{1}{t_p} = [e_p + c_p P_o]. \tag{2.22}$$

The concentration of holes is given by

$$P_o = N_v \, e^{\frac{E_v - E_f}{KT}} . \qquad (2.23)$$

Combining eqs. (2.14), (2.22) and (2.23), we get

$$\frac{1}{t_p} = c_p N_v \, e^{\frac{E_v - E_f}{KT}} [g_{au} \, e^{\frac{E_f - E_{au}}{KT}} + 1]. \qquad (2.24)$$

When the Fermi level is located above the trap level, the above equation becomes

$$\frac{1}{t_p} = c_p N_v \, g_{au} \, e^{\frac{E_v - E_{au}}{KT}} . \qquad (2.25)$$

The trap energy can be extracted from this equation by plotting $Ln(t_p T^2)$ versus $1000/T$ where it is assumed that the temperature dependence of c_p is weak.

From eq. (2.11) we get

$$\frac{S_{vv}(0)}{t_p V^2} = \frac{S_{PP}(0)}{t_p P^2} = \frac{4 \, Nau^+ e_p \, t_p}{L w d P^2} . \qquad (2.26)$$

Combining eqs. (2.13), (2.14), (2.17), (2.23) and (2.24), we get

$$\frac{S_{vv}(0)}{t_p V^2} = \frac{4 \, Nau}{\{1 + g_{au} \, e^{\frac{E_f - E_{au}}{KT}}\}^2} \, g_{au} \, e^{\frac{E_f - E_{au}}{KT}} \left[\frac{R w d e \mu_p}{L}\right]^2 \left[\frac{1}{w d L}\right],$$

or

$$\frac{S_{vv}(0) w d L}{t_p V^2} \left[\frac{L}{R w d e \mu_p}\right]^2 = \frac{4 \, Nau}{\{e^{-\gamma/2} + e^{\gamma/2}\}^2} , \qquad (2.27)$$

with

$$g_{au} \, e^{\frac{E_f - E_{au}}{KT}} = e^{\gamma} . \qquad (2.28)$$

Equation (2.27) shows a peak for $\gamma = 0$ where $T = T_o$. From this peak value the gold concentration can be determined. From eqs. (2.23) and (2.28), we get

$$g_{au} = \frac{P(T_0)\, e^{\frac{E_{au} - E_v}{KT}}}{N_v(T_0)} . \qquad (2.29)$$

When $\gamma > 0$, combining eqs. (2.23), (2.27) and (2.28), we get

$$\frac{S_{vv}(0) L w d N_V}{t_p V^2} \left[\frac{L}{R w d e \mu_p}\right] = \frac{4 Nau\, e^{\frac{E_{au} - E_v}{KT}}}{g_{au}} . \qquad (2.30)$$

When $\gamma < 0$, combining eqs. (2.23), (2.27) and (2.28), we get

$$\frac{S_{vv}(0) L w d}{t_p V^2 N_V} \left[\frac{L}{R w d e \mu_p}\right]^3 = 4 Nau\, g_{au}\, e^{\frac{E_v - E_{au}}{KT}} . \qquad (2.31)$$

The trap parameters can be extracted by using the following procedures as outlined in [20]

(1) The trap energy is extracted from eq. (2.30) or (2.31).

(2) The degeneracy factor is extracted from eq. (2.29).

(3) The gold concentration is extracted from eq. (2.27).

(4) The capture coefficient is extracted from eqs. (2.23) and (2.24).

(5) The emission coefficient is extracted from eq. (2.14).

2.2.3. Arbitrary Doping Levels

If the impurity concentration does not satisfy eq. (2.7) or eq. (2.20), the full expression for eq. (2.6) has to be considered; i.e.,

$$\frac{d\Delta P}{dt} = - [e_p + c_p P_o + c_p (Nau - Nauo^+)]\Delta P = - \frac{\Delta P}{t_p} , \qquad (2.32)$$

with

$$\frac{1}{t_p} = [e_p + c_p P_o + c_p (Nau - Nauo^+)]. \qquad (2.33)$$

Substituting for e_p, P_o and $Nauo^+$, we get

$$\frac{1}{t_p} = c_p \left[N_v g_{au} e^{\frac{E_v - E_{au}}{KT}} + P_o + \frac{Nau\ g_{au} e^{\frac{E_f - E_{au}}{KT}}}{1 + g_{au} e^{\frac{E_f - E_{au}}{KT}}} \right]. \qquad (2.34)$$

Equation (2.12) then becomes

$$\frac{S_{vv}(0)}{t_p V^2} = \frac{4 N_v g_{au} e^{\frac{E_v - E_{au}}{KT}}}{L w d P^2} \frac{Nau}{1 + g_{au} e^{\frac{E_f - E_{au}}{KT}}}$$

$$/ \left[N_v g_{au} e^{\frac{E_v - E_{au}}{KT}} + P + \frac{Nau\ g_{au} e^{\frac{E_f - E_{au}}{KT}}}{1 + g_{au} e^{\frac{E_f - E_{au}}{KT}}} \right]. \qquad (2.35)$$

Combining eqs. (2.17), (2.19), (2.23), (2.34) and (2.35), and using an optimization technique [18], we can get the degeneracy factor, gold concentration and trap energy level from eq. (2.35), and then from eq. (2.34) the capture coefficient. The emission coefficient is extracted from eq. (2.14).

2.3. Experimental Results and Discussion

For devices with small deep impurity concentrations, the method of section 2.2.2 applies, as is experimentally demonstrated in [20]. The experimental data obtained from our devices show that we deal with overcompensation. Therefore the theory of section 2.2.1 should apply.

A p^+-p^--p^+ resistor (CM24B-82 #1) shown in figure 2.1 is used in this experiment. An epi-layer of thickness 20.1 um is grown on a highly doped substrate with a resistivity of 0.02 Ohm-cm. The boron concentration in the epi-layer is 1.0×10^{15} cm^{-3}. The drive-in temperature is 900° Celsius; the drive-in time is 10.75 hours. The

junction diameter of the device is 7.5 x 10^{-2} cm and the calculated junction depth of the Ohmic contact is 1.93 um. The resistance of the device at room temperature is 64 Ohm. A guard ring to control the surface properties of the p^+-p^--p^+ device was included in the device design.

When the gold concentration is larger than the boron concentration and the shallow impurities are completely ionized, the gold impurities will be partially ionized and the Fermi level will be located between the gold donor energy level and the valance band edge. As it will be shown in Chapter V, the Fermi level is close to and significantly affected by the gold energy level, and varies linearly with temperature.

A block scheme of the experimental arrangement is shown in figure 2.3. The voltage Vs is the bias voltage, R_d represents the device and R_b the bias resistance. The device is mounted in a temperature controlled holder which allows for noise measurements between 77 and 300 K. The bias current I, supplied from a battery, is controlled by a variable series metal film resistor which is almost 20 times larger than the resistance of the device. A Brookdeal 5004 ultra-low noise preamplifier and a Hewlett Packard 3561A dynamic signal analyzer make it possible to measure the device noise at frequencies between 1 and 10^5 Hz.

A switch is used to connect the input of the amplifier to a dummy resistor, by which we are able to estimate the magnitude of the undesirable noise from the amplifier and the bias circuit. We found that the noise from the bias circuit is negligible when compared with the generation-recombination noise from the device.

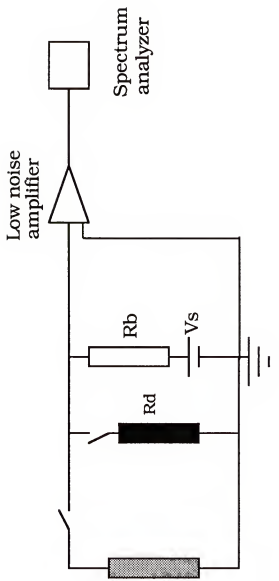

Figure. 2.3. Block scheme of the experimental set-up

The measured noise spectra show frequency independent excess noise up to frequencies where the bandwith of the measuring systems limits the signal transfer. The excess noise is interpreted in terms of G-R noise. Biasing of the guard ring has no effect on the measured spectral density. This indicates that the noise is generated in the bulk of the resistor.

Figure 2.4 shows the resistance of the device as a function of 1000/T. Figure 2.5 shows the measured values of the G-R noise plateau normalized to V^2 as a function of 1000/T. With the use of the semi-empirical formula (2.19) for the mobility and eqs. (2.16) and (2.18), we extract a hole capture cross section of $\sigma_{p1} = 3.2 \times 10^{-15}$ cm^2, a degeneracy factor of 16.25, a gold donor energy above the valence band of 0.336 eV, and a gold concentration of 2.51×10^{15} cm^{-3}.

Note that the extracted value of the gold degeneracy factor is quite close to 16 as found from Hall coefficient data [21], and that the value of the hole capture cross section is of the same order as published values [2,22]. This indicates that the above described noise method is an accurate technique to investigate deep level properties.

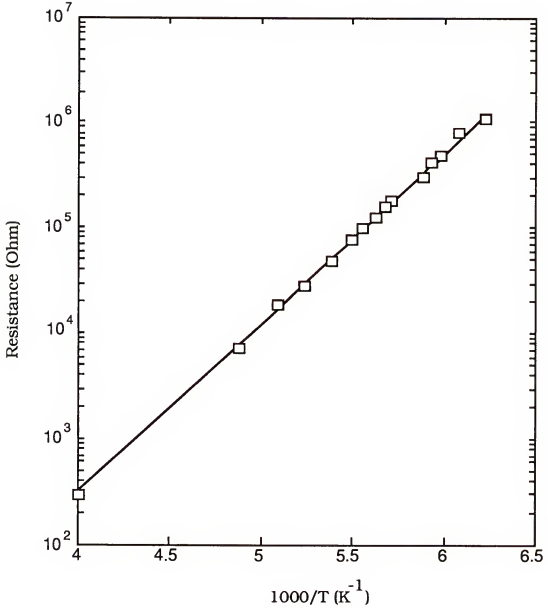

Figure 2.4. The resistance versus 1000/T of device CM24B-82 #1. The squares are the experimental data and the solid line represents the best fit to the data.

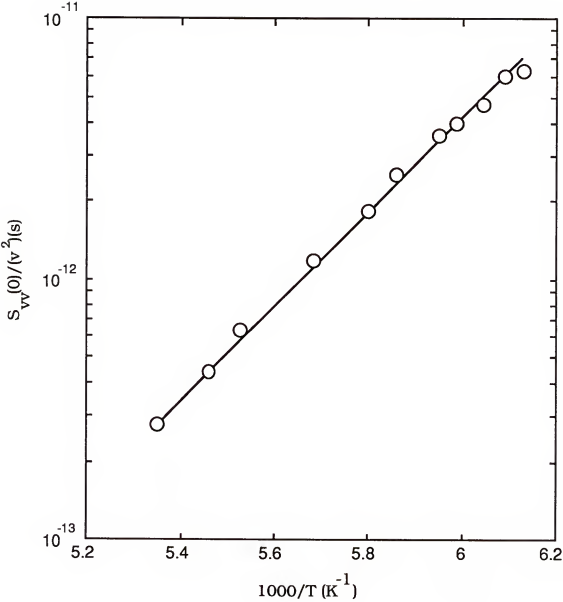

Figure 2.5. The normalized, low-frequency G-R noise plateau values versus 1000/T. The circles represent the experimental data and the solid line represents the best fit to the data.

CHAPTER III
EXPERIMENTAL EVIDENCE FOR A SECOND-DONOR LEVEL OF GOLD IN SILICON

3.1. Introduction

The complete signature of an impurity in a given semiconductor host should include information about its atomic configuration and wavefunction and the energy levels of bound electrons and/or holes. From these quantities it is possible to deduce all its electronic characteristics. The phenomenological electronic parameters, i.e., thermal-emission rates, capture cross sections and optical cross sections, can be measured by changing the carrier population in defects either thermally, optically, or electrically. In order to obtain the defect's electronic characteristics one relies on the sensitivity of the experimental techniques to the changes in defect characteristics when subjected to external disturbances. The experimental methods for characterization of electronic properties of defects can be divided into three groups namely, electrical techniques, optical techniques and techniques involving electron paramagnetic resonance [10]. The most widely used electrical techniques are the transient methods [11].

These transient measurement techniques are rather involved and mainly based on the assumption that there is only one dominant emission or capture process of either electrons or holes for each deep level during the transient. The effect from a small or slow response is not easily observed, simply because it has a minor contribution to the overall signal. For example, if two energy levels, say E_1, E_2, are very

close and the emission rate from level E_1 is smaller than that of level E_2, then we are unable to detect energy level E_1 by measuring emission rates versus 1000/T.

The activation energy for emission is obtained in these experiments by relating the emission rate to the energy level depth E_a by detailed balance. If the emission coefficient depends on electric field, then the activation energy extracted from these methods will show a variation with electric field strength.

In chapter II, we used resistivity and noise data to explore the defect properties of gold in silicon and found that the results are compatible with those obtained by other techniques. The variation of resistance versus temperature provides under certain conditions the activation energy, and the noise data give us the capture cross section and emission coefficient. In this noise experiment the magnitude of the electric field was controlled precisely by the externally applied voltage.

Despite the fact that gold in silicon has received so much attention, its behavior is not always predictable. The consensus seems to be that a donor and an acceptor level at 0.35 and 0.54 eV above the valence and below the conduction band respectively are introduced by gold in the silicon energy gap. This is the so-called two-level model. There are some indications, however, that gold can produce more than two levels. Newman [23] measured the photoconductive spectral response of p-type gold-doped silicon and pointed out that it is difficult to explain his data in terms of a two-level model.

A search for another acceptor level closer to the conduction band was conducted [24]. This was done by changing the

concentration ratio of gold (Nau) to residual donors (Nd-Na) in a single crystal by several additions of phosphorus from the case where Nau > (Nd-Na) to the case where 2 Nau > (Nd-Na) > Nau. No new level was discovered. A similar experiment in p-type silicon was carried out by Taft and Horn [25]. They doped p type silicon devices with different gold concentrations. No exact relationship between the gold and the shallow impurity concentration in the p-type silicon was specified, and no new energy level was found.

In this chapter we report on resistance and low frequency voltage noise measurements carried out as a function of temperature on a p^+-p^--p^+ device made of Si:Au with a boron concentration of 2.7×10^{15} cm^{-3}. Two different activation energies are observed. The normalized, low-frequency noise spectral density versus 1000/T shows an activation energy of 0.336 eV, which is in agreement with the well-established gold donor energy level. The plot of the resistance versus 1000/T reveals an activation energy of 0.267 eV. It is very unlikely that this energy level is caused by an unintended impurity since the devices were fabricated under very well controlled conditions. Therefore a double-donor model is proposed to interpret this behavior.

3.2. Theory

In this section, we discuss a method of using low-frequency generation-recombination noise involving a double donor as a tool for trap parameter extraction. The device is a p^+-p^--p^+ Si:Au:B resistor shown in figure 3.1. Figure 3.2 is the schematic energy band diagram of the device. As we will show in this chapter, gold in silicon creates

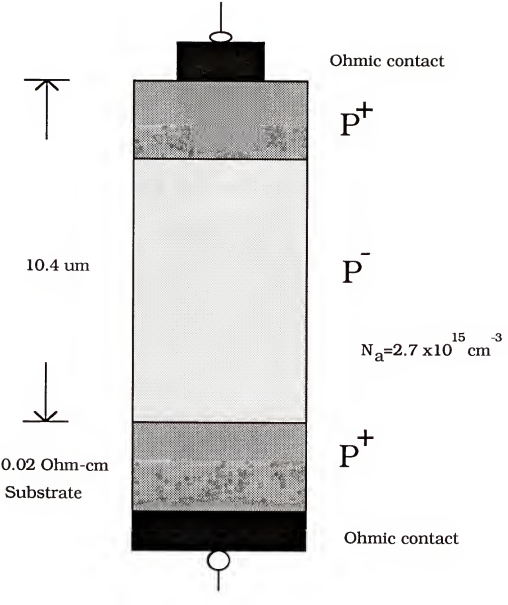

Figure 3.1. Device structure

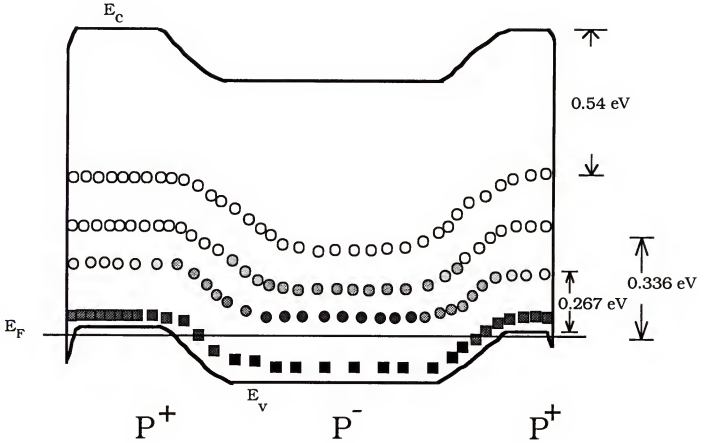

$(E_a - E_v) = 0.045$ eV

Figure 3.2. Schematic energy band diagram in equilibrium

two donor levels: the first donor level lies 0.336 eV above the valence band edge and the second donor level 0.267 eV above the valence band edge. The gold acceptor energy level is 0.54 eV below the conduction band edge. If the Fermi level is far away from the acceptor energy, the effects from the acceptor level can be neglected (see Chapter V). The boron activation energy is 0.045 eV.

In the previous chapter, we discussed a single-donor model in which the Fermi level is located above the second donor level. Consequently, the gold donor centers in silicon are almost singly ionized, and the effects of the second donor level on the electronic properties can be neglected. In this chapter, we consider a double-donor model, that under certain conditions may reduce to a single-donor model.

The calculations of the resistance and the voltage noise resulting from double donor centers interacting with the valence band are made based on the following assumptions: 1. space uniformity prevails; 2. only donor levels interact with the valence band, i.e., we neglect the interaction between the gold acceptor level at midgap and the valence band; 3. $P > N$; 4. $Na^- = Na$.

The pertinent hole transitions are described in Table 3.1. The parameter P is the hole density, N is the electron concentration, Na is the boron concentration, and Na^- is the ionized boron concentration. The total gold concentration is Nau, and Nau^+, Nau^{++}, Nau^o are the singly ionized, doubly ionized, and neutral gold concentration respectively. The symbol e^+ denotes a mobile hole, g_l, r_l are the hole generation rate and the hole recombination rate respectively, and e_{pl},

TABLE 3.1. Generation and recombination rates in terms of ionized gold and mobile hole concentrations.

Rate	Hole Transitions involved	Description of the rates
g_1	$Nau^+ \rightarrow Nau^o + e^+$	$e_{p1}\, Nau^+$
r_1	$Nau^o + e^+ \rightarrow Nau^+$	$c_{p1}\, Nau^o\, P$
g_2	$Nau^{++} \rightarrow Nau^+ + e^+$	$e_{p2}\, Nau^{++}$
r_2	$Nau^+ + e^+ \rightarrow Nau^{++}$	$c_{p2}\, Nau^+\, P$

c_{p1}, and e_{p2}, c_{p2} are the emission and capture coefficient for holes in the first-donor level and the second-donor level respectively.

According to W. Shockley and J. T. Last [26], the ionized impurity densities can be expressed as

$$Nau^{+} = \frac{1}{g_{au1}} Nau^{0} \, e^{\frac{E_{1d} - E_f}{KT}}, \tag{3.1}$$

$$Nau^{++} = \frac{1}{g_{au2}} Nau^{0} \, e^{\frac{E_{1d} + E_{2d} - 2E_f}{KT}}, \tag{3.2}$$

where E_{1d} is the first gold donor energy level, E_{2d} is the second gold donor energy level, E_f is the Fermi energy level, and g_{au1} and g_{au2} are the degeneracy factors for the first and second donor level respectively.

The total gold concentration is given by

$$Nau^{++} + Nau^{+} + Nau^{o} = Nau. \tag{3.3}$$

From eqs. (3.1), (3.2) and (3.3), the ionized gold concentrations are rewritten as

$$Nau^{+} = \frac{Nau}{1 + \frac{g_{au1}}{g_{au2}} e^{\frac{E_{2d} - E_f}{KT}} + g_{au1} e^{\frac{-(E_{1d} - E_f)}{KT}}}, \tag{3.4}$$

$$Nau^{++} = \frac{Nau}{1 + g_{au2} e^{\frac{-(E_{1d} + E_{2d} - 2E_f)}{KT}} + \frac{g_{au2}}{g_{au1}} e^{\frac{-(E_{2d} - E_f)}{KT}}}. \tag{3.5}$$

The value of P can be derived from eqs. (3.3) to (3.5) and eq. (2.23) with the use of the charge neutrality equation

$$2Nau^{++} + Nau^{+} + P = Na. \tag{3.6}$$

Our noise calculation applies to the low field Ohmic regime of device operation. Then

$$I = \frac{V}{R} = \frac{A}{L} q \mu_p \; P V, \tag{3.7}$$

where μ_p is the hole mobility, V is the applied voltage, and R is the resistance.

The rate equations for the hole and ionized gold densities read:

$$\frac{dNau^+}{dt} = - g_1 + r_1 + g_2 - r_2, \tag{3.8}$$

$$\frac{dNau^{++}}{dt} = - g_2 + r_2, \tag{3.9}$$

$$\frac{dP}{dt} = g_1 - r_1 + g_2 - r_2, \tag{3.10}$$

where g_1, r_1, g_2, r_2 are described in Table 3.1.

In order to calculate the noise spectral density, we express the carrier densities as sums of a steady-state term and a fluctuation term,

$$P = P_o + \Delta P, \tag{3.11}$$

$$Nau^+ = Nauo^+ + Nau^+, \tag{3.12}$$

$$Nau^{++} = Nauo^{++} + Nau^{++}, \tag{3.13}$$

where P, Nau^+, Nau^{++} are the hole concentration in the valence band, the singly ionized gold concentration and the doubly ionized gold concentration respectively. The terms ΔP, ΔNau^+, ΔNau^{++} are the corresponding fluctuations in the densities of hole and charged traps and P_o, $Nauo^+$, $Nauo^{++}$ are the corresponding densities in steady-state. From eqs. (3.3) and (3.6), we obtain

$$\Delta Nau^{++} + \Delta Nau^+ + \Delta Nau^o = 0, \tag{3.14}$$

and

$$2\Delta Nau^{++} + \Delta Nau^+ + \Delta P = 0. \tag{3.15}$$

We expand the carrier densities around steady-state in first order and obtain for eq. (3.10)

$$\frac{d\Delta P}{dt} = g_{10} - r_{10} + g_{20} - r_{20} + e_{p1}\,\Delta Nau^{+} - c_{p1}\,Nau^{o}\,\Delta P$$

$$- c_{p1}\,\Delta Nau^{o}\,P_o + e_{p2}\,\Delta Nau^{++} - c_{p2}\,\Delta Nau^{+}\,P_o - c_{p2}\,Nau^{+}\,\Delta P, \quad (3.16)$$

where g_{10}, r_{10}, g_{20}, r_{20} are the steady-state values of g_1, r_1, g_2, r_2, respectively.

Using eqs. (3.14), (3.15), (3.16) and the steady-state solution of eqs. (3.9) and (3.10), we get

$$\frac{d\Delta P}{dt} = -(e_{p1}-c_{p2}\,P_o+c_{p1}\,Nauo^{o}+c_{p2}\,Nauo^{+}+c_{p1}\,P_o)\Delta P -$$

$$(-e_{p2}+c_{p1}P_o+2e_{p1}-2c_{p2}P_o)\Delta Nau^{++}, \quad (3.17)$$

$$\frac{d\Delta Nau^{++}}{dt} = -(e_{p2} + 2c_{p2}\,P_o)\,\Delta Nau^{++} + (c_{p2}\,Nauo^{+} - c_{p2}\,P_o)\Delta P. \quad (3.18)$$

Using the Langevin approach, the rate equations including the noise can then be written as

$$\frac{d\Delta P}{dt} = -M_{11}\,\Delta P - M_{12}\,\Delta Nau^{++} + F_1 + F_2, \quad (3.19)$$

$$\frac{d\Delta Nau^{++}}{dt} = -M_{21}\,\Delta P - M_{22}\,\Delta Nau^{++} - F_2, \quad (3.20)$$

with relaxation matrix elements

$$M_{11} = e_{p1}-c_{p2}\,P_o+c_{p1}\,Nauo^{o}+c_{p2}\,Nauo^{+}+c_{p1}\,P_o,$$

$$M_{22} = e_{p2} + 2c_{p2}\,P_o,$$

$$M_{12} = -e_{p2}+c_{p1}P_o+2e_{p1}-2c_{p2}P_o,$$

$$M_{21} = -c_{p2}\,Nauo^{+} + c_{p2}\,P_o. \quad (3.21)$$

The Langevin noise source term F_1 models the noise in the hole transition rates between the valence band and the first-donor level,

whereas F_2 accounts for the noise in the hole transition rates between the valence band and the second-donor level.

Performing a Fourier transformation on eqs. (3.19) and (3.20), we obtain

$$\begin{bmatrix} j\omega+M_{11} & M_{12} \\ M_{21} & j\omega+M_{22} \end{bmatrix} \begin{bmatrix} \tilde{\Delta P} \\ \tilde{\Delta N}au^{++} \end{bmatrix} = \begin{bmatrix} \tilde{F}_1+\tilde{F}_2 \\ -\tilde{F}_2 \end{bmatrix}. \tag{3.22}$$

Inverting this expression results in

$$\tilde{\Delta P} = \frac{(j\omega+M_{22})(\tilde{F}_1+\tilde{F}_2)+M_{12}\tilde{F}_2}{Det}, \tag{3.23}$$

with

$$Det = -\omega^2+j\omega(M_{11}+M_{22})-M_{12}M_{21}+M_{22}M_{11}, \tag{3.24}$$

where $\tilde{\Delta P}$, $\tilde{F}_1$, $\tilde{F}_2$ are the Fourier components of ΔP, F_1 and F_2, respectively.

The eigenvalues λ_1, λ_2 of the phenomenological relaxation matrix M [3] are the roll-off frequencies of the noise spectra. The eigenvalue equation of M reads:

$$\lambda^2 - \lambda(M_{11}+M_{22})-(M_{12}M_{21}- M_{11}M_{22})=0.$$

The eigenvaules are therefore given by

$$\lambda_1 = \frac{(M_{11}+M_{22})+\sqrt{(M_{11}+M_{22})^2-4(M_{11}M_{22}-M_{12}M_{21})}}{2}, \tag{3.25}$$

$$\lambda_2 = \frac{(M_{11}+M_{22})-\sqrt{(M_{11}+M_{22})^2-4(M_{11}M_{22}-M_{12}M_{21})}}{2}. \tag{3.26}$$

Assuming that there is no correlation between the Langevin noise sources and that the transition rates show full shot noise, we obtain

$$S_{pp}(\omega)= \frac{(\omega^2+M_{22}^2)(S_{F1}+S_{F2}) + (M_{12}^2+2M_{12}M_{22})\,S_{F2}}{|Det|^2}, \tag{3.27}$$

with

$$S_{F1}= \frac{4r_1}{L\,w\,d},$$

and

$$S_{F2}= \frac{4r_2}{L\,w\,d},$$

where L, w, d are the length, width and thickness of the device.

Thus

$$S_{pp}(\omega)= \frac{G}{(\omega^2+\lambda_1^2)} + \frac{H}{(\omega^2+\lambda_2^2)}, \tag{3.28}$$

with

$$G = 4\,\frac{\lambda_1^2(r_1+r_2)-M_{22}^2\,(r_1+r_2)-(M_{12}^2+2M_{12}M_{22})\,r_2}{L\,w\,d\,(\lambda_1^2-\lambda_2^2)}, \tag{3.29}$$

and

$$H = 4\,\frac{-\lambda_2^2(r_1+r_2)+M_{22}^2\,(r_1+r_2)+(M_{12}^2+2M_{12}M_{22})\,r_2}{L\,w\,d\,(\lambda_1^2-\lambda_2^2)}. \tag{3.30}$$

Note that eq. (3.28) predicts two Lorentzian components for the overall noise spectrum. Equations (3.28) through (3.30) can be further simplified.

3.2.1. Deep Double-Donor Defects in Nearly Compensated Material

In this section, a device doped with a gold concentration satisfying Na > Nau > 0.5Na is studied. From the steady-state solution of eqs. (3.8) and (3.9), we find

$$e_{p1} = c_{p1}\,Nauo^0\,(\frac{P_o}{Nauo^+}), \tag{3.31}$$

and

$$e_{p2} = c_{p2}\,Nauo^+\,(\frac{P_o}{Nauo^{++}}). \tag{3.32}$$

At low temperatures we may assume $P_o << Nauo^+, Nauo^{++}, Nauo^o$. This assumption is substantiated by exact numerical calculations presented in section 3.3. We make this assumption at this point because it allows us to obtain simple analytical expression for the resistance and voltage

noise of the double donor model. With eqs. (3.31) and (3.32) and the above assumption eqs. (3.17) and (3.18) can be simplified to

$$\frac{d\Delta P}{dt} = -(c_{p1}\, Nau^{o} + c_{p2}\, Nau^{+})\Delta P - (-e_{p2} + c_{p1}P + 2e_{p1} - 2c_{p2}P)\Delta Nau^{++}, \tag{3.33}$$

$$\frac{d\Delta Nau^{++}}{dt} = (c_{p2}\, Nau^{+})\Delta P - (e_{p2} + 2c_{p2}\, P)\, \Delta Nau^{++}. \tag{3.34}$$

The relaxation matrix elements in eq. (3.21) become

$$M_{11} = c_{p1}\, Nau^{o} + c_{p2}\, Nau^{+}, \qquad M_{12} = -\, e_{p2} + c_{p1}P + 2e_{p1} - 2c_{p2}P,$$
$$M_{21} = -\, c_{p2}\, Nau^{+}, \qquad M_{22} = e_{p2} + 2c_{p2}\, P. \tag{3.35}$$

Note that eq. (3.28) predicts two Lorentzian components in the overall noise spectrum. However in the following we argue that the values of λ_1 and λ_2 are such that in our experiments where we measured the noise between 100 Hz and 1000 Hz, only $S_{pp}(\omega)$ for $\lambda_2 << \omega << \lambda_1$ was observed.

Since the coefficient c_{p2} is associated with a repulsive capture process, one may expect its value to be rather small [27], of the order of 10^{-11} to 10^{-14} cm^3/s. The coefficient c_{p1} on the other hand is related to a neutral capture process, and will be therefore of the order of 10^{-8} cm^3/s. Consequently we may assume

$$\frac{c_{p1}}{c_{p2}} >> \frac{Nau^{+}}{Nau^{o}} = \frac{1}{g_{au1}}\, e^{\frac{E_{1d^-} - E_f}{KT}}. \tag{3.36}$$

Using eqs. (3.25), (3.26) and (3.31), (3.32), (3.36), we obtain

$$M_{11} >> M_{21},\ M_{22},\ M_{12},$$
$$\lambda_1 >> \lambda_2,$$
$$\lambda_1 \cong M_{11} = c_{p1}\, Nau^{o} \cong \frac{1}{t_p}, \tag{3.37}$$

$$\lambda_2 \cong \frac{(M_{11}M_{22}-M_{12}M_{21})}{(M_{11}+M_{22})} < M_{22} = c_{p2} + 2c_{p2}\,P.$$

Our exact numerical calculations indicate an upper limit of 1 Hz for $\lambda_2/2\pi$ reached at a temperature of 221 K. This is consistent with the fact that we did not observe any Lorentzian spectrum in our low frequency noise window of 100 Hz to 1000 Hz.

Using eqs. (3.31), (3.32) and (3.37), we get

$$S_{pp}(\omega) \cong \frac{4(r_1+r_2)}{L\,w\,d\,(\omega^2+\lambda_1^2)}, \tag{3.38}$$

$$r_1+r_2 = (c_{p1}\,Nau^{o} + c_{p2}\,Nau^{+})P \cong M_{11}P,$$

$$\frac{S_{vv}(\omega)}{V^2} = \frac{S_{PP}(\omega)}{P^2} = \frac{4\,c_{p1}\,Nau^{o}\,P\,t_p^{\,2}}{L\,w\,d\,P^2\,(1+\omega^2\,t_p^{\,2})}\,. \tag{3.39}$$

Equation (3.39) can be approximated by

$$\frac{S_{vv}(\omega)}{V^2} = \frac{4}{L\,w\,d\,P\,c_{p1}\,Nau^{o}} \qquad \text{for} \qquad \lambda_2 << \omega << \lambda_1. \tag{3.40}$$

This equation can be simplified to eq. (2.16) if we use the hole concentration given by eq. (2.15). This shows that when the Fermi level is above the first donor energy level, the double-donor model reduces to a single-donor model. Equations (3.6), (3.7) and (3.40) can be used to extract trap parameters from the resistance data and noise data if we use the mobility formula (2.19).

The theoretical predictions for the noise and resistance can be further simplified by assuming $(E_{1d} - E_f) > KT \log(g_{au1})$ which is certainly valid for the low temperature region of our experiment. Then eq. (3.5) can be approximated by

$$Nau^{++} \cong \frac{Nau}{1 + \frac{g_{au2}}{g_{au1}}\,e^{\frac{-(E_{2d}-E_f)}{KT}}}\,. \tag{3.41}$$

Using eqs. (3.3), (3.6), neglecting P in eq. (3.6) and assuming Nau^{++}, $Nau^{+} > Nau^{o}$, the hole concentration at low temperature is given by

$$P = \frac{\frac{g_{au2}}{g_{au1}} (Na - Nau) N_v e^{\frac{E_v - E_{2d}}{KT}}}{2\,Nau - N_a}. \qquad (3.42)$$

Using the following approximations,

$$Nau^{++} \cong Na - Nau, \qquad (3.43)$$

$$Nau^{+} \cong 2Nau - Na, \qquad (3.44)$$

and substituting eqs. (3.1) and (3.42) into eq. (3.40), the expression for the normalized G-R noise becomes

$$\frac{S_{vv}(\omega)}{V^2} \cong \frac{4\, e^{\frac{E_{1d} - E_v}{KT}}}{L\,w\,d\,c_{p1}\,g_{au1}(2Nau - Na)\,N_v} \qquad \text{for } \lambda_2 << \omega << \lambda_1. \qquad (3.45)$$

Equations (3.42) and (3.45) illustrate that the noise contains the activation energy of the first donor level, whereas the carrier concentration or resistance shows the activation energy associated with the second donor level.

3.2.2. Simplified Double-Donor Noise Theory

Section 3.2.1 dealt with the double-donor model rigorously. However, the same results can be obtained using a simple idea. Suppose that carrier fluctuations can be caused by two processes: (1) carrier transitions between the first-donor level and the valence band such that $\Delta P \cong -\Delta Nau^{+}$, $\Delta Nau^{++} \cong 0$, (2) carrier transitions between the second-donor level and the valence band such that $\Delta P \cong \Delta Nau^{+} \cong -\Delta Nau^{++}$. We therefore approximate the rate equation as

For case 1,

$$\frac{d\Delta P}{dt} \cong e_{p1}\ \Delta Nau^{+} - c_{p1}\ Nau^{o}\ \Delta P\ - c_{p2}\ Nau^{+}\ \Delta P - c_{p2}\ \Delta Nau^{+}\ P,$$

$$\cong - (e_{p1} + c_{p1}\ Nau^{o}\ + c_{p2}\ Nau^{+} - c_{p2}\ P)\Delta P. \qquad (3.46)$$

Using eqs. (3.31), (3.32) and the conditions $P << Nau^{++}$, Nau^{+} at low temperature, we get

$$\frac{d\Delta P}{dt} \cong - (\ c_{p1}\ Nau^{o}\ + c_{p2}\ Nau^{+}\ )\Delta P. \qquad (3.47)$$

For case 2 we obtain

$$\frac{d\Delta P}{dt} \cong e_{p1}\ \Delta Nau^{+} - c_{p1}\ Nau^{o}\ \Delta P - c_{p2}\ Nau^{+}\ \Delta P$$

$$- c_{p2}\ \Delta Nau^{+}\ P + e_{p2}\ \Delta Nau^{++},$$

$$\cong - (-e_{p1} + c_{p1}\ Nau^{o}\ + c_{p2}\ Nau^{+} + c_{p2}\ P - e_{p2})\Delta P$$

$$\cong - (\ c_{p1}\ Nau^{o}\ + c_{p2}\ Nau^{+}\ )\Delta P = \frac{-\Delta P}{t_p}. \qquad (3.48)$$

Equations (3.47) and (3.48) show the same life time constant in both cases. Since the carrier fluctuations in the valence band arise from the processes listed in Table 3.1, the following spectral density expression for G-R noise is valid [17]

$$\frac{S_{vv}(\omega)}{V^2} = \frac{4\ g\ t_p^{\,2}}{L\ w\ d\ P^2\ (1+\omega^2\ t_p^{\,2})}\ , \qquad (3.49)$$

with

$$g = g_1 + g_2,$$

where g represents the total hole generation process. With the condition of eq. (3.36), eq. (3.39) readily follows.

3.3. Device Description, Experimental Results and Discussion

In this section we outline how we used the above procedures to extract trap parameters. When the electronic properties of the device

do not fit the deep defect density approximation made in the previous section, an exact numerical analysis should be employed.

A p^+-p^--p^+ resistor (M102-22 #1) shown in figure 3.1 is used in this experiment. An epi-layer of thickness 10.4 um is grown on a highly doped substrate with a resistivity of 0.02 Ohm-cm. The boron concentration in the epi-layer is 2.7×10^{15} cm^{-3}.

If the gold concentration is Na > Nau > 0.5Na and the shallow impurities are completely ionized, the gold impurities are either doubly ionized or singly ionized, and the Fermi level will be very close to the second-donor energy level. The device performance will be affected by both the first and the second donor level.

In chapter II, we investigated a p^+-p^--p^+ structure (device CM24B-82 #1) made of Si:Au:B with a boron concentration of 1.0×10^{15} cm^{-3}. In that particular case the resistance and noise data versus 1000/T showed identical activation energies of 0.34 eV. From the experimental data a gold concentration 2.51×10^{15} cm^{-3} was extracted. In the present work we use again a p^+-p^--p^+ structure (device M10B2-22 #1) but this time with a shorter p^- region and higher boron doping. An epi-layer of thickness 10.40 um was grown on a highly doped substrate with a resistivity of 0.02 Ohm-cm. The boron concentration in the epi-layer is 2.7×10^{15} cm^{-3}. The thickness of the wafer is 7.34 mil. The drive-in temperature is 900° Celsius; the drive-in time is 10.75 hours. The junction diameter of the device is 7.5×10^{-2} cm and the calculated junction depth of the Ohmic contact is 1.93 um. The resistance of the device at temperature T=300.8 K is 41.76 Ohm. The plot of the resistance versus 1000/T shows an activation energy of 0.267 eV as is indicated in figure 3.3. The

normalized, low-frequency noise spectral density plotted versus 1000/T in figure 3.4 on the other hand shows an activation energy of 0.336 eV. A combination of figure 3.3 and figure 3.4 is shown in figure 3.5. As we can clearly see from this figure, the values of the resistance show a smaller activation energy. The externally applied voltage during the noise measurement was about 0.12V which ensured that the device operated in the Ohmic regime. The voltage noise spectral density was measured between 100 and 1000 Hz.

Since the gold diffusion conditions for the devices discussed in Chapter II and this chapter were the same, but the thickness of the wafers and the length of the p^- region of the devices differed, we expect the gold concentration in M10B2-22 #1 to be larger than 2.51 x 10^{15} cm^{-3}. We have no reason, however, to believe that it is larger than 2.7 x 10^{15} cm^{-3}, since then the resistance versus 1000/T for this device is expected to have the same slope as in Chapter II, which is not in agreement with the data shown in figure 3.3. On the other hand if the concentration of gold is smaller than 2.7 x 10^{15} cm^{-3} and gold has only one donor level, then the resistance of the device is expected to decrease as temperature decreases due to an increase of the mobility. Again this is not what we measured. Therefore, we conclude that gold in silicon produces a second-donor level and that in our sample the condition $Na > Nau > 0.5\ Na$ is met.

Using the optimization procedures outlined in Chapter II and the semi-empirical mobility formula (2.19), we calculate the hole density P from the charge neutrality equation (3.6) and gold

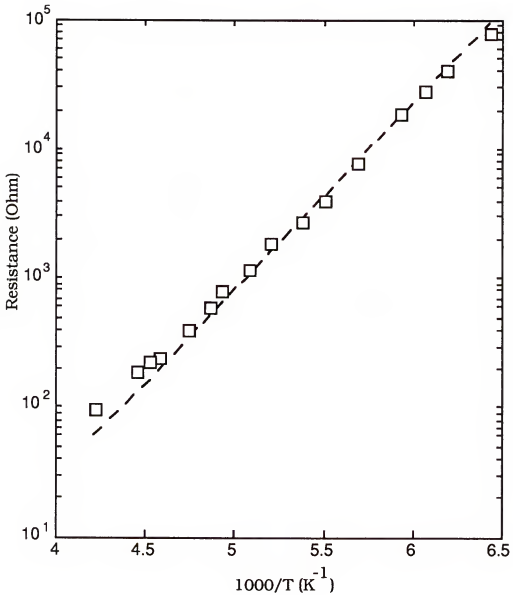

Figure 3.3. The resistance versus 1000/T of device M10b2-22 #1. The squares represent the experimental data. The dashed line shows the best fit to the data.

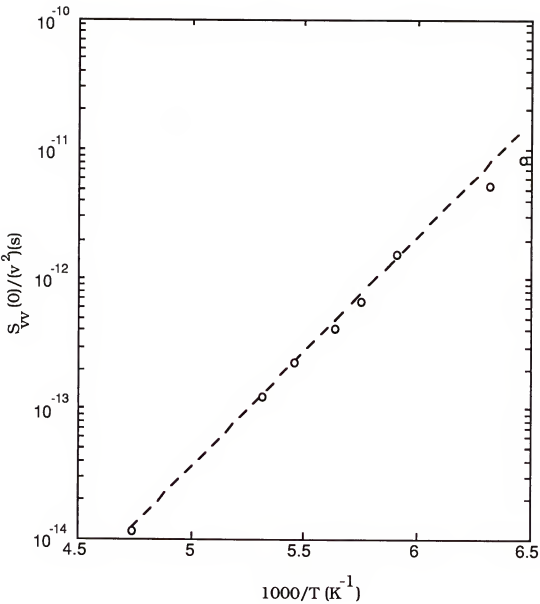

Figure 3.4. The relative, low-frequency G-R noise plateau values versus 1000/T. The circles represent the experimental data. The dashed line shows the best fit to the experimental data.

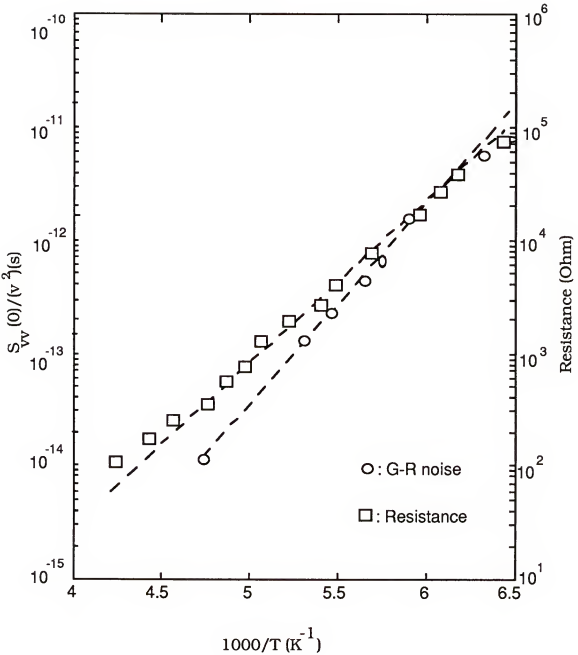

Figure 3.5. The relative, low-frequency G-R noise plateau values and the resistance versus 1000/T.

conservation equation (3.3) exactly, and fit the noise and the resistance data to eqs. (3.7) and (3.40), and extract the trap parameters listed in Table 3.2. The extracted hole capture cross section of $\sigma_{p1} = 6.5 \times 10^{-15}$ cm^2 is consistent with the hole capture cross section of the first-donor level published in the literature. The values of the other parameters listed in Table 3.2 justify the assumptions made in the previous section. The accuracy of the fitted results is limited by the mobility formula we used, the experimental accuracy and the fact that we assumed the activation energies of the gold donor and the hole capture cross section of the first donor to be temperature independent. The above data may therefore not represent the exact physical quantities. In fact, E_{1d} and E_{2d} may vary slightly with temperature because they contain a contribution from the entropy and because E_v varies slightly with temperature. These temperature-dependent factors have been accounted for in the degeneracy factors.

3.4. Summary

At low temperatures, when Na > Nau > 0.5Na, doubly ionized gold centers become electrically active and the Fermi energy level is located between E_{2d} and E_v. The average number of carriers in the valence band is then controlled by the second gold donor level. However, since the interaction between the mobile hole and the second-donor level is repulsive, the hole generation-recombination rates involving the second donor level will be smaller than the rates associated with the first gold donor level. The second-donor's contribution to the noise will therefore be small and the observed

TABLE 3.2. Trap parameter results obtained from extraction procedure.

Device parameters	Magnitude	Unit
σ_{p1}	6.5×10^{-15}	cm^2
Nau	2.58×10^{15}	cm^{-3}
g_{au1}	16	
g_{au2}	60.2	
$E_{1d} - E_v$	0.336	eV
$E_{1d} - E_v$	0.267	eV

generation-recombination noise will mainly come from the following processes: (a) hole emission, $Nau^+ \rightarrow Nau^o + e^+$ and (b) hole capture, $Nau^o + e^+ \rightarrow Nau^+$. This is why the resistance and noise data show different activation energies.

From the above discussion, it becomes clear that the activation energy of the resistance is associated with the second gold donor which lies 0.267 eV above the valence band edge, and that this level can be detected only within a certain window of doping densities, i.e., $Na > Nau > 0.5Na$.

3.5. Comparison of Experimental Results for the Single- and Double-Donor Model

In Chapter II and in sections of this chapter, we discussed trap parameter extraction using a single-donor and double-donor model. The facts are that the noise measured on devices (M102-22 #1) and (CM24B-82 #1) are produced by the same gold centers, and that the double donor model applies to both of the devices. Using the same optimization procedures as outlined in the previous chapter, the double donor model is fitted to the experimental data of Chapter II and this chapter, and the final results are shown in figure 3.6. The agreement is good in terms of the simplified models, except that the hole capture cross sections for the two devices are different: the hole capture cross-section $\sigma_{p1} = 6.5 \times 10^{-15}$ cm^2 for device (M102-22 #1) while the hole capture cross-section $\sigma_{p1} = 3.217 \times 10^{-15}$ cm^2 for device (CM24B-82 #1). Other parameters are listed in Table 3.2. The difference in the hole capture cross-sections may be caused by the fact that the device wafers are supplied by different manufacturers. Device

(CM24B-82 #1) uses a wafer supplied by Cincinetti while device (M102-22 #1) is made on a wafer supplied by Monsanto.

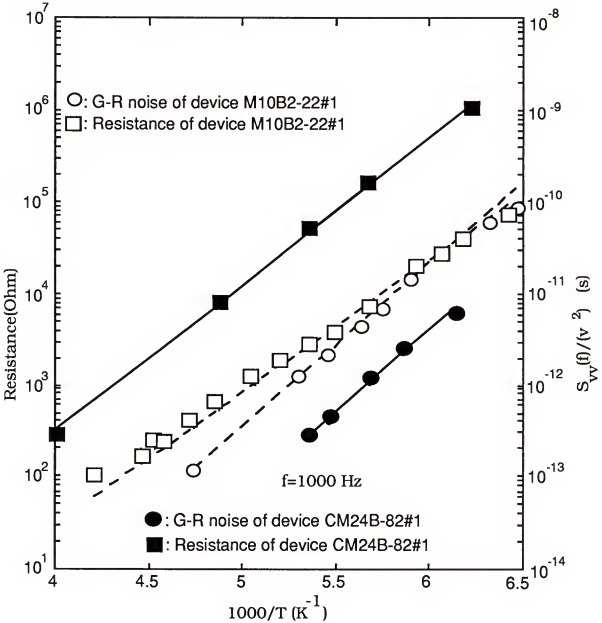

Figure 3.6. The normalized, low-frequency G-R noise plateau values and the resistance vs 1000/T.

CHAPTER IV
THE EFFECT OF FIELD-DEPENDENT EMISSION ON THE CURRENT-VOLTAGE CHARACTERISTICS OF A P^+-P^--P^+ Si:Au:B DEVICE

4.1. Introduction

Theoretical and experimental investigations of the current-voltage characteristics of high-low-high structures made of semi-insulating semiconductor devices with deep level doping have been carried out for decades. An excellent review of carrier injection in these materials is presented in the book by Lampert and Mark [28]. The current-voltage (I-V) behavior in high-resistivity materials can be described by (1) Ohm's law, (2) the trap free law, and (3) the trap-filled limited law [28]. The current in these devices is predominantly due to drift and might be affected by hot carrier phenomena. However, these laws are no longer sufficient to describe all aspects of the I-V characteristics in the domain where the capture and emission of carriers are field-dependent. Both superlinear and sublinear behavior can result from these competing mechanisms. Our experiments indicate that in the devices we investigated in Chapter II sublinear behavior prevails. We therefore develop in this chapter a model for sublinear I-V behavior and do not address superlinear aspects.

The occurrence of sublinear I-V behavior not associated with hot carrier mobility degradation has been reported by several researchers [29-32]. The possible mechanisms responsible for this phenomenon

are carrier exclusion [30,31] and field enhanced carrier capture into deep trap levels [32]. In steady state, the carrier concentration in a semi-insulating device is determined by the balance of emission and capture processes, in addition to junction effects. As a consequence, either a field-induced decrease in the emission coefficient, or a field-enhanced capture coefficient, or both can be reasons for observing sublinear I-V characteristics.

Most of the previous investigations on nonlinear I-V characteristics were based on I-V curves only. In Chapter II and III, we have used a combination of resistivity and noise data to explore the defect properties of gold in silicon, and we have shown that low-field device parameters can be extracted successfully by this method. In this chapter, we extend our noise measurement to a moderate high-field region to help unravel the generation-recombination effects on the I-V characteristics.

We measured the low temperature I-V characteristics of a p^+-p^--p^+ device made of Si:Au:B at various temperatures between 150 and 200K. The low-voltage region of the I-V characteristics shows Ohmic behavior, and is followed by a sublinear region at higher voltage. With the use of noise data, we found that the sublinear I-V behavior in our device is due to a significant decrease in the hole emission coefficient of gold donor centers with increasing bias.

In section 4.2, we describe the method we employed to interpret the I-V characteristics and noise spectra observed in our experiment. In section 4.3, the experimental details are presented and discussed.

4.2. Theory

In this section, we describe the theory used to interpret the sublinear I-V characteristics and the noise data. The device we investigated was a p^+-p^--p^+ silicon resistor, with boron dopants and a large gold concentration. We assume that the device is homogeneous and that the electric field is independent of position. In addition we assume that: (1) only the gold donors (0.336 eV above the valence band edge) interact with the valence band, (2) the electron density can be neglected, (3) the gold and boron densities are uniform, (4) the gold concentration Nau is larger than the boron concentration Na, (5) diffusion currents can be neglected.

The I-V characteristics are then given by eq. (3.7). The rate equation takes the form

$$\frac{dP}{dt} = e_p \, Nau^+ - c_p P \, (Nau - Nau^+), \tag{4.1}$$

where Nau^+ is the charged gold donor concentration, c_p is the hole capture coefficient, and e_p is the hole emission coefficient.

Next we expand the fluctuating parameters P and $N_{au}{}^+$ around their steady state values. Neglecting second and higher order terms we write

$$P = P_o + \Delta P$$

and

$$Nau^+ = Nauo^+ + \Delta Nau^+,$$

where the subscript o indicates steady state and ΔP and ΔNau^+ are the time-dependent fluctuations in P and Nau^+ respectively.

Substituting the above expressions in equation (4.1) we derive after separating d.c. and a.c. terms

$$e_p = c_p\ (Nau - Nauo^+)\left(\frac{P_o}{Nauo^+}\right), \tag{4.2}$$

$$\frac{d\Delta P}{dt} = -\ [e_p + c_p\ P_o + c_p\ (Nau - Nauo^+)]\Delta P. \tag{4.3}$$

In the derivation of equation (4.3) we used that $\Delta P \cong -\Delta Nau^+$, which can be justified by considering the condition for space charge neutrality, $P + Nau^+ = Na^-$, or in terms of density fluctuations $\Delta P + \Delta Nau^+ = \Delta Na^-$. Our low-frequency noise experiment does not probe the rapid fluctuations associated with the trapping and detrapping of holes in the shallow acceptor level, consequently we may assume $\Delta Na^- \cong 0$ or $\Delta P \cong -\Delta Nau^+$.

In our overcompensated p^+-p^--p^+ device, and at the temperatures selected for our experiments, 150< T < 250K, the equilibrium Fermi level lies below the deep gold donor level and far above the shallow acceptor level, resulting in equilibrium values for P between $10^9\ cm^{-3}$ and $10^{12}\ cm^{-3}$, specifically $P=2.2 \times 10^{11}\ cm^{-3}$ at T=200K. The equilibrium value of Nau^+ is of the order of the value of Na^- since the gold donor electrons will occupy the shallow acceptor sites. Due to the field dependence of e_p and c_p, P and Nau^+ will deviate from their equilibrium values when an electric field is applied. As we will demonstrate later, the changes in e_p and c_p in the field range we investigated are relatively minor so that P and Nau^+ do not change much from their equilibrium values. Consequently we may assume, using eq. (4.2) and the charge neutrality condition, that

$$[e_p + c_p\ P_o\ ] << [c_p\ (Nau - Nauo^+)], \tag{4.4a}$$

and

$$Nauo^+ \cong Nao^- \cong Na. \tag{4.4b}$$

These conditions simplify equation (4.3) to

$$\frac{d\Delta P}{dt} = - c_p \text{ (Nau- Na) } \Delta P = - \frac{\Delta P}{t_p}, \tag{4.5}$$

with

$$\frac{1}{t_p} = c_p \text{ (Nau - Na).} \tag{4.6}$$

The normalized, plateau value of the G-R noise has the form

$$\frac{S_{vv}(0)}{V^2} = \frac{4 \text{ Nauo}^+ e_p t_p^2}{L w d P_o^2}. \tag{4.7}$$

With the use of the previous assumptions and equations, eq. (4.7) can be written as

$$\frac{S_{vv}(0)}{V^2} = \frac{4}{L w d e_p \text{Nau}}. \tag{4.8}$$

If we now know the hole mobility as a function of electric field, then the hole concentration P can be calculated from eq. (3.7) and the hole emission coefficient from eq. (4.8). In addition the value of c_p can be derived from eq. (4.2).

The extraction of device parameters requires a model for the hole mobility since this quantity is not independently measured in our experiment. The experimental drift velocity versus electric field curve of lightly doped silicon for moderate electric field values can be found in the literature [33]. The measured field variation of velocity can be approximated with the following empirical expression proposed by Caughey and Thomas [34],

$$\upsilon = \upsilon_s \frac{\frac{E}{E_c}}{\left(1+\left(\frac{E}{E_c}\right)^{\beta}\right)^{1/\beta}}, \tag{4.9}$$

where υ_s is the saturation velocity, β is a fitting parameter, Ec is a critical field given by $Ec = \upsilon_s/\mu_o$, and μ_o is the low field carrier mobility.

Using $\upsilon_s=0.851x10^7$cm/s and $\mu_o=1280$ cm^2/(Vs) [35], we fitted eq. (4.9) to the experimental data [33], and obtained a best fit for β =1.252 at T=200.0K. The agreement between the experimental data and eq. (4.9) is shown in Fig. 4.1. The average error is 5%.

Equation (4.9) is strictly valid only for lightly doped silicon. In order to estimate the effect of ionized impurities on the hole mobility, we use the low-field, semi-empirical, mobility formula (2.19) to estimate the effects of a charged impurity concentration. We found from this equation that the effect of ionized impurity scattering is negligible for concentrations less than 3.0×10^{15} cm^{-3}. Since our devices have an ionized impurity concentration of the order of $2.0x10^{15}$ cm^{-3}, mobility degradation due to impurities can be neglected.

4.3. Experimental Details and Discussion

A p^+-p^--p^+ structure (CM24B-82 #2) made of Si:Au:B with a boron concentration of 1.0×10^{15} cm^{-3} is used in this work. The device details are described in Chapter II. From the experimental data, a gold concentration of 2.51×10^{15} cm^{-3} was extracted. The calculated length of the p^--device region is 18.1 um. The resistance of the device at T=298.9 K is 69.9 Ohm. The bias current I, supplied from a battery, is controlled by a variable series metal film resistor. The voltage noise spectral density was measured between 100 and 1000 Hz and was independent of frequency. The device was placed

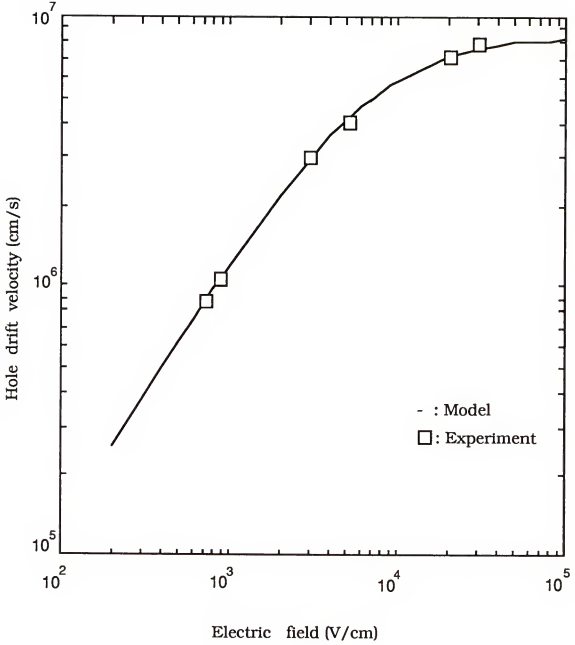

Figure 4.1. Hole drift velocity versus electric field at T=200.0K

inside a cryostat which allowed us to vary the device temperature between 77 and 300 K. Calculations show that the conditions for which the simple noise description given in section 4.2 are valid are met at temperatures between 150 and 250 K. We therefore concentrate on this temperature regime. The I-V characteristics at T=200.0 K measured as a function of bias polarity are shown in Fig. 4.2. Figure 4.3 shows the normalized plateau value of the G-R noise measured as a function of bias voltages at T=200.0 K. The measurements performed at other temperatures between 150 and 250 K show qualitatively similar behavior. We focus on the 200.0 K data however, since at this temperature accurate drift velocity data are available. In the moderate field regime of our investigations (E<1.5 kV/cm) the noise spectral density was independent of bias polarity.

As the voltage across the device increases, the electric field inside the device increases and the hole mobility will decrease at moderate to high electric field strength. However, the mobility reduction is very small in the field strength range of 0 to 1.5 kV/cm where the I-V characteristics deviate from ohmic behavior. Space charge injection is also negligible at these field strengths due to the large deep gold concentration. Hence, the sublinear I-V characteristics must be caused by other mechanisms among which are junction effects and generation-recombination processes.

In order to ensure that Joule heating was negligible and not responsible for the observed sublinearity in the I-V characteristics, we measured the noise data at T=192.5 K where the resistance of the device is significantly larger, and subsequently Joule heating is less

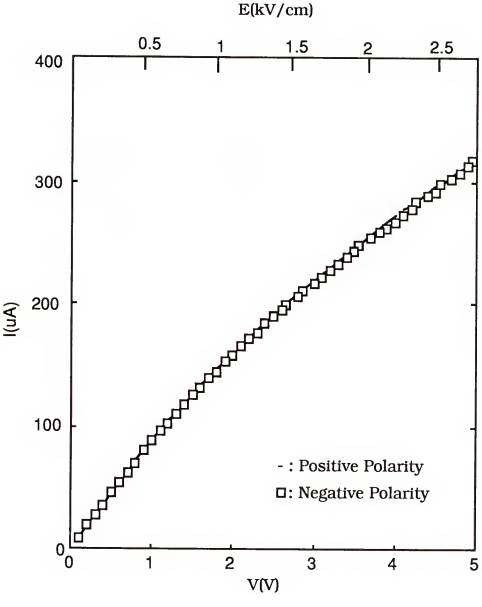

Figure 4.2. The current voltage characteristics at T=200.0K

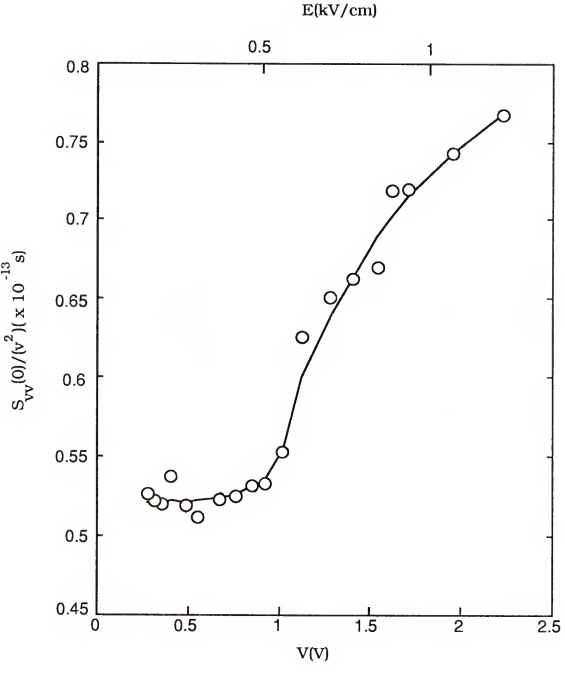

Figure 4.3. The normalized, low frequency G-R noise plateau versus voltage and electric field at T=200.0 K

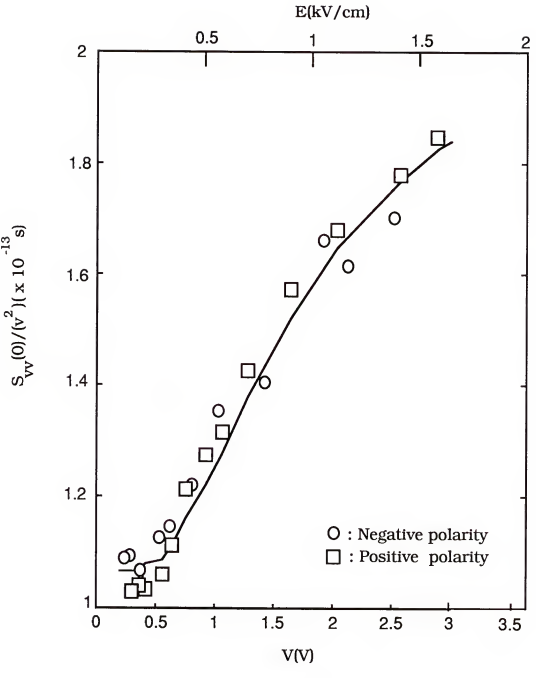

Figure 4.4. The normalized, low frequency G-R noise plateau versus voltage and electric field at T=192.5K

important. The noise data are shown in Fig. 4.4. The fact that the noise behavior observed at both temperatures is similar proves that our measurements were not affected by Joule heating.

Sublinear I-V characteristics observed in n^+ -n^- - n^+ structures made of Si:Au are attributed to carrier exclusion [30,31]. Carrier exclusion occurs at a reverse-biased high-low junction in a device and reduces the majority carrier density. A condition for exclusion to occur is a strong asymmetry of the electron and hole lifetimes. Exclusion effects can therefore not be used to account for the sublinear I-V characteristics of our device, since at low temperatures the lifetimes of the hole and electron carriers are of the same order, and the minority carrier density is negligible.

Hence, we opt for an interpretation of the sublinear I-V characteristics in terms of field-dependent generation-recombination processes. At low temperatures, the hole concentration is smaller than the gold concentration, and therefore a variation of the gold hole emission and capture coefficient with electric field will significantly affect the hole density in the device. Using the equations presented in the previous section, we extract from the experimental data the hole emission coefficient and the capture coefficient. The results are presented in Fig. 4.5 and show that the emission coefficient is independent of electric field in the low field region and then starts to decrease as the applied voltage approaches 1 V. In the same region, the I-V characteristics show sublinear behavior. Because the field-induced decrease in the hole emission coefficient is larger than the field-induced decrease in the hole capture coefficient, the net effect is that the hole carrier density in the valence band is reduced as the

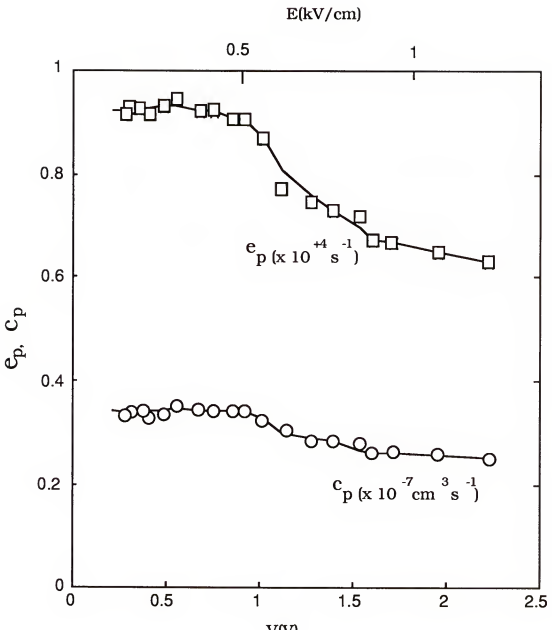

Figure 4.5. The hole emission and capture coefficients versus voltage at T=200K

electric field increases, resulting in the observed sublinear I-V characteristics.

4.4. High Field Effects

In the preceding sections, we have shown that the I-V characteristics are independent of device polarity at medium electric fields. At higher electric field strengths however, the device shows a bias polarity dependence. Figure 4.6 depicts the I-V characteristics of device (CM24B-82 #2). Positive polarity refers to a positive bias to the Ohmic contact at the diffusion region. Figures 4.7 and 4.8 represent the I-V characteristics of device (M102-22 #1). The asymmetry of the device geometry and the doping profiles, combined with the unknown field dependence of the defect parameters will affect the I-V characteristics in the high field regime and make it therefore difficult to analyze the measured polarity dependence of the I-V characteristics and the noise data and to extract trap parameters for this electric field regime.

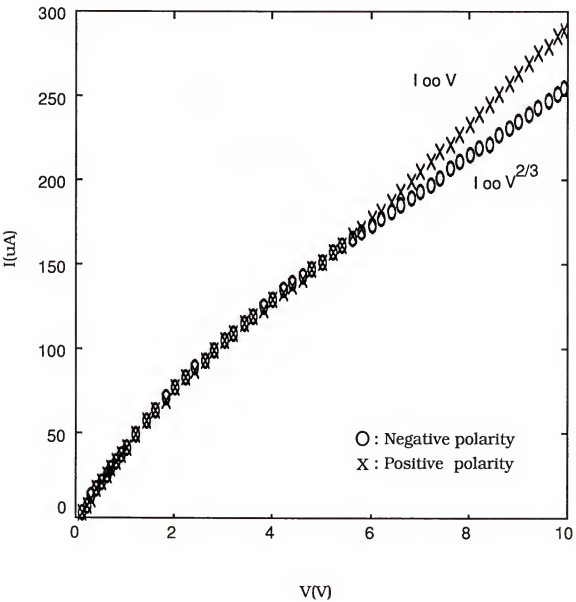

Figure 4.6. The I-V characteristics of device (CM24B-82#2) at T=192.5K.

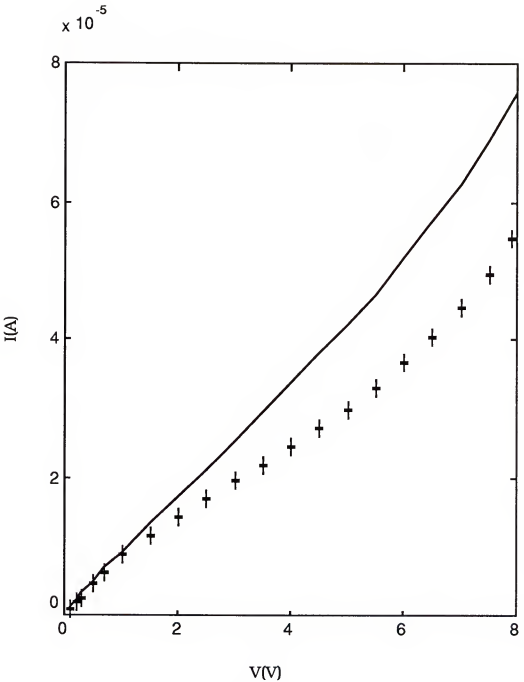

Figure 4.7. The I-V Characteristics of device (CM10B2-22#1) at T=156.0 K. The solid line represents the results of the measurements with negative polarity, the crosses refer to positive polarity results.

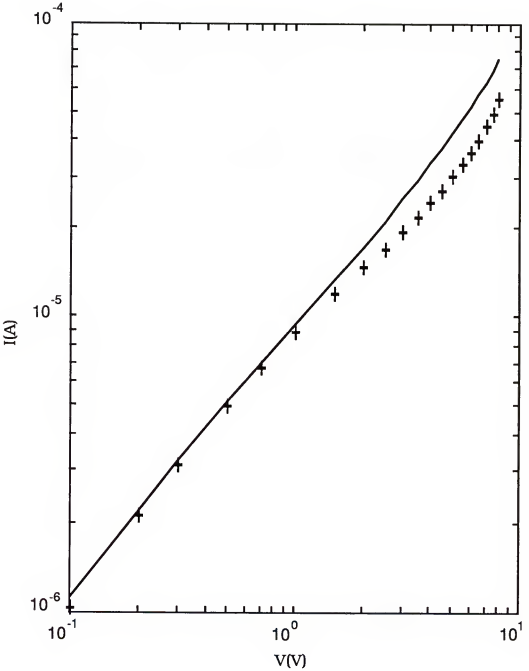

Figure 4.8. The I-V Characteristics of device (CM10B2-22#1) at T=156.0 K. The solid line represents the results of the measurements with negative polarity, the crosses refer to positive polarity results.

CHAPTER V
LOW-FREQUENCY GENERATION-RECOMBINATION NOISE AS A TOOL FOR INVESTIGATING DEEP DEFECTS, DEVICE DESIGN CONSIDERATIONS

5.1. Introduction

Electronic devices and systems exhibit random fluctuations in voltage (or current) at their terminals. These fluctuations are referred to as electronic noise. Since noise reflects the microscopic motion of carriers, it has been used as a tool for investigating the electrical characteristics of a device. Generation-recombination (G-R) noise is due to carrier transitions between traps and their associated conduction or valence band, and it can be used to investigate the properties of a defect in a semiconductor.

Up to now, most of the investigations of defects are done using transient capacitance methods [11]. These methods investigate transient capture and transient emission processes as two independent events. However, most problems of interest in device application are in steady-state or quasi-steady state situations in which generation and recombination processes occur simultaneously. Therefore the data from steady-state G-R noise measurements will provide without a doubt useful information concerning G-R mechanisms.

In the past, most G-R noise studies [4-6] have focused on traps producing a single energy level. Little work has been done on multi-

level G-R traps. Since defects can exist in several charge states in a device, other states may affect the measured data collected for a particular energy level. It is essential to understand the effects of other charge states on the observed energy level in order to obtain an accurate interpretation of measured data. To our knowledge, no work has been done on discrimination between donor and acceptor behavior of a defect energy level with G-R noise measurements. In Chapters II and III, we investigated G-R noise on samples with nearly- and over-compensated, deep impurity concentrations, and discovered a second-donor level of gold in silicon [Chapter III]. These investigations have motivated us to further explore this technique as a deep defect diagnostic tool.

Because device design is critical for the successful investigation of defects with G-R noise measurements, this chapter is written to provide information for designing a bulk semiconductor device for investigating the properties of defects. In the following section, we present several G-R noise models for defects with either one, or two energy levels in the lower half of the band gap of a p-type semiconductor, and study several special cases which make an analytical solution and an insightful device design scheme possible. These cases are: (a) the energy levels of a defect are separated by more than a few KT from each other and (b) the energy levels of a defect are within a few KT from each other. We layout the general theoretical background in section 5.2 and then explore various models. Finally, guidelines for proper device design are given.

5.2. Theory

In this chapter, we investigate the properties of defects with energy levels located in the lower half of the band gap of a p-type semiconductor. The resistance and voltage noise resulting from deep defects interacting with the valence band are calculated for the low field ohmic regime of device operation and are based on the following assumptions: (1) space charge neutrality and space uniformity prevail, (2) the electron density is neglected, (3) shallow impurities are fully ionized ($Na^- = Na$).

According to W. Shockley and J. T. Last [26], the ionized defect densities for a multi-level defect can be expressed as

$$Ni^- = g_{1a}\, Ni^o\, e^{\frac{E_f - E_{1a}}{KT}}, \tag{5.1.1}$$

$$Ni^+ = \frac{1}{g_{1d}} Ni^o\, e^{\frac{E_{1d} - E_f}{KT}}, \tag{5.1.2}$$

$$Ni^{++} = \frac{1}{g_{2d}} Ni^o\, e^{\frac{E_{1d} + E_{2d} - 2E_f}{KT}}, \tag{5.1.3}$$

where Ni, Ni^-, Ni^o, Ni^+, Ni^{++} are the total, singly negatively ionized, neutral, singly positively ionized, and doubly positively ionized defect concentration respectively. The symbols g_{1d}, g_{2d}, g_{1a} are the degeneracy factors for the first-donor, second-donor, and the acceptor level respectively. The energies E_{1a}, E_{1d}, E_{2d} are the defect acceptor, first-donor, second-donor energy level respectively, and E_f is the Fermi energy level. In this chapter, we restrict our discussion to a defect with energy levels satisfying $E_{1a} > E_{1d} > E_{2d}$, such as for example gold in silicon.

In order to calculate the noise spectral density, we express the carrier densities as sums of a steady-state term and a fluctuation term

$$Ni^{o} = Nio^{o} + \Delta Ni^{o}, \tag{5.1.4}$$

$$Ni^{+} = Nio^{+} + \Delta Ni^{+}, \tag{5.1.5}$$

$$Ni^{-} = Nio^{-} + \Delta Ni^{-}, \tag{5.1.5b}$$

$$Ni^{++} = Nio^{++} + \Delta Ni^{++}, \tag{5.1.6}$$

$$P = P_{o} + \Delta P, \tag{5.1.6b}$$

where N_{io}^{-}, N_{io}^{o}, N_{io}^{+}, N_{io}^{++} are the singly negatively charged, neutral, singly positively charged, and doubly positively charged defect densities in steady state respectively, and ΔN_{io}^{-}, ΔN_{io}^{o}, ΔN_{io}^{+}, ΔN_{io}^{++} are the corresponding fluctuations.

The carrier generation and recombination rates associated with a multi-level defect in a semiconductor are described in Table 5.1. The parameter P is the hole density, and N is the electron concentration. The symbol e^{+} denotes a mobile hole, and g_i and r_i, where i=1,2,3, are the hole generation and recombination rates respectively. The trap parameters e_{po}, c_{po}, e_{p1}, c_{p1}, and e_{p2}, c_{p2} are the emission and capture coefficients for holes in the acceptor, first-donor and second-donor level respectively.

In equilibrium, with the use of eqs. (5.1.1) through (5.1.3) and the principle of detailed balance, we get

$$e_{po} = c_{po}\, Nie^{-} \left(\frac{P_e}{Nie^{o}}\right) = c_{po}\, N_v\, g_{1a}\, e^{\frac{E_v - E_{1a}}{KT}}, \tag{5.1.7}$$

$$e_{p1} = c_{p1}\, Nie^{o} \left(\frac{P_e}{Nie^{+}}\right) = c_{p1}\, N_v\, g_{1d}\, e^{\frac{E_v - E_{1d}}{KT}}, \tag{5.1.8}$$

$$e_{p2} = c_{p2}\, Nie^{+} \left(\frac{P_e}{Nie^{++}}\right) = c_{p2}\, N_v \left(\frac{g_{2d}}{g_{1d}}\right) e^{\frac{E_v - E_{2d}}{KT}}, \tag{5.1.9}$$

where the subscript e denotes the equilibrium value.

TABLE 5.1. Generation and recombination rates in terms of ionized defect and mobile hole concentrations.

Rate	Hole Transitions involved	Description of the rates
g_o	$Ni^{o} \rightarrow Ni^{-} + e^{+}$	$e_{po}\ Ni^{o}$
r_o	$Ni^{-} + e^{+} \rightarrow Ni^{o}$	$c_{po}\ Ni^{-}\ P$
g_1	$Ni^{+} \rightarrow Ni^{o} + e^{+}$	$e_{p1}\ Ni^{+}$
r_1	$Ni^{o} + e^{+} \rightarrow Ni^{+}$	$c_{p1}\ Ni^{o}\ P$
g_2	$Ni^{++} \rightarrow Ni^{+} + e^{+}$	$e_{p2}\ Ni^{++}$
r_2	$Ni^{+} + e^{+} \rightarrow Ni^{++}$	$c_{p2}\ Ni^{+}\ P$

5.2.1. Single Level Noise Model

We first deal with the G-R noise model for a defect with a single donor level in a device with a shallow background doping. The following results have been derived in Chapter II. With the carrier densities given by eqs. (5.1.6b) and (5.1.5), the condition of charge neutrality gives the fluctuations in the carrier densities at low frequencies

$$\Delta P + \Delta Ni^{+}=0. \tag{5.2.1}$$

The rate equation takes the form

$$\frac{dP}{dt} = e_{p1}\, Ni^{+} - c_{p1}\, P\, (Ni - Ni^{+}). \tag{5.2.2}$$

Using eqs. (5.1.5), (5.1.6b) and (5.1.8), we get after linearization

$$\frac{d\Delta P}{dt} = - [e_{p1} + c_{p1}\, Po + c_{p1}\, (Ni\text{-}Nio^{+})]\Delta P. \tag{5.2.3}$$

This equation can be further simplified as we will show later.

5.2.1.1. Deep Defects in Overcompensated Devices

If the deep donor defect concentration is larger than the shallow impurity concentration, the Fermi level is located close to the defect donor energy level. At low temperatures, P is small, we may assume $P << (Ni - Nio^{+}), Nio^{+}, Ni$.

With the use of eq. (5.1.8), we can assume that

$$[e_{p1} + c_{p1}\, P_o] << [c_{p1}\, (Ni - Nio^{+})]. \tag{5.2.4}$$

Then eq. (5.2.3) simplifies to

$$\frac{d\Delta P}{dt} = - c_{p1}\, (Ni - Nio^{+})\, \Delta P = - \frac{\Delta P}{t_p}, \tag{5.2.5}$$

with

$$\frac{1}{t_p} = c_{p1}\, (Ni - Nio^{+}). \tag{5.2.6}$$

Assuming Na = Nio^+, eq. (5.2.6) becomes

$$\frac{1}{t_p} = c_{p1}\, Nio^o = c_{p1}\ (Ni - Na). \tag{5.2.7}$$

The temperature dependence of the capture coefficient can be derived from this equation. The normalized spectral density of G-R noise has the form [17]

$$\frac{S_{vv}(\omega)}{V_o^2} = \frac{S_{PP}(\omega)}{P_o^2} = \frac{4\ Nio^+\ e_{p1}\ t_p^2}{L\ w\ d\ P_o^2\ (1+\omega^2\ t_p^2)}\ . \tag{5.2.8}$$

where $Nio^+\ e_{p1}$ is the steady-state free carrier generation rate.

The normalized plateau value of the G-R noise is

$$\frac{S_{vv}(0)}{V^2} = \frac{4\ Nio^+\ e_{p1}\ t_p^2}{L\ w\ d\ P_o^2} = \frac{4}{L\ w\ d\ P_o\ c_{p1}\ Ni^o}\ . \tag{5.2.9}$$

At low temperatures P can be written as [Chapter II]

$$P = \frac{g_{1d}\ Na\ N_v\ e^{\frac{E_v - E_{1d}}{KT}}}{Ni - Na}, \tag{5.2.10}$$

with the aid of the charge neutrality equation

$$Na^- = P + Ni^+. \tag{5.2.11}$$

Using eqs. (5.1.8), (5.2.7), (5.2.9) and (5.2.10), and assuming the hole density is small, we get

$$\frac{S_{vv}(0)}{V^2} = \frac{4\ e^{\frac{E_{1d} - E_v}{KT}}}{L\ w\ d\ N_v\ c_{p1}\ N_a\ g_{1d}}\ . \tag{5.2.12}$$

Using eqs. (3.7) and (5.2.10), we get

$$R = \frac{L\ (N_i - N_a)\ e^{\frac{E_{1d} - E_v}{KT}}}{e\ w\ d\ \mu_p N_a\ N_v\ g_{1d}}\ . \tag{5.2.13}$$

Equations (5.2.12) and (5.2.13) show that the activation energies extracted from these equations should have the same value.

5.2.1.2. Deep Defects in Uncompensated Devices

If the deep impurity concentration is smaller than the shallow impurity concentration, we may assume from eq. (5.2.6) that

$$P >> Ni^{+}, Ni. \tag{5.2.14}$$

Equations (5.2.5) and (5.2.6) simplify to

$$\frac{d\Delta P}{dt} = - [e_{p\,1} + c_{p1} P_o] \Delta P = - \frac{\Delta P}{t_p}, \tag{5.2.15a}$$

with

$$\frac{1}{t_p} = [e_{p\,1} + c_{p1} P_o]. \tag{5.2.15b}$$

Combining eqs. (2.23), (5.1.8) and (5.2.15), we get

$$\frac{1}{t_p} = c_{p1} N_V \, e^{\frac{E_v - E_f}{KT}} [g_{1d} \, e^{\frac{E_f - E_{1d}}{KT}} + 1]. \tag{5.2.16a}$$

When the Fermi level is located above the trap level, the above equation becomes

$$\frac{1}{t_p} = c_{p1} N_V \, g_{1d} \, e^{\frac{E_v - E_{1d}}{KT}}. \tag{5.2.16b}$$

The trap energy can be extracted from this equation by plotting $Ln(t_p T^2)$ versus $1000/T$ where it is assumed that the temperature dependence of the hole capture cross section is weak.

From eq. (5.2.8), we get

$$\frac{S_{vv}(0)}{t_p V_o^2} = \frac{S_{PP}(0)}{t_p P_o^2} = \frac{4 \, Nio^{+} e_{p\,1} t_p}{L w d P_o^2}. \tag{5.2.17}$$

The trap energy, degeneracy factor, trap concentration can be extracted using the previous equations as discussed in section 2.2.2.

5.2.1.3. Device Design Consideration

The magnitude of G-R noise increases when the Fermi level approaches the trap energy level. This condition is critical for a device to be used for trap parameter extraction. For an overcompensated device, P is very small at low temperatures. Using eqs. (2.23) and (5.2.10), the Fermi level can be expressed as

$$E_f = E_{1d} - KT \log \left[\frac{g_{1d} N_a}{N_i - N_a} \right]. \qquad (5.2.18)$$

Once a device is overcompensated, the Fermi level will be close to the trap energy level. As the temperature is lowered, the Fermi level gets closer to the trap energy level, and the noise signal will therefore increase. The only design criterion to be considered is to have a device with suitable values of resistance for low-frequency noise measurements.

For a device that is lightly doped with deep defects, and in which the deep defect concentration is smaller than the shallow acceptor concentration, the Fermi level is controlled by the shallow impurity concentration and temperature. If the shallow dopants are almost fully ionized, then the hole density P can be written as

$$P = N_v e^{\frac{E_v - E_f}{KT}} = N_a. \qquad (5.2.19)$$

Thus the Fermi level becomes

$$E_f = E_v + KT \log \left[\frac{N_v}{N_a} \right]. \qquad (5.2.20)$$

From this equation, we find that the Fermi level can be moved across the lower half of energy band gap. This method is good for

investigating an unknown energy level. When Na << N_v is fulfilled, it can be used to investigate deep level defects.

5.2.1.4. Single-Acceptor Noise Model

When the device is lightly doped with deep single-acceptor defects, we obtain, following the same procedures as outlined in section 5.2.1.2,

$$\frac{S_{vv}(0)}{t_p V_o^2} = \frac{S_{PP}(0)}{t_p P_o^2} = \frac{4\ N_{io}^{\circ}\ e_{p\,o}\ t_p}{L\,w\,d\,P_o^2}, \tag{5.2.21}$$

with

$$\frac{1}{t_p} = [e_{p\,o} + c_{po}\,P_o]. \tag{5.2.22}$$

Equations (5.2.15) and (5.2.22) have the same form, and as a result we are unable to discriminate between acceptor-like and donor-like behavior of a defect by measuring G-R noise in a device with doping concentrations satisfying Ni<< Na. However, we can use the magnitude of the extracted capture coefficient to infer the donor or acceptor behavior of a defect energy level. At low temperatures, the coefficient c_{p2} (see Table 5.1) is associated with a repulsive capture process, and one may expect its value to be rather small [27], of the order of 10^{-11} to 10^{-14} cm^3/s; the coefficient c_{p1} is related to a neutral capture process, and will be therefore of the order of 10^{-8} cm^3/s; the coefficient c_{po} on the other hand is associated with an attractive capture process, and one may expect its value to be rather large, of the order of 10^{-5} to 10^{-8} cm^3/s.

Now, let's consider a device that is doped with a deep defect concentration larger than a large shallow dopant concentration. When the deep defect is acceptor-like, the Fermi level will behave, at lower

temperatures, according to eq. (5.2.20) provided that all shallow acceptors are ionized. With Na large, the temperature variation of Ef will be small making it difficult for Ef to reach values close to the deep acceptor level. As a consequence the hole transition rates between the deep acceptor level and the valence band will be small, providing negligible noise contributions to the overall noise spectrum. This makes it very difficult to detect deep acceptor-like traps in p-type material. However, when the deep defect is donor-like, the Fermi level is above the shallow acceptor level and close to the deep donor level (see eq. (5.2.18)), and a strong noise component results. Consequently, with the aid of a device with a deep defect concentration larger than the shallow dopant concentration, we are able to distinguish a donor from an acceptor by noise measurements.

5.2.2. Double-Donor Noise Model

In this section, we deal with a double-donor defect of which some aspects have been discussed in Chapter III. The total defect concentration is given by

$$Ni^{++} + Ni^{+} + Ni^{o} = Ni. \tag{5.3.1}$$

From eqs. (5.1.2), (5.1.3) and (5.3.1), the ionized defect concentrations can be written as

$$Ni^{+} = \frac{Ni}{1 + \frac{g_{1d}}{g_{2d}} e^{\frac{E_{2d} - E_f}{KT}} + g_{1d}\, e^{\frac{-(E_{1d} - E_f)}{KT}}}, \tag{5.3.2}$$

and

$$Ni^{++} = \frac{Ni}{1 + g_{2d}\, e^{\frac{-(E_{1d}+E_{2d}-2E_f)}{KT}} + \frac{g_{2d}}{g_{1d}}\, e^{\frac{-(E_{2d}-E_f)}{KT}}} . \qquad (5.3.3)$$

The value of P can be derived from eqs. (2.23) and (5.3.1) to (5.3.3) with the use of the charge neutrality equation

$$2Ni^{++} + Ni^{+} + P = Na. \qquad (5.3.4)$$

The rate equations for this system read:

$$\frac{dNi^{o}}{dt} = g_1 - r_1, \qquad (5.3.5a)$$

$$\frac{dNi^{+}}{dt} = - g_1 + r_1 + g_2 - r_2, \qquad (5.3.5)$$

$$\frac{dNi^{++}}{dt} = - g_2 + r_2, \qquad (5.3.6)$$

$$\frac{dP}{dt} = g_1 - r_1 + g_2 - r_2, \qquad (5.3.7)$$

where g_1, r_1, g_2, r_2 are described in Table 5.1.

From eqs. (5.3.1) and (5.3.4), we obtain

$$\Delta Ni^{++} + \Delta Ni^{+} + \Delta Ni^{o} = 0, \qquad (5.3.8)$$

$$2\Delta Ni^{++} + \Delta Ni^{+} + \Delta P = 0. \qquad (5.3.9)$$

Expanding the carrier densities around steady-state in first order, and using the Langevin approach, the rate equations including the noise can be written as

$$\frac{d\Delta P}{dt} = -M_{11}\,\Delta P - M_{12}\,\Delta Ni^{++} + F_1 + F_2, \qquad (5.3.10)$$

$$\frac{d\Delta Ni^{++}}{dt} = -M_{21}\,\Delta P - M_{22}\,\Delta Ni^{++} - F_2, \qquad (5.3.11)$$

with relaxation matrix elements

$$M_{11} = e_{p1} - c_{p2}\,P_o + c_{p1}\,Nio^{o} + c_{p2}\,Nio^{+} + c_{p1}\,P_o,$$

$$M_{22} = e_{p2} + 2c_{p2}\,P_o,$$

$$M_{12} = -e_{p2} + c_{p1} P_o + 2e_{p1} - 2c_{p2} P_o,$$

$$M_{21} = -c_{p2} Nio^{+} + c_{p2} P_o. \qquad (5.3.12)$$

The Langevin noise source terms F_1 and F_2 model the noise in the hole transition rates between the first-donor level, the second-donor level and the valence band respectively

Using the same procedures as outlined in Chapter III, and assuming that there is no correlation between the Langevin noise sources and that the transition rates show full shot noise, we obtain from eqs. (5.3.10) through (5.3.12)

$$S_{F1} = \frac{4r_1}{L\,w\,d}, \qquad S_{F2} = \frac{4r_2}{L\,w\,d}, \qquad (5.3.13)$$

$$S_{pp}(\omega) = \frac{G}{(\omega^2+\lambda_1^2)} + \frac{H}{(\omega^2+\lambda_2^2)}, \qquad (5.3.14)$$

$$G = 4\,\frac{\lambda_1^2(r_1+r_2) - M_{22}^2\,(r_1+r_2) - (M_{12}^2 + 2M_{12}M_{22})\,r_2}{L\,w\,d\,(\lambda_1^2-\lambda_2^2)}, \qquad (5.3.15a)$$

$$H = 4\,\frac{-\lambda_2^2(r_1+r_2) + M_{22}^2\,(r_1+r_2) + (M_{12}^2 + 2M_{12}M_{22})\,r_2}{L\,w\,d\,(\lambda_1^2-\lambda_2^2)}, \qquad (5.3.15b)$$

with

$$\lambda_1 = \frac{(M_{11}+M_{22}) + \sqrt{(M_{11}+M_{22})^2 - 4(M_{11}M_{22} - M_{12}M_{21})}}{2}, \qquad (5.3.16)$$

and

$$\lambda_2 = \frac{(M_{11}+M_{22}) - \sqrt{(M_{11}+M_{22})^2 - 4(M_{11}M_{22} - M_{12}M_{21})}}{2}. \qquad (5.3.17)$$

5.2.2.1. Deep Defects with Closely Spaced Energy Levels in Nearly-compensated Material

In this subsection, a device with a double-donor defect concentration satisfying $Na > Ni > 0.5Na$ is studied. At low temperatures we may assume $P << Ni^{+}, Ni^{++}, Ni^{o}$. This assumption is correct as long as the defect energy levels are closely spaced, i.e., not

more than a few KT apart. The relaxation matrix elements (5.3.12) become

$$M_{11}=c_{p1}\,Ni^{o}+c_{p2}\,Ni^{+}, \qquad M_{12}= -e_{p2}+c_{p1}P+2e_{p1}-2c_{p2}\,P_o,$$

$$M_{21}= -c_{p2}\,Ni^{+}, \qquad M_{22} =e_{p2}+2c_{p2}\,P_o. \tag{5.3.18}$$

Note that eq. (5.3.14) predicts two Lorentzian components in the overall noise spectrum. However, if λ_1 is too small, only $S_{PP}(\omega)$ for $\omega >> \lambda_2$ will be observed.

If $c_{p2} << c_{p1}$, we may assume

$$\frac{c_{p1}}{c_{p2}} >> \frac{Ni^{+}}{Ni^{o}} = \frac{1}{g_{1d}}\, e^{\frac{E_{1d}-E_f}{KT}} . \tag{5.3.19}$$

This assumption is valid if (E_{1d}-E_{2d}) is smaller than a few KT. Then E_f is close to E_{1d} and E_{2d}, and N_i^{+} and N_i^{o} are of the same order.

Using eqs. (5.1.8), (5.1.9), (5.3.16), (5.3.17) and (5.3.19), we obtain

$$M_{11} >> M_{21},\ M_{22},M_{12},$$

$$\lambda_1 >> \lambda_2 ,$$

$$\lambda_1 \cong M_{11} =c_{p1}\,Ni^{o} = \frac{1}{t_p} ,$$

$$\lambda_2 \cong \frac{(M_{11}M_{22}-M_{12}M_{21})}{(M_{11}+M_{22})} < M_{22} =e_{p2}+2c_{p2}\,P. \tag{5.3.20}$$

Using eqs. (5.1.8), (5.1.9), and (5.3.20), we get

$$S_{pp}(\omega)\cong \frac{4(r_1+r_2)}{L\,w\,d\,(\omega^2+\lambda_1^2)} ,$$

$$r_1+ r_2= (c_{p1}\,Nio^{o}+c_{p2}\,Nio^{+})P_o \cong M_{11}P_o,$$

$$\frac{S_{vv}(\omega)}{V_o^2} = \frac{S_{PP}(\omega)}{P_o^2} = \frac{4\,c_{p1}\,Nio^{o}\,P_o\,t_p^2}{L\,w\,d\,P_o^2\,(1+\omega^2\,t_p^2)} \quad \text{for } \lambda_2<< \omega. \tag{5.3.21}$$

Equation (5.3.21) can be approximated by

$$\frac{S_{vv}(\omega)}{V_o^2} = \frac{4}{L\,w\,d\,P_o\,c_{p1}\,Nio^{o}} \qquad \text{for } \lambda_2<< \omega << \lambda_1. \tag{5.3.22}$$

Equations (3.7), (5.3.1) to (5.3.4) and (5.3.22) can be used to extract trap parameters from the resistance data and noise data if we use the mobility formula (2.19).

The theoretical predictions for the noise and resistance can be further simplified by assuming (E_{1d} - E_f) > KT log(g_{1d}) which is certainly valid at low temperatures. Equation (5.3.3) can be approximated by

$$Ni^{++} \cong \frac{Ni}{1 + \frac{g_{2d}}{g_{1d}} e^{\frac{-(E_{2d} - E_f)}{KT}}} .$$

Using eqs. (5.3.1) and (5.3.4), neglecting P in eq. (5.3.4) and assuming Ni^{++}, $Ni^{+} > Ni^{o}$, the hole concentration at low temperatures is given by

$$P = \frac{\frac{g_{2d}}{g_{1d}} (Na - Ni)\, N_v\, e^{\frac{E_v - E_{2d}}{KT}}}{2\,Ni - Na} . \qquad (5.3.23)$$

Using the following approximations,

$$Ni^{++} \cong Na - Ni, \qquad (5.3.23a)$$

$$Ni^{+} \cong 2Ni - Na, \qquad (5.3.23b)$$

and substituting eqs. (5.1.2) and (5.3.23) into eq. (5.3.22), the expression for the normalized G-R noise becomes

$$\frac{S_{vv}(\omega)}{V^2} \cong \frac{4\, e^{\frac{E_{1d} - E_v}{KT}}}{L\, w\, d\, c_{p1}\, g_{1d} (2Ni - Na)\, N_v} \quad \text{for } \lambda_2 << \omega << \lambda_1. \qquad (5.3.24)$$

Equations (5.3.23) and (5.3.24) illustrate that the noise contains the activation energy of the first-donor level, whereas the carrier concentration or resistance shows the activation energy associated with the second-donor level.

Equation (5.3.22) is the same as eq. (5.2.9). This shows that when the doping concentrations satisfy Na<<Ni, and the hole density can be approximated by eq. (5.2.10), the double-donor model reduces to the single-donor model.

5.2.2.2. Deep Defects with Closely Spaced Energy Levels in Uncompensated Material

If the defect concentration is smaller than the boron concentration, we may assume that P = Na, P >> Ni, Ni^{o}, Ni^{+}, Ni^{++} hold. In the following, we limit our discussion to the conditions: $c_{p1} >> c_{p2}$ as assumed in section 5.2.2.1, and $e_{p1} >> e_{p2}$, from which we derive, with the use of eqs. (5.1.8) and (5.1.9),

$$\frac{c_{p1}}{c_{p2}} >> \frac{g_{2d}}{g_{1d}^{2}} e^{\frac{E_{1d} - E_{2d}}{KT}} .$$

The relaxation matrix elements (5.3.12) become

$$M_{11} = e_{p1} + c_{p1} P_o, \qquad M_{21} = e_{p2} + 2c_{p2} P_o,$$

$$M_{12} = c_{p1}P_o + 2e_{p1}, \qquad M_{22} = c_{p2} P_o. \qquad (5.3.25)$$

In this section, we discuss the situation where the defect energy levels are close to each other. With the use of eqs. (5.1.2), and (5.1.3), we obtain that Ni^{o}, Ni^{+}, Ni^{++} are almost of the same order. With the use of eqs. (5.1.8), and (5.1.9), we infer that e_{p1}, $c_{p1} P_o$, and e_{p2}, $c_{p2} P_o$ are almost of the same order, respectively. Using these results and eqs. (5.3.16), (5.3.17) and (5.3.25), we obtain

$$M_{11}, M_{12} >> M_{22}, M_{21},$$

$$\lambda_1 \cong M_{11} = e_{p1} + c_{p1} P_o = \frac{1}{t_p},$$

$$\lambda_2 \cong \frac{(M_{11}M_{22} - M_{12}M_{21})}{(M_{11} + M_{22})}$$

$$= \frac{e_{p2}\, c_{p1}\, P_o + 2\, e_{p1}\, e_{p2} + c_{p1}\, c_{p2}\, P_o^2 + 3 e_{p1}\, c_{p2}\, P_o}{e_{p1} + c_{p1}\, P_o + c_{p2}\, P_o} .$$

Since M_{11} is of the same order as e_{p1}, λ_2 is of the same order of $-e_{p2}$, the observed noise spectra will have only one Lorentzian component in a certain frequency window because $-\lambda_2$ is smaller than λ_1 and the same reason used in section 5.2.2.1 applies to this case. The roll-off time constant is the same as given by eq. (5.2.15) of the single-donor model.

From eq. (5.3.19) and Table 5.1 we get $r_1 >> r_2$. Equation (5.3.14) can be approximated by

$$S_{pp}(\omega) \cong \frac{4 r_1}{L\, w\, d\, (\omega^2 + \lambda_1^2)} \qquad \text{for } -\lambda_2 << \omega, \tag{5.3.26}$$

$$r_1 = c_{p1}\ Nio^o\ P_o,$$

$$\frac{S_{vv}(\omega)}{V_o^2} = \frac{S_{PP}(\omega)}{P_o^2} = \frac{4\, c_{p1}\, Nio^o\, P_o\, t_p^2}{L\, w\, d\, P_o^2\, (1+\omega^2 t_p^2)} \qquad \text{for } -\lambda_2 << \omega. \tag{5.3.26a}$$

Using $r_1 \cong g_1$, eq. (5.3.26a) transforms to

$$\frac{S_{vv}(0)}{t_p V_o^2} = \frac{S_{pp}(0)}{t_p P_o^2} = \frac{4\ Nio^+\ e_{p1}\ t_p}{L\, w\, d\, P_o^2} \qquad \text{for } -\lambda_2 << \omega << \lambda_1. \tag{5.3.27}$$

Note that eqs. (5.2.17) and (5.3.27) are of the same form with the same lifetime constant. In this case, we are unable to measure the second-donor level of defects.

5.2.2.3. Deep Defects with Energy Levels Far Apart from Each Other in Overcompensated Material

For an overcompensated device, with Ni >Na, but of the same order, and with the energy levels spaced by more than a few KT, we may assume at low temperatures that $Na \cong Ni^+$, and $Ni - Na \cong Ni^o$ using the same reasoning as described in 5.2.1.1. The Fermi level is

close to the first-donor level and Nio^{++}, $P_o << Nio^+$, Na holds. Using $c_{p1} >> c_{p2}$ as assumed in section 5.2.2.1, and assuming that $e_{p1} << e_{p2}$, which is possible because the conditions $E_{1d}-E_{2d}$ > a few KT and $c_{p1} >> c_{p2}$ hold, eq. (5.3.12) becomes

$$M_{11} = c_{p1}\, Nio^o, \qquad M_{22} = e_{p2},$$

$$M_{12} = -e_{p2}, \qquad M_{21} = -c_{p2}\, Nio^+. \tag{5.3.29}$$

If $c_{p1}\, Nio^o >> e_{p2}$ holds, i.e.,

$$(Ni - Na) >> \left(\frac{c_{p2}}{c_{p1}}\right) N_v \left(\frac{g_{2d}}{g_{1d}}\right) e^{\frac{E_v - E_{2d}}{KT}},$$

we obtain with the use of eqs. (5.3.14) through (5.3.17) and (5.3.29)

$$M_{11} >> M_{21},$$

$$M_{11} >> -M_{12} = M_{22},$$

$$\lambda_1 \cong M_{11} = c_{p1}\, Nio^o = \frac{1}{t_p} >> \lambda_2,$$

$$\frac{S_{vv}(\omega)}{V_o^2} = \frac{S_{PP}(\omega)}{P_o^2} = \frac{4\, c_{p1}\, Nio^o\, P_o\, t_p^2}{L\, w\, d\, P_o^2\, (1+\omega^2 t_p^2)} \quad \text{for } \lambda_2 << \omega. \tag{5.3.30}$$

Equation (5.3.30) can be approximated by

$$\frac{S_{vv}(\omega)}{V_o^2} = \frac{4}{L\, w\, d\, P_o\, c_{p1}\, Nio^o} \qquad \text{for } \lambda_2 << \omega << \lambda_1, \tag{5.3.31}$$

which is the same as given by eq. (5.2.9) of the single-donor model.

If the hole concentration P is approximated by eq. (5.2.10), the double-donor reduces to the single-donor model discussed in 5.2.1.1.

For a device with a defect concentration satisfying $Na > Ni > 0.5Na$, we may assume $c_{p1}/c_{p2} << Ni^+/Ni^o$ because the Fermi level is close to the second-donor level and far away from the first-donor level.

We start with the rate equations including the noise

$$\frac{d\Delta P}{dt} = -M_{11}\,\Delta P - M_{12}\,\Delta Ni^{o} + F_1 + F_2, \qquad (5.3.32)$$

$$\frac{d\Delta Ni^{o}}{dt} = -M_{21}\,\Delta P - M_{22}\,\Delta Ni^{o} + F_1, \qquad (5.3.33)$$

with relaxation matrix elements

$$M_{11} = -e_{p1}+c_{p2}\,P_o + c_{p2}\,Nio^{+} + c_{p1}\,Nio^{o} + e_{p2},$$

$$M_{12} = 2e_{p1} - 2c_{p2}\,P_o + c_{p1}\,P_o - e_{p2},$$

$$M_{21} = c_{p1}\,Nio^{o} - e_{p1},$$

$$M_{22} = 2e_{p1} + c_{p1}\,P_o. \qquad (5.3.34)$$

Using the condition $P_o << N_{io}^{+}$, eq. (5.1.8) and similar approximation procedures as outlined in section 5.2.2.1, we get

$$\frac{S_{vv}(\omega)}{V_o^{2}} = \frac{4}{L\,w\,d\,P_o\,c_{p2}\,Nio^{+}} \quad \text{for} \quad \lambda_2 << \omega << \lambda_1, \qquad (5.3.35)$$

which is in the same form as given by eq. (5.2.9) of the single-donor model.

Using eq. (5.3.23b), eq. (5.3.35) becomes

$$\frac{S_{vv}(\omega)}{V_o^{2}} = \frac{4}{L\,w\,d\,P_o\,c_{p2}\,[2Ni-Na]} \quad \text{for} \quad \lambda_2 << \omega << \lambda_1. \qquad (5.3.36)$$

Under the conditions studied here, the normalized G-R noise is inversely proportional to the hole concentration P, indicating the noise and resistance show the same donor activation energy.

5.2.2.4. Deep Defects with Energy Levels Far Apart from Each Other in Uncompensated Material

When the Fermi level is close to the second-donor level and far away from the first-donor level in a situation where the levels are spaced by more than a few KT, we can assume $S_{F2} >> S_{F1}$ which can be transformed to $e_{p2}\,N_i^{++} >> e_{p1}\,N_i^{+}$ with the use of eq. (5.3.13) and

Table 5.1. From eqs. (5.1.2), (5.1.3), (5.1.8), (5.1.9) and (5.3.13), this condition translates into

$$\frac{c_{p1}}{c_{p2}} << \frac{1}{g_{1d}} e^{\frac{E_{1d}-E_f}{KT}} . \qquad (5.3.37)$$

The condition $S_{F2} >> S_{F1}$ implies $F_2 >> F_1$. The carrier fluctuations will then mainly come from the fluctuations in the emission and capture rates associated with the second-donor level, and therefore eq. (5.3.9) becomes

$$-\Delta Ni^{+} \cong - \Delta P = \Delta Ni^{++}. \qquad (5.3.38)$$

The rate equations including the noise can then be written as

$$\frac{d\,\Delta P}{dt} = -M_{11}\Delta P - M_{12}\,\Delta Ni^{++} + F_2, \qquad (5.3.39)$$

$$\frac{d\,\Delta Ni^{++}}{dt} = -M_{21}\Delta P - M_{22}\,\Delta Ni^{++} - F_2, \qquad (5.3.40)$$

with relaxation matrix elements

$$M_{11} = e_{p1}-c_{p2}\,P_o+c_{p1}\,Nio^{o}+c_{p2}\,Nio^{+}+c_{p1}\,P_o,$$

$$M_{21} = e_{p2} + 2c_{p2}\,P_o,$$

$$M_{12} = -e_{p2}+c_{p1}P_o+2e_{p1}-2c_{p2}P_o,$$

$$M_{22} = - c_{p2}\,Nio^{+} + c_{p2}\,P_o. \qquad (5.3.41)$$

With additional conditions $e_{p1}/e_{p2} << 1$, and $P >> Ni, Ni^{o}, Ni^{+}, Ni^{++}$, and with the aid of eq. (5.1.9), one can show that eqs. (5.3.39) and (5.3.40) have the same time constant defined by

$$\frac{1}{t_p} \cong e_{p2} + c_{p2}\,P_o. \qquad (5.3.42)$$

Under the above stated conditions, the double-donor model reduces to the single-donor model discussed earlier. However, this time we can only measure the activation energy of the second-donor level.

When the Fermi level is close to the first-donor level and far away from the second-donor level, we can assume $S_{F2} << S_{F1}$, which becomes, with the use of eqs. (5.1.2), (5.1.3), (5.1.8), (5.1.9), (5.3.13) and Table 5.1,

$$\frac{c_{p1}}{c_{p2}} >> \frac{1}{g_{1d}} e^{\frac{E_{1d}-E_f}{KT}} . \qquad (5.3.43)$$

The condition $S_{F2} << S_{F1}$ implies $F_2 << F_1$. The carrier fluctuations will come mainly from first-donor level transitions, and therefore eq. (5.3.9) becomes

$$\Delta Ni^+ \cong - \Delta P \cong -\Delta Ni^o.$$

The rate equations including the noise can then be written as

$$\frac{d\,\Delta P}{dt} = -M_{11}\,\Delta P - M_{12}\,\Delta Ni^o + F_1, \qquad (5.3.44)$$

$$\frac{d\,\Delta Ni^o}{dt} = -M_{21}\,\Delta P - M_{22}\,\Delta Ni^o + F_1, \qquad (5.3.45)$$

with relaxation matrix elements given by (5.3.34).

With additional conditions $c_{p2}/c_{p1} << 1$ and $P >> Ni, Ni^o, Ni^+, Ni^{++}$, eqs. (5.3.44) and (5.3.45) have the same time constant defined by

$$\frac{1}{t_p} \cong e_{p1} + c_{p1}\,P_o. \qquad (5.3.46)$$

Again, the double-donor model reduces to the single-donor model discussed earlier. In this case however we can only measure the G-R noise caused by the first-donor level.

5.2.3. Acceptor-Donor Noise Model

In this section, we calculate the resistance and the voltage noise resulting from deep defects with an acceptor and a donor level that

interacts with the valence band. The total deep defect concentration is given by

$$Ni^- + Ni^+ + Ni^o = Ni. \tag{5.4.1}$$

From eqs. (5.1.1), (5.1.2) and (5.4.1), the ionized deep defect concentrations are rewritten as

$$Ni^+ = \frac{Ni}{1 + g_{1d}\, g_{1a}\, e^{\frac{2E_f - E_{1a} - E_{1d}}{KT}} + g_{1d}\, e^{\frac{(E_f - E_{1d})}{KT}}}, \tag{5.4.2}$$

and

$$Ni^- = \frac{Ni}{1 + \frac{1}{g_{1a}}\, e^{\frac{(E_{1a} - E_f)}{KT}} + \frac{1}{g_{1a}\, g_{1d}}\, e^{\frac{(E_{1d} + E_{1a} - 2E_f)}{KT}}}. \tag{5.4.3}$$

The value of P can be derived from eqs. (5.4.1) to (5.4.3) and eq. (2.23) with the use of the charge neutrality equation

$$Ni^+ + P = Na^- + Ni^-. \tag{5.4.4}$$

The rate equations for the carrier densities read:

$$\frac{dNi^+}{dt} = -g_1 + r_1, \tag{5.4.5}$$

$$\frac{dNi^-}{dt} = g_o - r_o, \tag{5.4.5a}$$

$$\frac{dNi^o}{dt} = -g_o + r_o + g_1 - r_1, \tag{5.4.6}$$

$$\frac{dP}{dt} = g_1 - r_1 + g_o - r_o, \tag{5.4.7}$$

where g_1, r_1, g_o, r_o are described in Table 5.1.

From eqs. (5.4.1) and (5.4.4), we obtain

$$\Delta Ni^- + \Delta Ni^+ + \Delta Ni^o = 0, \tag{5.4.8}$$

and

$$-\Delta Ni^- + \Delta Ni^+ + \Delta P = 0. \tag{5.4.9}$$

Expanding the densities around steady-state and using the Langevin approach, the rate equations including the noise can be written as

$$\frac{d\Delta P}{dt} = -M_{11}\Delta P - M_{12}\,\Delta Ni^{+} + F_o + F_1, \tag{5.4.10}$$

$$\frac{d\Delta Ni^{+}}{dt} = -M_{21}\Delta P - M_{22}\,\Delta Ni^{+} - F_1, \tag{5.4.11}$$

with relaxation matrix elements

$$\begin{aligned} M_{11} &= e_{po}-c_{p1}\,P_o+c_{po}\,Nio^{-}+c_{p1}\,Nio^{o}+c_{po}\,P_o,\\ M_{21} &= e_{p1}+2c_{p1}\,P_o,\\ M_{12} &= -e_{p1}+c_{po}\,P_o+2e_{po}-2c_{p1}\,P_o,\\ M_{22} &= -c_{p1}\,Nio^{o}+c_{p1}\,P_o, \end{aligned} \tag{5.4.12}$$

where F_o, F_1 are Langevin noise source terms modeling the noise in the hole transition rates between the acceptor level, the first-donor level, and the valence band respectively.

Assuming that there is no correlation between the Langevin noise sources and that the transition rates show full shot noise, we obtain

$$S_{Fo}=\frac{4r_o}{L\,w\,d}, \qquad S_{F1}=\frac{4r_1}{L\,w\,d}, \tag{5.4.13}$$

$$S_{pp}(\omega)=\frac{G}{(\omega^2+\lambda_1^2)}+\frac{H}{(\omega^2+\lambda_2^2)}, \tag{5.4.14}$$

$$G = 4\,\frac{\lambda_1^2(r_1+r_o)-M_{22}^2\,(r_1+r_o)-(M_{12}^2+2M_{12}M_{22})\,r_o}{L\,w\,d\,(\lambda_1^2-\lambda_2^2)}, \tag{5.4.15}$$

$$H = 4\,\frac{-\lambda_2^2(r_1+r_o)+M_{22}^2\,(r_1+r_o)+(M_{12}^2+2M_{12}M_{22})\,r_o}{L\,w\,d\,(\lambda_1^2-\lambda_2^2)}, \tag{5.4.16}$$

with

$$\lambda_1 = \frac{(M_{11}+M_{22})+\sqrt{(M_{11}+M_{22})^2-4(M_{11}M_{22}-M_{12}M_{21})}}{2}, \tag{5.4.17}$$

and

$$\lambda_2 = \frac{(M_{11}+M_{22})-\sqrt{(M_{11}+M_{22})^2-4(M_{11}M_{22}-M_{12}M_{21})}}{2} \quad . \qquad (5.4.18)$$

5.2.3.1. Deep Defects with Energy Levels Close to Each Other in Overcompensated Devices

At low temperatures we may assume $P << Ni^+, Ni^-, Ni^o$ in an overcompensated device with Ni > Na. The assumption is valid as long as the energy levels of the deep defects are within a few KT of each other. With the aid of eq. (5.1.7), the relaxation matrix elements (5.4.12) become

$$M_{11}=c_{po}N_i^- + c_{p1}\,Ni^o, \qquad M_{12} = -e_{p1}+c_{po}P_o+2e_{po}-2c_{p1}P_o,$$

$$M_{21} = e_{p1} + 2c_{p1}P_o, \qquad M_{22} = -c_{p1}\,Ni^o. \qquad (5.4.19)$$

In the following, we limit our discussion to the situation where $c_{po} >> c_{p1}$ and

$$\frac{c_{po}}{c_{p1}} >> \frac{Ni^o}{Ni^-} = \frac{1}{g_{1a}}\, e^{\frac{E_{1a}-E_f}{KT}} \quad . \qquad (5.4.20)$$

The condition $c_{po}/c_{p1} >> N_i^o/N_i^-$ is obtained when the acceptor and donor levels are very close to each other and the Fermi level is close to both E_{1d} and E_{1a}.

Using eqs. (5.1.7), (5.1.8), (5.4.17), (5.4.18) and (5.4.20), we obtain

$$M_{11} >> M_{21}, M_{22}, M_{12}, \qquad (5.4.21)$$

$$\lambda_1 >> \lambda_2, \qquad (5.4.22)$$

$$\lambda_1 \cong M_{11} = c_{po}\,Nio^- = \frac{1}{t_p}, \qquad (5.4.23)$$

$$\lambda_2 \cong \frac{(M_{11}M_{22}-M_{12}M_{21})}{(M_{11}+M_{22})} < M_{22}. \qquad (5.4.24)$$

Using eqs. (5.4.14) through (5.4.16) and (5.4.23), we get

$$S_{pp}(\omega) \cong \frac{4(r_1+r_o)}{L\,w\,d\,(\omega^2+\lambda_1^2)} \qquad \text{for } \lambda_2 << \omega, \qquad (5.4.25)$$

$$r_1 + r_2 = (c_{p1}\ Nio^{o} + c_{po}\ Nio^{-})P_o \cong M_{11}P_o, \tag{5.4.26}$$

$$\frac{S_{vv}(\omega)}{V_o^{\,2}} = \frac{S_{PP}(\omega)}{P_o^{\,2}} = \frac{4\ c_{po}\ Nio^{-}\ P_o\ t_p^{\,2}}{L\ w\ d\ P_o^{\,2}\ (1+\omega^2\ t_p^{\,2})} \quad \text{for } \lambda_2 << \omega. \tag{5.4.27}$$

Equation (5.4.27) can be approximated by

$$\frac{S_{vv}(\omega)}{V_o^{\,2}} = \frac{4}{L\ w\ d\ P_o\ c_{po}\ Nio^{-}} \quad \text{for } \lambda_2 << \omega << \lambda_1. \tag{5.4.28}$$

Equations (3.7), (5.4.1) to (5.4.4) and (5.4.28) can be used to extract trap parameters from the resistance data and noise data if we use the semi-empirical mobility formula (2.19).

The theoretical predictions for the noise and resistance can be further simplified if $KT \log(g_{1a}\ c_{po}/c_{p1}) > (E_{1a} - E_f) > KT \log(g_{1a})$ and $(E_{1d}-E_f) > KT \log(g_{1d})$. Then eq. (5.4.2) can be approximated by

$$Ni^{+} \cong \frac{Ni}{1 + g_{1d}\ e^{\frac{-(E_{1d}-E_f)}{KT}}}. \tag{5.4.29}$$

Using the following approximations,

$$Ni^{-} < Ni,\ Ni^{+},\ Ni^{o},$$

$$Ni^{+} \cong Na,$$

$$Ni^{o} \cong Ni - Na, \tag{5.4.30}$$

and eqs. (2.23), (5.4.29) and (5.4.30), the hole concentration at low temperatures is given by

$$P = \frac{g_{1d}\ Na\ N_v\ e^{\frac{E_v - E_{1d}}{KT}}}{Ni\text{-}Na}. \tag{5.4.31}$$

Using eqs. (5.1.1) and (5.4.31) into eq. (5.4.28), the expression for the normalized G-R noise becomes

$$\frac{S_{vv}(\omega)}{V_o^2} \cong \frac{4\, e^{\frac{E_{1a}-E_v}{KT}}}{L\, w\, d\, c_{po}\, g_{1a}(Ni-Na)\, N_v} \quad \text{for} \quad \lambda_2 << \omega << \lambda_1. \quad (5.4.32)$$

Equations (5.4.31) and (5.4.32) illustrate that the noise contains the activation energy of the acceptor level, whereas the carrier concentration or resistance shows the activation energy associated with the the donor level.

5.2.3.2. Deep Defects with Energy Levels Far Away from Each Other in Overcompensated Material

Instead of eq. (5.4.20) we limit our discussion in this section to the condition $c_{po}/c_{p1} << Ni^o/Ni^-$, which prevails when the acceptor and donor levels are separated by more than a few KT, such that the Fermi level is close to E_{1d} and far away from E_{1a}. We find, with the use of eqs. (5.1.1) and (5.1.2), that $Ni^o >> Ni^-$.

We start with the rate equations including the noise

$$\frac{d\Delta P}{dt} = -M_{11}\,\Delta P - M_{12}\,\Delta Ni^- + F_o + F_1, \quad (5.4.33)$$

$$\frac{d\Delta Ni^-}{dt} = -M_{21}\,\Delta P - M_{22}\,\Delta Ni^- + F_o, \quad (5.4.34)$$

where

$$M_{11} = c_{p1}\, Nio^o + c_{po}\, N_{io}^- + e_{p1} + c_{p1}\, P_o - e_{po}, \quad M_{21} = -e_{po} + c_{po}\, Nio^-,$$

$$M_{12} = -e_{p1} + c_{po}\, P_o + 2e_{po} - 2c_{p1}P_o, \quad M_{22} = c_{po}\, P + 2e_{po}. \quad (5.4.35)$$

At low temperatures P_o is small in overcompensated devices, and if Nio^o is large, we may assume $P_o << Nio^o$. Using eqs. (5.1.8), (5.1.7) and similar approximation procedures as outlined in section 5.2.3.1, we get

$$\frac{S_{vv}(\omega)}{V_o^2} = \frac{4}{L\, w\, d\, P_o\, c_{p1}\, Ni^o} \quad \text{for} \quad \lambda_2 << \omega << \lambda_1. \quad (5.4.36)$$

This is of the same form as eq. (5.2.9). Using eq. (5.4.30), eq. (5.4.36) becomes

$$\frac{S_{vv}(\omega)}{V_o^2} = \frac{4}{L\, w\, d\, P_o\, c_{p1}\, [Ni\text{-}Na]} \qquad \text{for} \quad \lambda_2 << \omega << \lambda_1. \qquad (5.4.37)$$

The hole density P can be approximated by eq. (5.2.10). The acceptor-donor model reduces to the single-donor model discussed in 1.A. The results are straightforward, because when the Fermi level is close to the donor level, the negatively charged defect concentration is negligible, and the contribution of acceptor levels to the G-R noise can be neglected. In this case, we are unable to measure the properties of the acceptor level using G-R noise measurements.

5.2.3.3. Deep Defects with Energy Levels Closely Spaced to Each Other in Uncompensated Material

If the defect concentration is smaller than the shallow impurity concentration and the energy levels of a defect are very close, then we may assume P= Na, P >> Ni, Ni^o, Ni^+, Ni^-. The relaxation matrix elements (5.4.12) become

$$M_{11} = e_{po} - c_{p1} P_o + c_{po} P_o, \qquad M_{21} = e_{p1} + 2c_{p1} P_o,$$

$$M_{12} = -e_{p1} + c_{po} P_o + 2e_{po} - 2c_{p1} P_o, \qquad M_{22} = c_{p1} P_o. \qquad (5.4.38)$$

Using $c_{po} >> c_{p1}$ as assumed in section 5.2.3.1, the relaxation matrix elements (5.4.38) become

$$M_{11} = e_{po} + c_{po} P_o, \qquad M_{21} = e_{p1} + 2c_{p1} P_o,$$

$$M_{12} = c_{po} P + 2e_{po}, \qquad M_{22} = c_{p1} P_o. \qquad (5.4.39)$$

Using eqs. (5.4.17), (5.4.18), (5.4.20) and (5.4.39), we obtain

$$M_{11}, M_{12} >> M_{22}, M_{21},$$

$$\lambda_1 \cong M_{11} = e_{po} + c_{po}\ P_o = \frac{1}{t_p},$$

$$\lambda_2 \cong \frac{(M_{11}M_{22}-M_{12}M_{21})}{(M_{11}+M_{22})}$$

$$= \frac{e_{p1}\ c_{po}\ P_o + 2\ e_{po}\ e_{p1} + c_{po}\ c_{p1}\ P_o^2 + 3e_{po}\ c_{p1}\ P_o}{e_{po} + c_{po}\ P_o + c_{p1}\ P_o}.$$

Since M_{11} is of the same order as M_{12}, $-\lambda_2$ is of the same order as M_{22}, and the observed noise spectra will have only one Lorentzian component in a certain frequency window because $-\lambda_2$ is smaller than λ_1. The same reasoning as used in section 3.1 applies to this case. The roll-off time constant is the same as given by eq. (5.2.22) for the single-acceptor model.

From eq. (5.4.20) and Table 5.1 we get $r_1 >> r_2$. Equation (5.4.14) can be approximated by

$$S_{pp}(\omega) \cong \frac{4r_o}{L\ w\ d\ (\omega^2+\lambda_1^2)} \qquad \text{for } -\lambda_2 << \omega, \qquad (5.4.40)$$

$$r_1 = c_{po}\ Nio^-\ P_o,$$

$$\frac{S_{vv}(\omega)}{V_o^2} = \frac{S_{pp}(\omega)}{P_o^2} = \frac{4\ c_{po}\ Nio^-\ P_o\ t_p^2}{L\ w\ d\ P_o^2\ (1+\omega^2\ t_p^2)} \qquad \text{for } -\lambda_2 << \omega. \qquad (5.4.41)$$

Using $r_o \cong g_o$, eq. (5.4.41) transforms to

$$\frac{S_{vv}(0)}{t_p V_o^2} = \frac{S_{PP}(0)}{t_p P_o^2} = \frac{4\ Nio^o\ e_{po}\ t_p}{L\ w\ d\ P_o^2} \qquad \text{for } -\lambda_2 << \omega << \lambda_1. \qquad (5.4.42)$$

Note that eqs. (5.4.42) and (5.2.17) are of similar form. In this case, we are unable to measure the donor level of defects.

5.2.3.4. Deep Defects with Energy Levels Separated by More than a Few KT from Each Other in Uncompensated Material

At high temperatures we may assume $P >> Ni^+, Ni^-, Ni^o$ in devices with defect concentrations satisfying $Na > Ni$. When the Fermi

level is close to the acceptor level and far away from the donor level, we may assume $S_{Fo} >> S_{F1}$ which implies $F_o >> F_1$. The rate equations including the noise can then be written as

$$\frac{d\Delta P}{dt} = -M_{11}\,\Delta P - M_{12}\,\Delta N_i^- + F_o, \tag{5.4.43}$$

$$\frac{d\Delta N_i^-}{dt} = -M_{21}\,\Delta P - M_{22}\,\Delta N_i^- + F_o, \tag{5.4.44}$$

with the relaxation elements given by eq. (5.4.35).

With eqs. (5.1.2), (5.1.7), (5.1.8), (5.4.13) and Table 5.1, $S_{Fo} >> S_{F1}$ results in

$$\frac{c_{po}}{c_{p1}} >> \frac{1}{g_{1a}} e^{\frac{E_{1a} - E_f}{KT}}. \tag{5.4.45}$$

The carrier fluctuations will come mainly from the acceptor level, therefore eq. (5.4.9) becomes

$$\Delta N_i^- \cong \Delta P. \tag{5.4.46}$$

With an additional condition $c_{po}/c_{p1} >> 1$, eqs. (5.4.43) and (5.4.44) have the same time constant defined by

$$\frac{1}{t_p} \cong M_{11} = e_{po} + c_{po}\,P_o. \tag{5.4.47}$$

Consequently, the acceptor-donor model reduces to the single-acceptor model discussed earlier.

When the Fermi level is close to the donor level and far away from the acceptor level, we may assume $S_{Fo} << S_{F1}$, which becomes with eqs. (5.1.2), (5.1.7), (5.1.8), (5.4.13) and Table 5.1

$$\frac{c_{po}}{c_{p1}} << \frac{1}{g_{1a}} e^{\frac{E_{1a} - E_f}{KT}}. \tag{5.4.48}$$

Equations (5.4.10) and (5.4.11) become

$$\frac{d\Delta P}{dt} = -M_{11}\,\Delta P - M_{12}\,\Delta Ni^{+} + F_1, \tag{5.4.49}$$

$$\frac{d\Delta Ni^{+}}{dt} = -M_{21}\,\Delta P - M_{22}\,\Delta Ni^{+} - F_1, \tag{5.4.50}$$

with relaxation matrix elements

$$M_{11} = e_{po}-c_{p1}\,P_o+c_{po}\,Nio^{-}+c_{p1}\,Nio^{o}+c_{po}\,P_o,$$

$$M_{12} = -e_{p1}+c_{po}\,P_o+2e_{po}-2c_{p1}\,P_o,$$

$$M_{21} = e_{p1} + 2c_{p1}\,P_o,$$

$$M_{22} = -c_{p1}\,Nio^{o} + c_{p1}\,P_o. \tag{5.4.51}$$

The carrier fluctuations will come mainly from the donor level, therefore eq. (5.4.9) becomes

$$\Delta N_i^{+} \cong -\Delta P. \tag{5.4.52}$$

Since we discuss the condition $(E_{1a} - E_{1d})$ larger than a few KT, we may assume $e_{po}/e_{p1} \ll 1$, i.e.,

$$\frac{c_{po}}{c_{p1}} \ll \frac{g_{1d}}{g_{1a}} e^{\frac{E_{1a}-E_{1d}}{KT}},$$

with which we find that eqs. (5.4.49) and (5.4.50) have the same time constant defined by

$$\frac{1}{t_p} \cong e_{p1} + c_{p1}\,P_o. \tag{5.4.53}$$

Hence, the acceptor-donor model reduces to the single-donor model discussed earlier.

5.3. Conclusions

In the design of a device for investigating defect properties from G-R noise spectra, the following facts should be considered:

1. Most of the energy levels of defects can be detected in uncompensated devices. Under certain conditions, G-R noise spectra

of double-level defects reduce to G-R noise spectra of single-level defects. However, in uncompensated devices, the noise signal is rather small compared to that of overcompensated devices.

2. In order to measure a particular energy level of a defect in devices doped with an intended deep defect and a shallow dopant, the doping impurity concentrations should satisfy the following conditions: Na > Ni > 0.5Na for a second-donor level, and Ni > Na for a first-donor level. We are able to measure the capture coefficients as a function of temperature and electric field if the values of the device resistance are such that the cut-off frequency of the circuit is larger than the roll-off frequency of the G-R noise spectra.

3. If the energy levels of a double-level defect are very close and there is a very large difference in the magnitude of capture coefficients associated with each level, the noise and resistance data in a nearly compensated device are likely to show different activation energies associated with the different levels of the same defect. It is only possible to detect the energy level that has the larger capture coefficient in an uncompensated device.

4. For a defect with an acceptor and a donor level, or double or triple acceptor levels, it is difficult to detect the acceptor level in a p-type device doped with an intended defect concentration larger than the shallow dopant concentration, because the Fermi level is far away from the deep acceptor energy levels.

5. For an uncompensated device, defect activation energies can be extracted from the roll-off time constants of G-R noise spectra measured as a function of temperature. In a p-type device doped with an intended defect concentration larger than the shallow dopant

concentration, defect activation energies are extracted from noise plateau and/or resistance data.

6. For a defect with multi-energy levels, which are separated by more than a few KT from each other, the multi-level G-R noise model reduces to the single-level G-R noise model in both uncompensated and overcompensated devices.

7. For an uncompensated device, eqs. (2.15) and (2.23) can be used to extract the defect activation energy. We can not determine whether the activation energy is associated with an acceptor or a donor center. This can only be deduced from the magnitude of the carrier capture coefficient associated with the defect. Using a device doped with an intended deep defect concentration larger than the shallow dopant concentration, the electrical nature of a defect can be determined since a deep acceptor center is unlikely to be detected in a p-type device, whereas a deep donor level will contribute a strong noise component.

8. The methods presented in this chapter can be extended to design a device for investigating a defect with more than two energy levels in the band gap.

CHAPTER VI
CARRIER CAPTURE, EMISSION AND RECOMBINATION

6.1. Carrier Capture and Emission

In a well-known paper [36], Lax proposed a "cascade capture" model: the electron is captured by one of the highly excited recombination center levels, which are quasi-continuously arranged, and by emitting phonons rolls down through these excited levels. The capture cross section resulting from this model is proportional to T^{-4}. V. N. Abakumov et al. [37] argue that the capture is dominated by electrons of energy $m^*v_l^2$ rather than KT, where v_l is the velocity of sound, and m^* is the electron effective mass. In the latter case, the capture cross section is calculated to be proportional to T^{-3}.

The cascade capture in charged centers relies on closely spaced, Rydberg-like bound states. Neutral centers however do not have excited states [38], and therefore the energy must be released by other mechanisms. During capture, the released energy can be (a) emitted in the form of light (radiative transitions), (b) transferred to another electron or hole (Auger process), or (c) transferred to phonon modes. The phonon emission processes include cascade mechanisms and multiphonon emission (nonradiative transitions).

Nonradiative transitions play a role in many processes, examples include the broadening of sharp optical transitions, and various device degradation mechanisms. Defects are likely to act as lifetime killer

centers [39] if they have favorable nonradiative (i.e., vibrational) properties such as large-amplitude modes promoting transitions and large-energy modes to take up the electronic energy to facilitate nonradiative carrier capture.

Emission processes can be considered as the reverse processes of carrier capture in equilibrium. As far as field-enhanced emission processes are concerned, there are three mechanisms used to account for its enhancement: (1) the Poole-Frenkel effect, where the electron climbs over a barrier lowered by the presence of the field, (2) pure tunneling, and (3) phonon-assisted tunneling, where the electron absorbs thermal energy from the lattice and then tunnels through a field-lowered barrier at a higher energy [40].

In this chapter, we discuss nonradiative transitions, specifically, as they apply to carrier transitions via neutral centers.

6.2. Microscopic Capture Model

6.2.1. Introduction

The Monte Carlo technique has been used to unravel the nonlinear transport phenomena of carriers in semiconductors for more than a decade. The advantages of using the Monte Carlo (MC) technique in device simulations are that it provides an accurate microscopic description of the physical processes, that it does not require any assumption on form of the carrier distribution function, and that it is very easy to include band-structure effects. In order to implement this technique, microscopic models for the physical processes should be developed. It is difficult to use the MC technique to investigate phenomena occurring in a semiconductor device with

deep generation-recombination (G-R) centers because there are not many well-accepted physical models for G-R process available to be implemented. Although a cascade capture G-R mechanism for a shallow impurity has been developed [37] and used to calculate G-R noise [15], and nonradiative multiphonon (NMP) carrier capture models by attractive and repulsive centers have been described by R. Passler [41,42], microscopic theories for neutral deep levels can not be found.

Defects create localized electronic states in the forbidden band of semiconductors. Phenomenologically, the interaction between deep states and conduction or valence bands can be described by Shockly-Hall-Read (SHR) statistics [43]. In SHR statistics, the rate equations involve capture and emission rates of carriers. Carrier capture efficiencies of traps are quantitatively described by capture coefficients, which give the actual size of the crystal volume swept out, in unit time, due to capture into the individual trap considered. A theory for a realistic capture coefficient C(T,E) should describe both its temperature and carrier energy dependence. The phenomenological capture coefficient C(T) results from the microscopic C(T,E) averaged over the carrier distribution. Preliminary knowledge of the dependences of microscopic carrier capture coefficients C(T,E) on E thus represents in general the prerequisite for actual calculations of any observed capture coefficient.

The theory of nonradiative multiphonon capture of free carriers belongs to the very few fields of solid state physics where a satisfactory solution has not been achieved so far. The multiphonon problem involves a complex many-body Hamiltonian and, in order to induce

transitions, some perturbation [44]. The G-R process can be described only by (1) approximating the unperturbed Hamiltonian, (2) assuming some sensible wavefunctions for the unperturbed Hamiltonian, and (3) assuming some perturbation. Once the basic approach is selected, there are still many possible variations regarding the electron-phonon interaction, the vibration modes, and the electron wavefunctions.

The microscopic nonradiative multiphonon (NMP) carrier capture by attractive or repulsive centers has been described by R. Passler [41,42]. The complete dependence of microscopic carrier capture coefficients C(T,E) on variables T and E is derived from the semi-phenomenological relation $C(T,E) = So(E)\ C^{o}(T,E)$, where So(E) is the Sommerfeld factor, accounting for the influence of non-vanishing center charges $Z|e|$ on a free-carrier wavefunction, and $C^{o}(T,E)$ takes into account the energy-loss mechanism. The condition of energy conservation can be satisfied when

$$p\,\hbar\omega = E_k + E_{to},$$

where E_k is the kinetic energy of the carrier, E_{to} is the energy depth of the traps below the band edge, p is the number of phonons emitted during the capture process, and ω is the vibrational radian frequency. In Passler's papers, p is not necessary an integer.

Generally speaking, capture of a carrier by a deep center occurs in three steps: firstly, the free wavefunction is modified by the electric field surrounding the capture center when the carrier approaches the deep level center, i.e., coulomb scattering; secondly, the electron releases its energy through delocalized phonon emission. If the process goes on, the capture becomes a cascade process. The carrier arrives at a bound vibronic state by either tunnelling, by a thermally

activated transition, or by a direct transition. Thirdly, the carrier drops to the ground state by multi-phonon emission. The capture cross section is proportional to the product of the three transition probabilities associated with these three steps. If any step is rate limiting, then that process will be sensed by an experiment designed to probe the capture cross section.

In contrast to the semi-phenomenological approach by R. Passler [41,42], we derive a microscopic nonradiative multiphonon carrier capture coefficient for a neutral deep center based on quantum mechanics in the following sections. In our model, the carrier releases its energy through delocalized optical phonon emission and directly jumps from a free vibronic state to a bound vibronic state. We assume that this step is the rate-limiting one. Therefore the capture coefficient can be calculated by evaluating this transition probability. In our model, the energy conservation condition with non-integer p as used by R. Passler [41,42] is avoided by a mechanism in which the delocalized phonon frequency is adjustable. Both the long-range and short-range electron-phonon interactions are accounted for by including localized and delocalized phonons in the representation of vibronic states. We focus on silicon material, but the basic ideas on which this theory is based apply to other materials as well.

6.2.2. Theory

In this section, we derive the transition probability for a free carrier to be captured by a deep neutral center. The direct influence of the externally applied electric field on the discrete levels may be

appreciable only if the field strength E is the order of the interior field in the lattice, and is therefore neglected in the following discussion.

6.2.2.1. Transition Probability

The Hamiltonian of the impurity-electron system can be generally expressed as

$$H_{tot} = H_e + H_L + H_{eL}, \tag{6.1}$$

with

$$H_L = T_n(Q) + \frac{K_1 Q^2}{2}, \tag{6.2}$$

where $T_n(Q)$ is the vibrational kinetic energy, and Q is the lattice coordinate; H_e, H_L, H_{eL} are the electronic part, the vibrational part and the electron-phonon interaction of H_{tot}, respectively. The electron-phonon interaction Hamiltonian H_{eL} for a free state is smaller than H_e and H_L, and is therefore neglected in the discussion of a free state.

The problem is to determine the probability w_{ct} of finding the system in the impurity ground state as t -> oo, if it was in the free state at t -> - oo. The exact eigenstates Ψ satisfy

$$(H_{tot} - E_t) \Psi = 0. \tag{6.3}$$

This equation can not be solved because the Hamiltonian does not allow a separation of variables. Hence a static approximation is used.

In the static approximation [45], the electronic wavefunction φ_k is assumed to be independent of the lattice coordinate and taken as

$$H_e \varphi_k = E_e \varphi_k . \tag{6.4}$$

The total wavefunction is written as [45]

$$\Psi = \sum_{k} \varphi_k(r)\, \chi_{kt}(r,Q) , \tag{6.5}$$

where Q is the configuration coordinate, and χ_{kt} is the lattice wavefunction which is derived in the following.

Taking the electron-phonon interaction to be of the form $H_{eL}=UQ$, where U is constant, and substituting eq. (6.5) into eq. (6.3), the following expression is derived for the lattice wavefunctions

$$(H_L + E_e + \sum_{k} \langle k|U\,Q|j\rangle - E_t)\, \chi_{kt}(r,Q) = 0, \tag{6.6}$$

i.e.,

$$(H_L + E_e + U\,Q - E_t)\, \chi_{kt}(r,Q) = 0. \tag{6.7}$$

This can be written as

$$\left(T_n(Q) + \frac{K_1(Q+\frac{U}{K_1})^2}{2} + E_e - \frac{U^2}{2K_1} - E_t\right) \chi_{kt}(r,Q) = 0. \tag{6.8}$$

Equations (6.4) and (6.7) give a vibronic state wavefunction

$$\Psi_{k,t} = \varphi_k(r,Q_o)\, \chi_{kt}(r,Q) . \tag{6.9}$$

The total vibronic energy is given by

$$E_t = (\frac{1}{2} + n_t)\hbar\omega - E_{to}, \tag{6.10}$$

with

$$E_{to} = -E_e + \frac{U^2}{2K_1} = E_{eg} + \frac{U^2}{2K_1}, \tag{6.11}$$

where E_{eg} is the electronic ground state energy of a carrier.

We define

$$\frac{U^2}{2K_1} = S\,\hbar\omega, \tag{6.11a}$$

where S is the Huang-Rhys factor, and $S\hbar\omega$ is the relaxation energy.

For a carrier in a free state, H_{eL} is negligible, and therefore

$$E_k = (\frac{1}{2} + n_k)\hbar\omega + \frac{\hbar^2 k^2}{2m^*}, \qquad (6.12)$$

where E_k is the energy of the carrier in the free state, k is the carrier wavevector, and m^* is its effective mass.

The wavefunctions $|k,n_k>$ and $|t,n_t>$ can be written in the static approximation as

$$|k,n_k> = |k>\ |n_k>,$$
$$|t,n_t> = |t>\ |n_t>. \qquad (6.13)$$

The wavefunctions $|k,n_k>$ and $|t,n_t>$ are orthogonal, because of the orthogonality relations

$$\int_\Omega \varphi_j\, \varphi_{k\,dr} = \delta_{j,k},$$
$$\int_\Omega \chi_{kt2}\, \chi_{kt1\,dr} = \delta_{t2,\,t1}, \qquad (6.14)$$

where Ω is the crystal volume.

In general, the transition rate between two states can be computed using the Golden Rule

$$P_{12} = \frac{2\Pi}{\hbar}\ |<2|H'|1>|^2\ \delta(E_2-E_1), \qquad (6.15)$$

where $|1>$ and $|2>$ represent many-electron, many-phonon states, and E_1, E_2 are the corresponding total energies.

Equation (6.15) can be written as

$$P_{12} = \frac{2\Pi}{\hbar}\ |<t,n_t,n_{2'}|H'|k,n_k,n_{1'}>|^2\ \delta(E_2-E_1).$$

where $|k,n_k,n_{1'}>$ and $|t,n_t,n_{2'}>$ refer to the electronic, delocalized and localized wavefunctions of the states $|1>$ and $|2>$ respectively.

We assume that the optical deformation potential is the perturbation Hamiltonian H' which is given by [14]

$$H' = D \sum_{q} \left(\frac{\hbar}{2\rho\Omega\omega_q}\right)^{1/2} e^{i\bar{q}\cdot\bar{r}} (a_q + a_q^{+}), \tag{6.16}$$

where ρ is the density of the crystal, D is the optical deformation potential constant, a_q is the phonon creation operator, a_q^{+} is the phonon annihilation operator.

If however acoustic deformation dominates carrier capture, the perturbation Hamiltonian is given by [14]

$$H' = D_a \sum_{q} q \left(\frac{\hbar}{2\rho\Omega\omega_q}\right)^{1/2} e^{i\bar{q}\cdot\bar{r}} (a_q + a_q^{+}), \tag{6.16a}$$

where ρ is the density of the crystal, D_a is the acoustic deformation potential constant, a_q is the phonon creation operator, a_q^{+} is the phonon annihilation operator.

The transition rate for capture of a carrier by vibronic states through emitting an optical phonon is given by

$$W_{kt} = \frac{2\pi}{\hbar^2} ave_{nk} \sum_{n_t} (\bar{n}_q + 1) |\langle t, n_t | V' | k, n_k \rangle|^2 \delta\left(\frac{E_k - E_t - \hbar\omega_q}{\hbar}\right), \tag{6.17}$$

where $\hbar\omega_q$ is the energy of a delocalized optical phonon, and ave_{nk} is an average over the quantum states of delocalized phonons. The vibrational wavefunctions $|n_t\rangle$, and $|n_k\rangle$ are assumed to have the same vibration frequency ω, the unit of δ is second,

$$V' = D \sum_{q} \left(\frac{\hbar}{2\rho\Omega\omega_q}\right)^{1/2} e^{i\bar{q}\cdot\bar{r}}, \tag{6.18}$$

and

$$\bar{n}_q = \frac{1}{\exp(\frac{\bar{\hbar}\omega_q}{KT}) - 1}. \qquad (6.18a)$$

Assuming that the dynamics of delocalized and localized phonons are independent, we get

$$\langle t, n_t | V' | k, n_k \rangle = \langle t | V' | k \rangle \langle n_t | n_k \rangle. \qquad (6.19)$$

The probability of a transition involving p phonons can be determined by summing over the transitions between an initial state with quantum number n and a final state with quantum number n+p. Equation (6.17) can be written as a sum of the transition probabilities involving p phonons

$$W_{kt} = \frac{1}{\bar{\hbar}^2} (\bar{n}_q + 1) | \langle t | V' | k \rangle |^2 \sum_p P_p \, \delta(\frac{E_k - E_t - \bar{\hbar}\omega_q}{2\pi\bar{\hbar}}), \qquad (6.20)$$

with

$$P_p = (1 - \exp(\frac{-\bar{\hbar}\omega}{KT})) \sum_n \exp(\frac{-n\bar{\hbar}\omega}{KT}) | \langle n+p | n \rangle |^2. \qquad (6.21)$$

Let the position of the energy E_t be so smeared out [46] that we may describe it only by the probability $Y(E_t)\, dE_t$ of finding it between E_t and $E_t + dE_t$, and with $g(f_t) = 2\pi\bar{\hbar}\, Y(E_t)$ so that

$$\int g(f_t)\, df_t = 1.$$

With the energy conservation connection and eq. (6.18), the transition probability rate becomes

$$W_{kt} = \frac{1}{\bar{\hbar}^2} (\bar{n}_q + 1) | \langle t | V' | k \rangle |^2 \sum_p P_p \, g(f_t).$$

This equation can be further approximated, if we assume that E_t is peaked around E_{to}.

The transition probability rate from the free state φ_k to the bound state φ_t becomes

$$W_{kt} = \frac{1}{\hbar^2} D^2 \left(\frac{\hbar}{2\rho\Omega\omega_q}\right)(\bar{n}_q+1) \cdot \left[\int_\Omega \varphi_t \, e^{i\bar{q}\cdot\bar{r}} \varphi_k \, dr\right]^2 2\pi \, \Xi(\omega_q) \sum_p P_p , \tag{6.23}$$

where

$$p\,\hbar\omega = \frac{\hbar^2 k^2}{2m^*} + E_{to} - \hbar\omega_q, \tag{6.24}$$

where φ_t is the bound electronic wavefunction, φ_k is the free state wavefunction, ω_q is the frequency of a delocalized optical phonon mode. We define $\Xi(\omega_q)$ such that $\Xi(\omega_q)\, d\omega_q$ is the fraction of modes with radian frequency between ω_q and $\omega_q + d\omega_q$.

At low temperatures ($p > \bar{n}$) [47], we get

$$P_p = \frac{S^p}{p!} e^{-S(2\bar{n}+1)} (\bar{n}+1)^p \left(1 + \frac{S^2 \bar{n}(\bar{n}+1)}{p+1}\right), \tag{6.25}$$

where

$$\bar{n} = \frac{1}{\exp\left(\frac{\hbar\omega}{KT}\right)-1} . \tag{6.26}$$

The way that a carrier is trapped in a vibronic ground state is illustrated in Fig. 6.1. When a free carrier loses its energy $\hbar\omega_q$ by

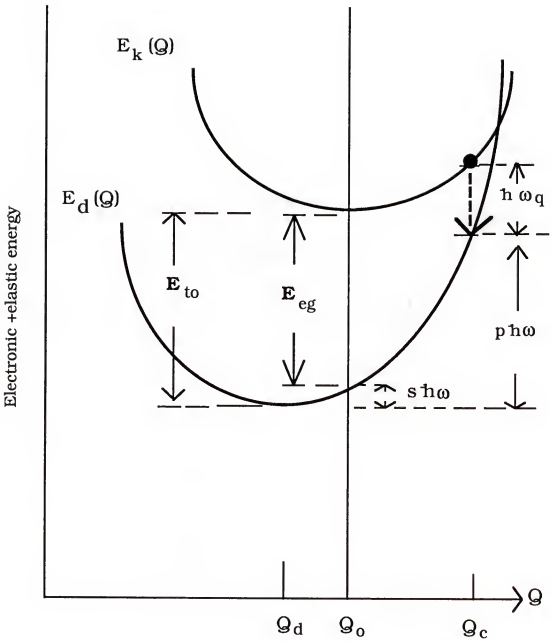

Figure 6.1. The configuration coordinate diagram-electronic + elastic energy versus Q

emitting an optical phonon, it directly transits to a vibronic bound state, and subsequently drops to the ground vibrational state by multiphonon emission.

6.2.2.2. Density of States of Delocalized Optical Phonons

The dispersion curves of phonons in silicon in the [1,0,0] direction can be described by the following branches [48]: the transverse branch

$$M\omega_q^2 = 4\xi + 4\gamma(1-\cos(\pi q_1)) \mp 2\sqrt{2}\sqrt{[\xi^2+\eta^2+(\xi^2-\eta^2)\cos(\pi q_1)]}\ , \quad (6.27)$$

and the longitudinal branch

$$M\omega_q^2 = 4\xi + 8\gamma(1-\cos(\pi q_1)) \mp 2\sqrt{2}\,\xi\sqrt{1+\cos(\pi q_1)}\ , \quad (6.28)$$

where the - sign refers to the acoustic phonon branch and the + sign indicates the optical phonon branch, $q_1 = q/q_{max}$ is the reduced phonon wavevector, $q_{max} = \pi/a$, a is the lattice constant of silicon (5.43095×10^{-8}cm), and M is the mass of host lattice (4.666×10^{-23}g). We fit eqs. (6.27) and (6.28) to the experimental results [49], and get the constants:

$\xi = 0.5804 \times 10^5$ dynes/cm,

$\gamma = 0.4069 \times 10^2$ dynes/cm,

$\eta = 0.4667 \times 10^5$ dynes/cm.

The fitted results are shown in Fig. 6.2.

The density of states for optical phonon is calculated from the following formula

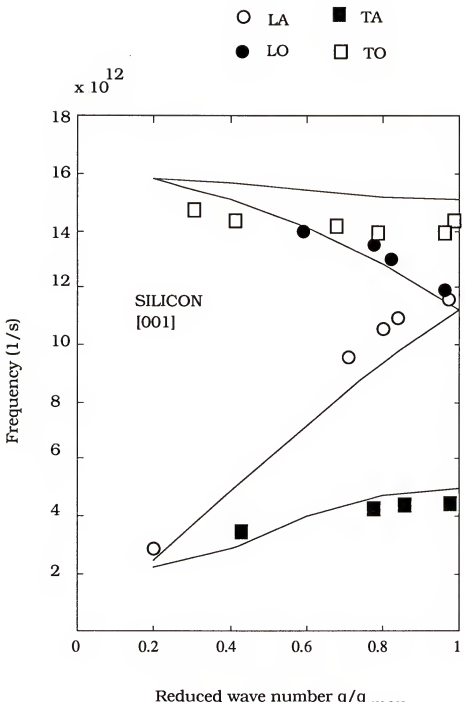

Figure 6.2. Phonon dispersion curves of silicon. The full lines are the fitted results.

$$\int_{\omega_l}^{\omega_u} (\Xi(\omega_q))\, d\omega_q = \frac{\Omega}{8\pi^3} \int_{-q_{xm}}^{q_{xm}} \int_{-q_{ym}}^{q_{ym}} \int_{-q_{zm}}^{q_{zm}} dq_x dq_y dq_z, \qquad (6.29)$$

where ω_u and ω_l are the upper and lower limit of the radian frequency for each dispersion branch, and q_{im} is the upper limit of q_i.

For simplicity, we approximate the density of states for phonons by

$$\Xi(\omega_q) = 2\frac{\Omega}{8\pi^3}\left(\frac{2\pi}{a}\right)^2 \frac{|dq_z|}{d\omega_{q_z}} . \qquad (6.30)$$

From eqs. (6.27) and (6.29), we get for the density of states of the transverse optical branch

$$\Xi_t(\omega_q) = \frac{\Omega}{a^3\pi} \cdot \frac{\sqrt{M\{4\xi+8\gamma(1-\cos(\pi q_1))+2\sqrt{2}\sqrt{[\xi^2+\eta^2+(\xi^2-\eta^2)\cos(\pi q_1)]}\}}}{\frac{(\xi^2-\eta^2)\sin(\pi q_1)}{\sqrt{2[\xi^2+\eta^2+(\xi^2-\eta^2)\cos(\pi q_1)]}} - 2\gamma\sin(\pi q_1)} . \qquad (6.31)$$

The density of states of the longitudinal optical branch is given by

$$\Xi_l(\omega_q) = \frac{\Omega}{a^3\pi} \frac{\sqrt{M\{4\xi+8\gamma(1-\cos(\pi q_1))+2\sqrt{2}\xi\sqrt{1+\cos(\pi q_1)}\}}}{\frac{\xi\sin(\pi q_1)}{\sqrt{2[1+\cos(\pi q_1)]}} - 4\gamma\sin(\pi q_1)} . \qquad (6.32)$$

6.2.2.3. Evaluation of Electronic Matrix Elements

A theory for the magnitude of the capture cross section is difficult to develop because the explicit form of the electron wavefunction for a deep state is not well known. The initial and final electronic wavefunctions are rather complicated, and depend on what we assume for the potential of the defect. Since the defect potential is not explicitly known, we assume the potential of a neutral deep defect

to be a spherical square well of depth Vo, and radius b. If we further assume the potential is a Lucovsky's delta-function [50], then $Vo\ b \cong \pi^2\hbar^2/(8m)$ as b -> 0. The electronic wavefunctions form an orthogonal set. The approximate, normalized ground state electronic wavefunction is given by

$$\varphi_t(r) = \sqrt{\frac{\alpha}{2\pi}}\ \frac{e^{-\alpha r}}{r}, \tag{6.33}$$

with

$$\alpha = \sqrt{\frac{2m\ E_{eg}}{\hbar^2}}\ , \tag{6.34}$$

where m is the electron mass.

For simplicity, the free electronic wavefunction is approximated by

$$\varphi_k(r) = \frac{1}{\sqrt{\Omega}}\ e^{i\bar{k}\cdot\bar{r}}. \tag{6.35}$$

The electronic matrix element is then given by

$$M_e = \int_{\Omega} \varphi_t\, e^{i\bar{q}\cdot\bar{r}}\, \varphi_k\, dr = 2\sqrt{\frac{2\pi\alpha}{\Omega}}\left(\frac{1}{\alpha^2 + |\bar{k}+\bar{q}|^2}\right). \tag{6.36}$$

Because $|\bar{k}+\bar{q}| = |k+q\cos(\Theta)|$, where Θ is the angle between $\bar{k}$ and $\bar{q}$, the average electronic matrix element is given by

$$\frac{-1}{4\pi}\int 2\sqrt{\frac{2\pi\alpha}{\Omega}}\left(\frac{1}{\alpha^2 + |\bar{k}+\bar{q}|^2}\right) d\cos(\Theta)\, d\phi$$

$$= \frac{1}{2kq}\sqrt{\frac{2\pi}{\alpha\Omega}}\ \mathrm{Ln}\left(\frac{\alpha^2+k^2+q^2+2kq}{\alpha^2+k^2+q^2-2kq}\right). \tag{6.37}$$

where ϕ is the azimuthal angle.

6.2.2.4. Calculation of the Capture Coefficient

With eqs. (6.23), (6.25), and (6.36), and by assuming that the transition probability mainly comes from the p-phonon emission process, the transition probability via optical phonon emission becomes

$$W_{kt}(T,E,p)= \frac{1}{\hbar^2} D^2 \left(\frac{\hbar}{2\rho\Omega\omega_q}\right) M_e^2 (\bar{n}_q + 1)\, 2\pi\, (\Xi_l(\omega_q)+2\,\Xi_t(\omega_q)) \cdot \frac{S^p}{p!} e^{-S(2\bar{n}+1)} (\bar{n}+1)^p \left(1+ \frac{S^2 \bar{n}(\bar{n}+1)}{p+1}\right). \qquad (6.38)$$

with the conditions that the optical phonon wavevector satisfies eqs. (6.27) and (6.28), and the carrier energy satisfies eq. (6.24).

The microscopic capture coefficient is given by

$$C(T,E,p)= \Omega\ W_{ct}(T,E,p). \qquad (6.39)$$

The phenomenological capture coefficient C(T) results from the microscopic C(T,E) after averaging over the carrier distribution. The capture cross section is given by

$$\sigma(T,E)= \sum_p \frac{m^* \Omega\ W_{ct}(T,E,p)}{\hbar k}\ . \qquad (6.40)$$

The average capture coefficient reads

$$C(T)= \sum_p \frac{\int_E n(E) C(T,E,p)\, dE}{\int_E n(E)\, dE}\ , \qquad (6.41)$$

where n(E) represents the carrier distribution function.

The observed capture cross section is C(T) divided by the thermal velocity of the carriers. In the following, we calculate the value of the electron capture coefficient of the gold acceptor in silicon.

Equation (6.41) can be rewritten as

$$C(T)= \sum_{p} \frac{\int_{E} D(E)f(E,T)C(T,E,p)\,dE}{\int_{E} D(E)f(E,T)\,dE}, \qquad (6.42)$$

where D(E) represents the density of states in the conduction band, and f[E,T] is the carrier distribution function.

At low field and $E_c - E_f >> KT$, f[E,T] is given by

$$f(E,T) = e^{-\frac{\hbar^2 k^2}{2m^* KT}} e^{-\frac{E_c - E_f}{KT}}. \qquad (6.43)$$

With the following expressions for D(E) and the various masses,

$$D(E)= \frac{\sqrt{2}\, M_c\, (m_{de})^{3/2}\, E^{1/2}}{\hbar^3\, \pi^2}, \qquad (6.44a)$$

$$D(E)dE= \frac{\sqrt{2}\, M_c\, (m_{de})^{3/2}\, E^{1/2}\, k}{m^*\, \hbar\, \pi^2} dk, \qquad (6.44b)$$

$$m_{de} = \left(m_l^*\, m_t^*\, m_t^*\right)^{1/3}, \qquad m^* = 3\left(\frac{1}{m_l^*} + \frac{2}{m_t^*}\right)^{-1},$$

we get for the root mean square velocity

$$v_{rms} = \sqrt{\frac{3KT}{m^*}}. \qquad (6.45)$$

Considering that the transition probability is dominated by the p-phonon emission process, we can estimate the capture coefficient from eq. (6.38),

$$C(T,E,p) = \Omega \frac{1}{\hbar^2}\left(\frac{\hbar}{2\rho\Omega\omega_q}\right) 2\pi \left(D_l^2 \Xi_l(\omega_q) + 2 D_t^2 \Xi_t(\omega_q)\right)(\bar{n}_q + 1)$$

$$\cdot \left\{\frac{1}{2kq}\sqrt{\frac{2\pi}{\alpha\Omega}} Ln\left(\frac{\alpha^2+k^2+q^2+2kq}{\alpha^2+k^2+q^2-2kq}\right)\right\}^2$$

$$\cdot \frac{S^p}{p!} e^{-S(2\bar{n}+1)} (\bar{n}+1)^p \left(1+\frac{S^2\bar{n}(\bar{n}+1)}{p+1}\right), \qquad (6.46)$$

where D_l is the longitudinal optical deformation constant, D_t is the transverse optical deformation constant.

If we take the radian frequency of localized optical phonon as $\omega = 0.1218 \times 10^{+15}$/s, and use the following electronic constants

$m_l^* = 0.98 * 0.91095 \times 10^{-27}$g, $m_t^* = 0.19 * 0.91095 \times 10^{-27}$g,

$a = 5.43095 \times 10^{-8}$cm, $M_c = 1$, $M = 4.666 \times 10^{-23}$g,

$N_c = 2.8 \times 10^{19} \left(\frac{T}{300}\right)^{3/2}$/cm^3, $\rho = 2.328$ g/cm^3,

$D_l = 11 \times 10^8$eV/cm, $D_t = 2 \times 10^8$eV/cm

for the gold acceptor level in silicon, we can calculate the electron capture cross section with eqs. (6.45) and (6.46) if we use $E_{to} = 0.540$ eV, S=2.743 and p=6. The results are shown in Fig. 6.3. The theory gives values for the electron capture coefficient which are of the same order as the experimental data. The slight temperature dependence of our model may be due to some of the approximations we used and might not be real.

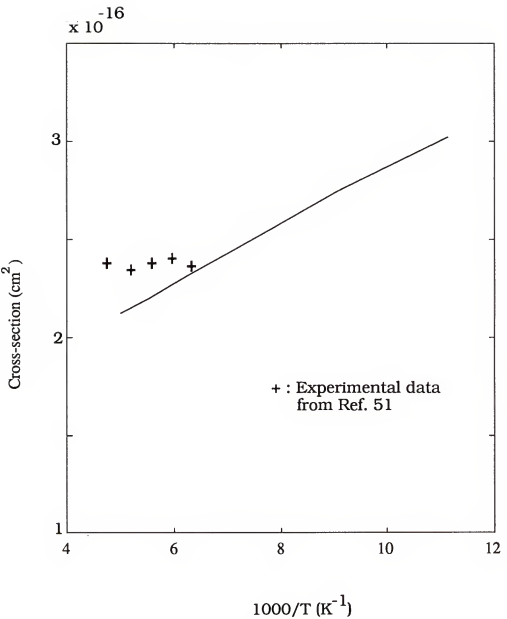

Figure 6.3. Electron capture cross section of the gold acceptor level versus 1000/T. The full line represents the results of the microscopic model outlined in the text.

CHAPTER VII
DEFECT PARAMETER EXTRACTION FROM FIELD-EFFECT TRANSISTORS

Junction-gate transistors are particularly attractive for use in the input stages of low-frequency, low-noise amplifiers, and offer substantial improvements over bipolar amplifiers when the signal source impedance is large. MOS transistors, on the other hand, tend to generate considerably large amounts of low-frequency noise. However, in the MHz range their noise is comparable to the junction-gate device, and this, together with a very low cross-modulation performance, make them particularly useful for low-noise RF amplification.

There are three major noise sources in MOSFETs and JFETs: the thermal noise in the channel, the 1/f noise, and the generation-recombination (G-R) noise due to random emission of electrons and holes from defect centers in the depletion region of the semiconductor and the G-R noise originating from the random trapping and releasing of current carriers from deep centers or shallow impurities in the channel.

In this chapter, we analyze the posibilities for using the G-R noise spectra of MOSFETs and JFETs as a tool for trap parameter extraction. We discuss MOSFETs first, and then describe JFETs.

7.1. Fluctuations in the Charge States of Shockley-Hall-Read Centers Located in the Space Charge Region

The rate equation for the trapped electron concentration, taking the four processes indicated in Fig. 7.1 into account, may be written as

$$\frac{dn_t}{dt} = N_t [(c_n f_{tp} N - e_n f_t) - (c_p f_t P - e_p f_{tp})], \tag{7.1}$$

where P, N are the hole, electron concentration in the valence band and conduction band, respectively; n_t, N_t are the occupied and total trap concentration, respectively; c_p, e_p are the hole capture and emission coefficient, respectively; c_n, e_n are the electron capture and emission coefficient, respectively; f_t is the fraction of occupied traps.

We express in terms of Fermi-Dirac statistics

$$f_{tp} = 1 - f_t = \frac{1}{1 + g_t e^{\frac{E_f - E_t}{kT}}}, \tag{7.2}$$

where E_t is the trap energy level, E_f is the Fermi level and g_t is the degeneracy factor.

Using the principle of detailed balance and eq. (7.1), eq. (7.2) can be rewritten as

$$f_{tp} = 1 - f_t = \frac{c_p P + e_n}{c_p P + e_n + c_n N + e_p}. \tag{7.3}$$

Using the principle of detailed balance and eq. (7.2), we get

$$e_p = c_p N_v g_t e^{\frac{E_v - E_t}{kT}}. \tag{7.4}$$

Similarly,

$$e_n = c_n N_c \frac{1}{g_t} e^{\frac{E_t - E_c}{kT}}. \tag{7.5}$$

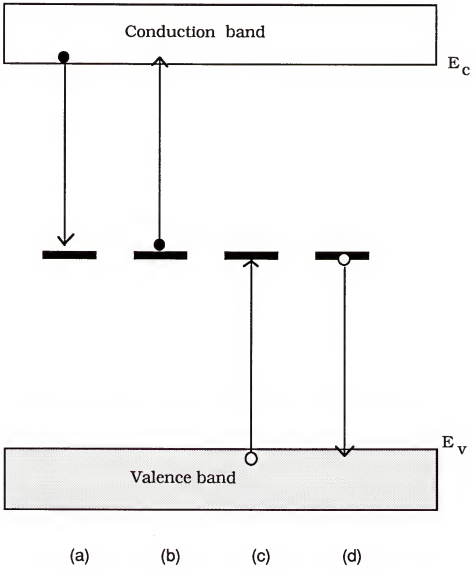

Figure 7.1. The electron and hole generation-recombination processes: (a) electron capture, (b) electron emission, (c) hole capture, (d) hole emission.

The carrier densities can be expanded around their steady-state values

$$N = N_o + \Delta N, \tag{7.6}$$

$$P = P_o + \Delta P, \tag{7.7}$$

$$n_t = n_{to} + \Delta n_t, \tag{7.8}$$

where N_o, P_o, n_{to} are the electron, hole and occupied trap concentration in steady-state, respectively; ΔN, ΔP, Δn_t are the corresponding density fluctuations.

Using eqs. (7.1) and (7.6) through (7.8), we get after linearization

$$\frac{d\Delta n_t}{dt} = -[(c_n N_o + e_n) + (c_p P_o + e_p)]\Delta n_t + c_n(N_t - n_{to})\Delta N - c_p n_{to} \Delta P. \tag{7.9}$$

The noise from the carrier fluctuations ΔN and ΔP may be neglected, since they have much shorter time constants, i.e., the transit time across the transition layer, than Δn_t. For a nearly depleted region in a semiconductor, the solution of eq. (7.9) is relatively simple, if we concentrate on low-frequency fluctuations only. Thus we get

$$\frac{1}{t_p} = [(c_n N_o + e_n) + (c_p P_o + e_p)]. \tag{7.10a}$$

When the carrier densities are very small, it becomes

$$\frac{1}{t_p} = [e_n + e_p]. \tag{7.10b}$$

If $e_n >> e_p$ or $e_n << e_p$ holds, as for example in the case of the acceptor level of gold in silicon where e_n is 20-50 times greater than e_p [8], we are able to extract the activation energy of the trap from a measurement of the lifetime of the G-R noise spectrum versus temperature. Equations (7.4) and (7.5) are often assumed to be independent of electric field, and the activation energies and capture

coefficients are therefore extracted from these equations. In reality however, field-dependent factors should be taken into account in the interpretation of experimental data.

7.2. Generation-Recombination Noise in Metal-Oxide-Semiconductor Field-Effect Transistors

7.2.1. Low-Field Noise Theory

The MOS transistor device structure, with an induced n-channel structure in a p-type substrate, is shown in Fig. 7.2. According to the theory of low-frequency G-R noise derived by Yau and Sah [52], the equivalent gate voltage spectral density is of the form

$$S_{V_{gs}}(\omega) = \frac{2\,q^2\,N_t\,(2V_{gsa}-V_{ds})}{C_o^2\,Z\,L\,v_{ds}} \cdot \int_0^{V_{ds}} \int_0^{W} \left\{ \frac{(V_{gsa}-V)}{\left[(V_{gsa}-V)+\frac{kT}{q}\left(1+\frac{C_W}{C_o}\right)\right]^2} \frac{t_p}{(1+\omega^2 t_p^2)} f_t(1-f_t)\left[1-\frac{x}{W}\right]^2 \right\} dx\,dV, \tag{7.11}$$

with

$$t_p = \frac{1}{e_n + e_p}\,, \tag{7.12}$$

$$f_t\,(1-f_t) = \frac{e_n\,e_p}{[e_n+e_p]^2}\,, \tag{7.13}$$

and

$$C_W = \frac{\varepsilon_s}{W} = \frac{\varepsilon_s}{\left[\frac{2\varepsilon_s}{q\,N_a}(2\,\phi_F + V(y))\right]^{\frac{1}{2}}}\,,$$

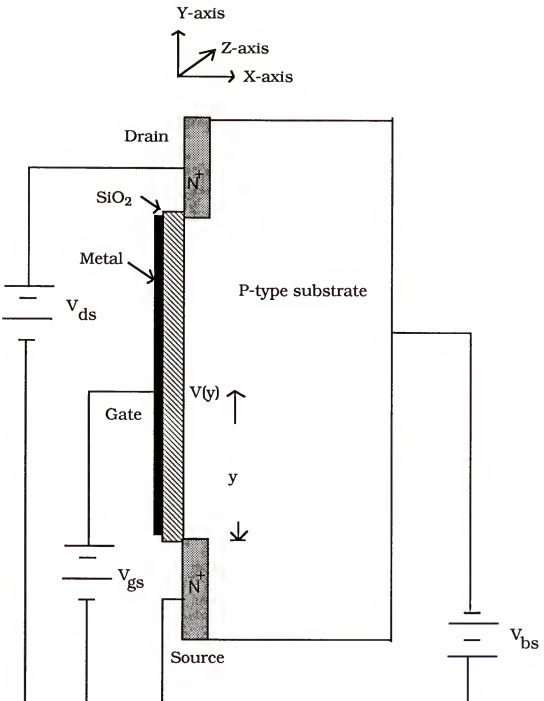

Figure 7.2. MOS transistor structure

$$C_o = \frac{\varepsilon_o}{x_o}\ , \qquad (7.14)$$

where V=V(x) is the voltage along the channel, W is the depletion region thickness of the MOSFET, ϕ_F is defined by $\phi_F = (E_f - E_i)/q$, E_i is the intrinsic Fermi level in the bulk; x_o is the thickness of the silicon dioxide of the gate, and ε_o is its associated dielectric constant; Vgsa is the gate-source voltage minus the threshold voltage, Vds is the drain-source voltage; x is the distance from the silicon-dioxide interface, and N_a is the shallow acceptor concentration.

Assuming that t_p and f_t are constants, eq. (7.11) becomes

$$S_{Vgs}(\omega) = \frac{t_p}{(1+\omega^2 t_p^2)} f_t(1-f_t)\, Fg, \qquad (7.15)$$

where Fg contains the geometrical factors and the d.c. bias voltages which are kept constant during a particular noise measurement versus temperature.

Using eq. (7.13), and if $e_p << e_n$, eq. (7.15) may be simplified to

$$\frac{S_{vgs}(\omega \to 0)}{Fg\, t_p} = \frac{e_p}{e_n}\ . \qquad (7.16)$$

Combining eqs. (7.12) and (7.16), we get e_p and e_n. Constructing Arrhenius plots and using eqs. (7.3) and (7.4), we get the activation energies of the trap involved. Recently, Scholz et al. [9] used this technique and DLTS to measure trap parameters and found that the results from both techniques are in agreement.

7.2.2. Field Dependent Noise Theory

According to the arguments of Yau and Sah [8], the major noise contribution comes from the random thermal emission from gold

centers located near the interface. The electric field can be varied by varying the substrate bias. If we approximate the electric field by $E = Emax = 2V_{bs}/W(V=0)$, where V_{bs} is the substrate-source voltage, the field dependent emission coefficients can be extracted.

7.3. Generation-Recombination Noise in Junction-Gate Field-Effect Transistors

7.3.1. Low-Field Junction Generation-Recombination Noise

The JFET device structure, with a n-channel structure, is shown in Fig. 7.3. The low-frequency excess noise in junction-gate FET's was first analyzed in detail by Lauritzen and Sah [53,54,55]. The theoretical expression for G-R noise due to SHR centers in the gate-channel transition region of an abrupt junction, symmetrical JFET is written in the form [54,55]

$$S_{Vgs}(\omega)= \frac{a^3 q^2 t_p}{6 \varepsilon_s^2 L Z(1+\omega^2 t_p^2)} f_t(1-f_t) F(u_s,u_L), \qquad (7.17)$$

where ε_s is the dielectric constant of the substrate.

The function $F(u_s,u_L)$ is given by

$$F(u_s,u_L)= \frac{\frac{2}{3}[3(u_s^2- u_L^2)-2(u_s^3- u_L^3)][\ln(\frac{u_s}{u_L})-2(u_s- u_L)+\frac{1}{2}(u_s^2- u_L^2)]}{(u_s- u_L)^2}, \qquad (7.18)$$

with

$$u_s=1- \left[\frac{V_{gs}+V_{bg}}{V_{pd}}\right]^{1/2} = 1- U_s, \qquad (7.19)$$

and

$$u_L=1- \left[\frac{V_{gs}-V_{ds}+V_{bg}}{V_{pd}}\right]^{1/2} = 1- U_d, \qquad (7.20)$$

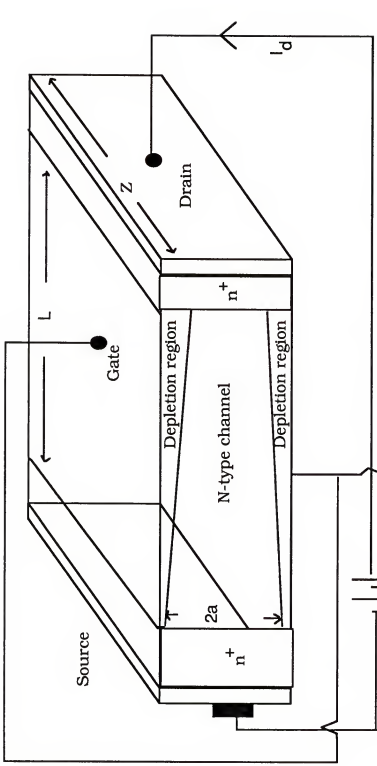

Fig. 7.3. Schetch of an n-channel junction-gate FET showing coordinate system and dimensions used in the analysis.

where V_{pd} is the pinch-off potential, and V_{bg} is the built-in potential of the gate junction.

Above pinch-off, eq. (7.20) is replaced by

$$u_L=\left[\frac{a\, I_{d'}}{6\, L\, I_{do}}\right]^{1/2}, \tag{7.22}$$

with

$$\frac{I_{d'}}{I_{do}} = 3(u_s^2 - u_L^2) - 2(u_s^3 - u_L^3)\ . \tag{7.23}$$

Expressions (7.12) and (7.13) for f_t and t_p respectively, indicate that defects with energies away from the center of the gap give negligible noise. K. K. Wang et al. [56] reevaluated f_t and t_p by not neglecting the free carrier density density at the edge of the depletion region. The drain current noise is then given by

$$S_{di}(\omega)= \frac{4\, q\, \mu_n\, I_d\, W_d\, J_o}{N_d\, a\, L^2\, (1+\omega^2\, t_p^2)} \left[(U_d^{1/2} - U_s^{1/2}) - \ln\left(\frac{1- U_d^{1/2}}{1- U_s^{1/2}}\right)\right], \tag{7.24}$$

where J_o depends on N_t and the geometry of the depletion region, I_d is the d.c. drain current, N_d is the shallow donor concentration in the channel, μ_n is the electron mobility, and

$$t_p = \frac{2}{3e_n}\ . \tag{7.25}$$

Hence, a noise measurement of t_p (T) versus T gives the defect activation energy.

7.3.2. Generation-Recombination Noise in the Channel of Junction Field-Effect Transistors

The expression for the drain current G-R noise from the channel region has been derived by different authors [4,54,57]. It can be written as

$$S_{di}(\omega) = \frac{4\, I_d}{L^2} \int_0^{V_{ds}} \frac{q\, \alpha\, \mu_n\, t_p}{(1+\omega^2\, t_p^2)}\, dV, \qquad (7.26)$$

with

$$\alpha = N_t\, f_t(1-f_t) \,/\, N_d.$$

At relatively low fields, α, f_t and t_p are constants, and eq. (7.26) can be written as

$$S_{di}(\omega) = \frac{4\, I_d\, V_{ds}}{L^2} \frac{q\, \alpha\, \mu_n\, t_p}{(1+\omega^2\, t_p^2)}. \qquad (7.27)$$

Using similar techniques as presented in Chapters II through V, trap parameters can be extracted from channel G-R noise.

In summary, using eqs. (7.15) and (7.17), we can extract, from a measurement of the roll-off time constant as a function of temperature, the trap activation energies from defect centers located in junction depletion regions. The trap parameter extraction from gate-junction G-R noise is complicated by the geometrical factors of a device and the assumption of field-independent capture and emission coefficients required to take the frequency-dependent factors $t_p/(1+\omega^2\, t_p^2)$ outside the integral. G-R noise from the junction transition region of a MOSFET or FET is generation noise, while that from the channel or from a bulk p-type or n-type semiconductor is trapping and detrapping noise.

CHAPTER VIII
GENERATION-RECOMBINATION NOISE IN POLYSILICON RESISTORS

8.1 Introduction

The use of polycrystalline silicon has become increasingly widespread in solar cells and VLSI circuits, including polycrystalline MOS devices, static RAM's, PROM's, ECL, D/A converters, CCD detectors, distributed RC filters, and as redundancy fusing elements. The polysilicon film is composed of aggregates of single-crystalline silicon grains with grain boundaries between adjacent grains. The grain boundaries contain trapping states that are capable of trapping mobile carriers and contribute to the creation of space charge potentials, and may also serve as a sink for the dopants, which cause them to become inactive [58]. Several distribution functions, such as an ideal δ-distribution, uniform distribution, Gaussian distribution [58], U-shaped distribution [59] and exponential distribution [60], have been used to describe these grain-boundary trapping states. Since G-R noise is generated by carrier transitions between the conduction band and trapping states, it possibly can be used to investigate and shine light on trapping related phenomena.

Several researchers [61,62] have studied the noise properties of low or moderately doped n-type polysilicon films. A large amount of pure 1/f noise was observed at low frequencies. Number fluctuations and mobility fluctuations can be the origins of 1/f noise

[17]. The observed 1/f noise in general is attributed to electron mobility fluctuations occurring in the depletion region near the grain boundaries. There is not a general theory describing number fluctuation related 1/f noise in polycrystalline resistors. Recently, M. Y. Luo [61] found noise spectra of the form $C/(1+\omega^2 t_p^2)$ and $D/(1+\omega^4 t_p^4)$ on LPCVD phosphorus-doped thin films with a doping concentration of 5.4×10^{19} cm^{-3}, where D is slightly frequency dependent.

In this chapter, we analyze G-R noise models associated with the defects in the grain boundary regions. We explore lightly and moderately doped n-type materials for the sake of simplicity and hope that it will stimulate further research on the uncommon $D/(1+\omega^4 t_p^4)$-type noise.

8.2. Theory

The polycrystalline semiconductor material we investigated is assumed to satisfy the following conditions: (1) the grain-boundary space charge region is fully depleted and its width is small compared to the grain size, (2) its physical properties are the same in adjacent grains, (3) the boundaries may be considered as surfaces characterized by an effective interface state density n_{ss}.

The equilibrium energy band diagram of the investigated polysilicon resistors is illustrated in Fig. 8.1. The symbol Vb represents the potential barrier, w is the width of the depletion region, and 2d is the width of the grain-boundary. We use the simple, symmetrical Schottky-barrier band model [63], and assume that

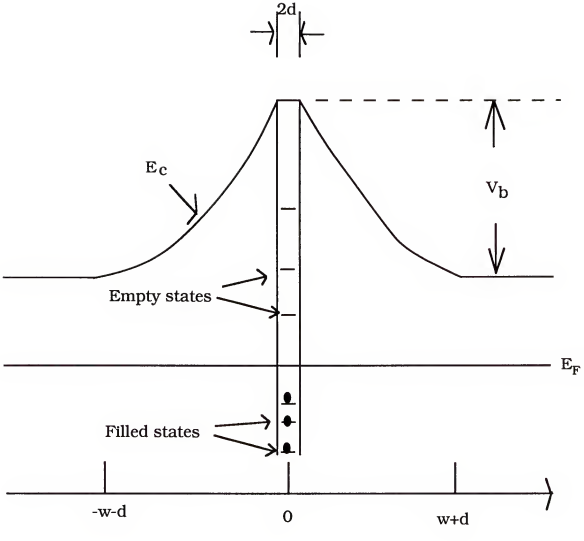

Figure 8.1. Energy band diagram of a single grain-boundary region

the voltage drop across a grain boundary region is equally distributed over each side of the depletion region of a grain boundary. To model charge transport in Schottky diodes, several authors [64] have combined the diffusion theory and the thermionic emission theory by considering the two mechanisms in series. The current flow is described by the diffusion theory in the depletion region, while at the metal-semiconductor interface the net current is described by

$$I = A\, q\, V_r\, (N(d) - N_{th}(d)), \tag{8.1}$$

where N(d) is the electron density at x=d when the current is flowing, and $N_{th}(d)$ is the electron density at x=d when the current is equal to 0. The parameter V_r is the effective recombination velocity at the interface. The general current voltage relationship for one grain can then be written as [64]

$$Ig = 2\, q\, Ag\, Ng \left(\frac{V_r V_d}{V_r + V_d}\right) e^{\frac{-qVb}{KT}} \sinh\left(\frac{q\, Vg}{2KT}\right), \tag{8.2a}$$

with

$$Vg = \frac{Va}{N_{fg}}\ , \tag{8.2b}$$

where Va is the applied voltage, Vg is the voltage drop across a grain, Ng is the effective doping concentration in the grain-bulk region, N_{fg} is the effective number of grains, and Ag is the cross section of a grain. The total current is then given by

$$I = 2\, q\, A\, Ng \left(\frac{V_r V_d}{V_r + V_d}\right) e^{\frac{-qVb}{KT}} \sinh\left(\frac{q\, Va}{2\, N_{fg}\, KT}\right), \tag{8.3}$$

where A is the cross section of the device.

In polysilicon resistors, G-R noise sources can originate from possibly three regions: the grain-bulk, the depletion and the grain-boundary region. The G-R noise in the grain-bulk regions can be calculated using the bulk G-R noise theories given in Chapters II to V and some small signal circuit calculations if we assume that the dynamic resistance of the grain-boundary and depletion region is larger than that of the grain-bulk region. With eq. (2), we can calculate the dynamic resistance associated with a single grain-boundary region from the following equation

$$Rg = \frac{dIg}{dVg}. \tag{8.4}$$

The general theory for G-R noise generated by traps in the depletion region has been described elsewhere [65]. The equivalent saturated diode current of the noise in the depletion region can be written as

$$I_{eqg} = \int_{d}^{w+d} \left[\frac{I_{eqL}}{(1+\omega^2 t_p^2)} + I_{eqH} \frac{\omega^2 t_p^2}{(1+\omega^2 t_p^2)} \right] dx, \tag{8.5a}$$

where t_p is the trap time constant, and I_{eqL} and I_{eqH} are complicated functions of material and device parameters.

The equivalent output, saturated diode current of the noise in the depletion regions then becomes after taking circuit considerations into account

$$I_{eq} = \frac{A}{Ag}\frac{2}{Nfg} \int_{d}^{w+d} \left[\frac{I_{eqL}}{(1+\omega^2 t_p^2)} + I_{eqH} \frac{\omega^2 t_p^2}{(1+\omega^2 t_p^2)} \right] dx. \tag{8.5b}$$

Next, we focus on G-R noise from the trap states in the grain-boundary region. Assuming that the depletion approximation applies, Poisson's equation becomes

$$\frac{d^2V}{d^2x} = \frac{q\ Ng}{\varepsilon_s}, \qquad d < x < w+d . \tag{8.6}$$

The potential barrier height (V_b-V_{g1}) is the difference between V(w+d) and V(d), that is

$$V_b - V_{g1} = \frac{q\ w^2\ Ng}{2\varepsilon_s}, \tag{8.7}$$

where V_{g1} is the voltage drop in the depletion region, and ε_s is the dielectric constant of the grain-bulk material.

Hence,

$$w = \sqrt{\frac{2\varepsilon_s\ (V_b - V_{g1})}{q\ Ng}} . \tag{8.8}$$

For simplicity, we limit our discussion to the condition $V_b > V_{g1}$. From the charge conservation relation, we get

$$2\ q\ w\ Ng = q\ n_{ss}, \tag{8.9}$$

where n_{ss} is the effective grain-boundary, charged trap density per unit area.

The current equation can be described by

$$I = A\ J = A\ q[D_n \frac{dN}{dx} - \mu_n\ N \frac{d\Psi_n}{dx}], \tag{8.10}$$

where μ_n is the electron mobility, and D_n is the electron diffusion constant.

The electron density is given by

$$N = N_c\ e^{\frac{-q(\Phi_n - \Psi_n)}{K\ T}}, \tag{8.11}$$

where Ψ_n is the electron potential, and Φ_n is the electron quasi-Fermi level.

In the following discussion, we neglect mobility fluctuations. Expanding the carrier densities around steady-state in first order, the current equation can be written as

$$\Delta I = A\, q[D_{no}\frac{d\Delta N}{dx} - \mu_{no} N_o \frac{d\Delta\Psi_n}{dx} - \mu_{no}\Delta N \frac{d\Psi_{no}}{dx}]. \tag{8.12}$$

Using eq. (8.12) and the following equations

$$D_{no}\frac{d\Delta N e^{\frac{-q\Psi_n}{KT}}}{dx} = \frac{-q}{KT} D_{no}\Delta N e^{\frac{-q\Psi_n}{KT}}\frac{d\Psi_n}{dx} + D_{no} e^{\frac{-q\Psi_n}{KT}}\frac{d\Delta N}{dx}],$$

and

$$\frac{KT}{q} = \frac{D_{no}}{\mu_{no}}, \tag{8.13}$$

we get

$$\Delta I e^{\frac{-q\Psi_n}{KT}} = Aq[D_{no}\frac{d\Delta N e^{\frac{-q\Psi_n}{KT}}}{dx} - \mu_{no} N_o e^{\frac{-q\Psi_n}{KT}}\frac{d\Delta\Psi_n}{dx}], \tag{8.14}$$

with

$$\Psi_n(x) = (V_b - V_{g1}) - \frac{q\,(w+d-x)^2\, N_g}{2\varepsilon_s}. \tag{8.15}$$

Using eq. (8.14) and the following equations

$$I_{in} = \int_d^{w+d}\left[e^{\frac{-q\Psi_n}{KT}}\right] dx, \tag{8.16}$$

$$I_{uu} = \int_d^{w+d}\left[H_u e^{\frac{-q\Psi_n}{KT}}\right] dx, \tag{8.17}$$

we get

$$\Delta I = \frac{A\,q}{I_{in}}[D_{no}\Delta N(w+d) e^{\frac{-q(V_b - V_{g1})}{KT}} - D_{no}\Delta N(d)] - \frac{A\,q}{I_{in}}\mu_{no} N_c \int_d^{w+d}\left[e^{\frac{-q\Phi_n}{KT}}\frac{d\Delta\Psi_n}{dx}\right] dx. \tag{8.18}$$

The derivative of the potential fluctuation is calculated as follows:

$$\frac{d\Psi_n}{dx} = \frac{q\,(w+d-x)\,N_g}{\varepsilon_s},$$

$$\frac{d\Delta\Psi_n}{dx} = \frac{q\,\Delta w\,N_g}{\varepsilon_s}. \qquad (8.19)$$

Substituting eq. (8.19) into eq. (8.18), we get

$$\Delta I = \frac{A\,q}{I_{in}}\left[D_{no}\,\Delta N(w+d)\; e^{\frac{-q(V_b - V_{g1})}{K\,T}} - D_{no}\,\Delta N(d)\right]$$
$$- \frac{A\,q}{I_{in}}\mu_{no}N_c\,\frac{q\,\Delta w\,N_g}{\varepsilon_s}\int_d^{w+d}\left[e^{\frac{-q\Phi_n}{K\,T}}\right]dx,$$

which can be written as

$$\Delta I = \frac{A\,q}{I_{in}}\left[D_{no}\,\Delta N(w+d)\,e^{\frac{-q(V_b - V_{g1})}{K\,T}} - D_{no}\,\Delta N(d)\right]$$
$$- \frac{A\,q}{I_{in}}\mu_{no}N_c\,\frac{q\,\Delta w\,W_{efo}N_g}{\varepsilon_s}, \qquad (8.20a)$$

with

$$W_{efo} = \int_d^{w+d}\left[e^{\frac{-q\Phi_n}{K\,T}}\right]dx. \qquad (8.20b)$$

Using eq. (8.1), the current fluctuation can be written as

$$\Delta I = A\,qV_r\,\Delta N(d). \qquad (8.21a)$$

Thus the carrier fluctuations at x=d becomes

$$\Delta N(d) = \frac{\Delta I}{A\,qV_r}. \qquad (8.21b)$$

Substituting eq. (8.21b) into eq. (8.20), we get

$$\Delta I = \frac{A\,q}{I_{in}}\left[D_{no}\Delta N(w+d)\,e^{\frac{-q(V_b - V_{g1})}{K\,T}} - D_{no}\,\frac{\Delta I}{A\,qV_r}\right]$$
$$- \frac{A\,q}{I_{in}}\mu_{no}N_c\,\frac{q\,\Delta w\,W_{efo}\,N_g}{\varepsilon_s}, \qquad (8.22a)$$

or

$$\Delta I(1+\frac{D_{no}/I_{in}}{V_r}) = -\frac{A\,q}{I_{in}}\mu_{no}N_c\frac{q\,\Delta w\,W_{efo}N_g}{\varepsilon_S}) + \frac{A\,q}{I_{in}}[D_{no}\Delta N(w+d)e^{\frac{-q(V_b-V_{g1})}{K\,T}}]. \quad (8.22b)$$

Considering only the low-frequency noise behavior of the device, we can assume

$$\Delta N(w+d) = 0, \quad (8.23)$$

then eq. (8.22b) becomes

$$\Delta I = \frac{-A\,q}{I_{in}\,C_{1o}}\mu_{no}N_c\frac{q\,\Delta w\,W_{efo}N_g}{\varepsilon_S},$$

with

$$C_{1o} = (1+\frac{D_{no}/I_{in}}{V_r}). \quad (8.24)$$

Fluctuations in the charged trap density of the grain-boundary region cause fluctuations of the depletion width w,

$$\Delta n_{ss} = 2\,\Delta w\,Ng. \quad (8.25)$$

Thus

$$\Delta I = \frac{A\,q}{I_{in}\,C_{1o}}\mu_{no}N_c\frac{q\Delta n_{ss}\,W_{efo}}{2\varepsilon_S}.$$

The noise spectral density becomes

$$S_I(\omega) = [\frac{A\,q^2\,\mu_{no}N_c\,W_{efo}}{2\,I_{in}\,C_{1o}\,\varepsilon_S}]^2\,Sn_{ss}(\omega). \quad (8.26)$$

Trap carrier fluctuations are calculated as follows. Let $n_{ss}=2d\,n_t$, where n_t is the trap density of a grain boundary. The rate equation is given by [Chapter VII]

$$\frac{dn_t}{dt} = -\frac{\Delta n_t}{t_p}, \quad (8.27)$$

$$\frac{1}{t_p} = [(c_n N_o + e_n) + (c_p P_o + e_p)]. \tag{8.28}$$

The spectral density of G-R noise has the form [17]

$$S_{n_t}(\omega) = \frac{4 g t_p^2}{2d Ag (1+\omega^2 t_p^2)}, \tag{8.29}$$

where g (= $e_n n_t$) is the electron generation rate.

The output current spectral density of G-R noise becomes

$$S_I(\omega) = \left[\frac{A q^2 \mu_{no} N_c W_{efo}}{2I_{in} C_{1o} \varepsilon_S}\right]^2 \frac{8 d g t_p^2}{Ag (1+\omega^2 t_p^2)}. \tag{8.30}$$

With eq. (8.20b), and assuming that the Fermi level does not vary much throughout the depletion region, we get

$$W_{efo} = \int_d^{w+d} \left[e^{\frac{-q\Phi_n}{K T}}\right] dx \cong w \left[e^{\frac{-q\Phi_n(w+d)}{K T}}\right]$$

$$\cong w\, e^{\frac{-q(V_b - V_{g1} + V_n)}{K T}}, \tag{8.31}$$

where $V_n = Ln(N_g/N_c)$.

Equation (8.30) describes the G-R noise from one depletion region. Assuming that the fluctuations of barrier heights are independent. After some circuit manipulation we get for the total device 1/f noise

$$S_I(\omega) = \frac{A}{Ag\, Nfg}\left[\frac{A w q^2 \mu_{no} N_a}{2I_{in} C_{1o} \varepsilon_S}\right]^2 H \frac{4 e_n n_{ss} t_p^2}{Ag (1+\omega^2 t_p)}, \tag{8.32a}$$

with

$$H = \left[e^{\frac{-2q(V_b - V_{g1})}{K T}} + e^{\frac{-2q(V_b + V_{g1})}{K T}}\right]. \tag{8.32b}$$

In the preceding discussion, we have assumed that the trap states have a δ-distribution function. If however the energy of the trap states is distributed over a specific energy range such that [17]

$$S_{n_t}(\omega) = \frac{\beta n_t}{f \, Ln(\frac{\tau_1}{\tau_o})}, \qquad (8.33)$$

where β, τ_1, τ_o are functions of material properties, the output current spectral density of G-R noise becomes

$$S_I(\omega)=[\frac{A\, w\, q^2 \mu_{no} N_a}{2\, I_{in}\, C_{1o}\, \varepsilon_S}]^2 H \frac{4d^2\ \beta\, n_t}{f \, Ln(\frac{\tau_1}{\tau_o})}. \qquad (8.34a)$$

Equation (8.34a) describes the 1/f noise from one depletion region of a grain, we get after some circuit manipulation

$$S_I(\omega)= \frac{A}{A_g\, N_{fg}}[\frac{A\, w\, q^2 \mu_{no} N_a}{2\, I_{in}\, C_{1o}\, \varepsilon_S}]^2 H_1 \frac{4d^2\ \beta\, n_t}{f \, Ln(\frac{\tau_1}{\tau_o})}, \qquad (8.34b)$$

with

$$H_1= \left[e^{\frac{-2q(V_b-V_a/2N_{fg})}{K\ T}} + e^{\frac{-2q(V_b+V_a/2N_{fg})}{K\ T}} \right]. \qquad (8.32c)$$

Equation (8.34b) describes 1/f noise produced by G-R processes in the grain-boundary region. Since the observed 1/f noise is proportional to the square of the device current, the fluctuations of the charged trap density in the grain-boundary can not be used to account for the published 1/f noise in polysilicon resistors.

CHAPTER IX
CONCLUSIONS AND SUGGESTIONS FOR FURTHER RESEARCH

9.1. Conclusions

We have studied deep trap parameter extraction methods in semiconductors using G-R noise measurements. In the course of our experimental investigations, we found that proper device design is critical for application of these methods. Deep trap parameters can be measured on devices with an intended deep defect concentration larger or smaller than the shallow dopant concentration.

Gold in silicon has been widely studied in the past, its behavior is not always predictable however. In this thesis noise measurements are described with which we look at the role of this impurity in silicon. We carefully set up three experiments to fully exploit noise measurement techniques. The first experiment deals with low-field noise measurements, which were done on p^+-p^--p^+ silicon devices doped with a boron concentration of 10^{15} cm^{-3} and an initially unknown gold concentration. The measured trap energy, hole capture cross section and degeneracy factor, which were extracted from the experimental noise and resistance data, are in good agreement with the generally-accepted data for the gold donor level, indicating that this method is accurate for investigating deep-defect properties.

Since defects can exist in several charged states in a device, other states may affect the measured data collected for a particular energy level. Our second experiment was done on p^+-p^--p^+ silicon

devices doped with a boron concentration of 2.7 $x10^{15}$ cm^{-3}. The plot of the device resistance versus temperature indicates that gold produces an activation energy of 0.267 eV, and the plot of the voltage noise versus temperature indicates that gold produces an activation energy of 0.336 eV. These results are explained in terms of double donor centers interacting with the valence band. We conclude that when the energy levels of a defect are within a few KT from each other, the collected data for a particular energy level will be affected by the behavior of a nearby energy level.

We analyzed the noise of several multi-level trap centers, and derived the conditions for which the noise of a multi-level trap center reduces to the noise of a single-level trap center. For a defect with multi-energy levels, which are separated by more than a few KT from each other, the multi-level G-R noise model reduces to the single-level G-R noise model in both uncompensated and overcompensated devices. Intuitively, this is consistent with the fact that very often a single level G-R noise model is used to extract defect parameters. We also devised a method by which G-R noise measurements can be used to discriminate between donor-like and acceptor-like trap behavior. Using a device doped with an intended deep defect concentration larger than the shallow dopant concentration, we can determine whether a defect is an acceptor or a donor center. A deep acceptor center is unlikely to be detected in a p-type device because the Fermi level is far away from the deep acceptor energy levels. When the deep defect is donor-like, the Fermi level is close to the trap energy level and the noise becomes a strong function of temperature and defect parameters.

Since emission and capture coefficients may be a function of electric field, and the free carrier concentration in a strongly doped device is determined by the balance of emission and capture processes in traps, a field-induced decrease in the emission coefficient or a field-enhanced capture coefficient, or both can reduce the free carrier concentration in a semiconductor device when subject to electric field. The current-voltage (I-V) characteristics of the devices used in the first experiment were measured and they showed sublinear behavior at moderately high fields. With the use of low frequency voltage noise data measured as a function of electric field, we found that the sublinear I-V behavior was caused by a decrease in the hole concentration with increasing electric field. This decrease is caused by a field-induced decrease in the hole emission coefficient, which is larger than the associated field-induced decrease in the hole capture coefficient.

In addition to the above described macroscopic G-R noise mechanisms, a microscopic model for calculating the carrier capture coefficient for deep traps is derived. In our model, the carrier releases its energy through delocalized optical phonon emission and directly jumps from a free vibronic state to a bound vibronic state. The calculated capture coefficient shows a slight temperature dependence and agrees with the experimental data measured between 160 and 200K.

Theories for G-R noise generated in field-effect devices are discussed. Trap parameters can be extracted from G-R noise generated in junction devices. Its interpretation however is more

involved than is the case for bulk devices. Finally, we analyzed G-R noise models associated with defects in the grain boundary regions of n-type silicon resistors.

In summary, this thesis provides comprehensive information on how to use noise data from G-R processes to investigate trap parameters.

9.2. Suggestions for Future Research

Firstly, the capture coefficients in our experiment are extracted using optimization techniques. From eq. (2.9) we find that the roll-off time constant provides information about the temperature-dependence of the capture coefficient. One can reduce the doping concentration of shallow acceptors and deep impurities and increase the device cross section such that the roll-off time constants can be measured. Then the device can be used to extract directly the information about the temperature and field dependence of capture coefficients.

Secondly, with further modifications of our microscopic capture model developed in Chapter VI and coupling this model with the Monte Carlo simulation technique, high field studies of G-R processes and carrier transport become possible.

Thirdly, knowledge of the field dependence of capture and emission coefficients is very useful for the interpretation of capture and emission mechanisms and the possible deformation of bound carrier potentials. This knowledge can be obtained by measuring the I-V and noise characteristics of a symmetric device with doping profiles and a geometry that eliminate a bias polarity dependence of

the I-V characteristics, so that the I-V behavior is determined only by the field-dependent G-R processes and the electric field distribution.

Finally, we developed a simple G-R noise model for polysilicon in Chapter VIII based on the symmetrical Schottky-barrier band model. This model needs further modifications. It should include the asymmetrical behavior of the crystallites, of the voltage distribution, and of the band structure of grain boundaries. We also may dope an intended defect in the grain boundary such that the Fermi level is nearby the defect energy level and is therefore known. This will make it easier to characterize grain-boundary defects. Once these steps have been taken, it may be easier to find a solution for the $D/(1+\omega^4 t_p^4)$-type noise problem.

REFERENCES

1. Sokrates T. Pantelides, Rev. Mod. Phys. 50, 797 (1978).

2. L. S. Lu, T. Nishida and C. T. Sah, J. Appl. Phys. 62, 4773 (1987).

3. K. M. Van Vliet and J. R. Fassett, in Fluctuation Phenomena in Solids (Academic Press, New York, R.E. Burgess (Ed.), 1965).

4. A. van der Ziel, Noise: Sources, Characterization, Measurement (Prentice-Hall, Englewood Cliffs, New Jersey, 1970).

5. D. Gasquet, B. Azais, J. C. Vassiere and J. P. Nougier, "Generation recombination noise in p-Si at 77 K," Noise in Physical Systems and 1/f Noise-1985, (edited by A. D'Amico and P. Mazzetti (North-Holland, Amsterdam, 1985).

6. F. Hofman, R. J. J. Zijlstra and J. C. M. Henning, Solid State Electron. 31, 279 (1988).

7. P. O. Lauritzen, Solid-State Electron. 8, 41 (1965).

8. L. D. Yau and C. T. Sah, Solid-State Electron. 13, 1213 (1970).

9. F. Scholz, J. M. Hwang and D. K. Schroder, Solid-State Electron. 31, 205 (1988).

10. J. C. Bourgoin, H. J. von Bardeleben and D. Stievevard, J. Appl. Phys. 64, R65 (1988).

11. G. L. Miller, D. V. Lang and L. C. Kimberling, Ann. Rev. Mater. Sci. 7, 377 (1977).

12. C. T. Sah, L. Forbes, L. L. Rosier and A. F. Tasch, Jr., Solid-State Electron. 13, 759 (1970).

13. J. A. Pals, Solid-State Electron. 17, 1139 (1974).

14. C. Jacoboni and L. Reggiani, Rev. Mod. Phys. 55, 645 (1983).

15. L. Reggiani and Paolo Lugli, Appl. Phys. Lett. 51, 925 (1988).

16. G. D. Watkins, Physica, 117B & 118B, 9 (1983).

17. A. van der Ziel, Noise in Solid State Devices and Circuits (John Wiley & Sons, Inc., New York, 1986).

18. S. L. Jang and G. Bosman, J. Appl. Phys. 65, 201 (1989).

19. N. D. Arora, J. R. Hauser and D. J. Roulston, IEEE Trans. Electron Devices, ED-29, 292 (1982).

20. A. D. van Rheenen, G. Bosman and R. J. J. Zijlstra, Solid-State Electron. 30, 259 (1987).

21. B. Bruckner, Phys. Status Solidi 4, 685 (1971).

22. R. H. Wu and A. R. Peaker, Solid-State Electron. 25, 643 (1982).

23. R. Newman, Phys. Rev. 94, 1530 (1954).

24. C. B. Collins, R. O. Carlson and C. J. Gallagher, Phys. Rev. 105, 1168 (1957).

25. E. A. Taft and F. Hubbard Horn, Phys. Rev. 93, 64 (1954).

26. W. Shockley and J. T. Last, Phys. Rev. 107, 392 (1957).

27. A. G. Milnes, Deep Impurities in Semiconductors (John Wiley & Sons, Inc., New York, 1973).

28. M. A. Lampert and P. Mark, Current Injection in Solids (Academic Press, New York, 1970).

29. B. V. Knornilov and A. V. Anfinov, Sov. Phys. Semicond. 1, 279 (1967).

30. Yu. A. Bykovskii, V. V. Zuev, A. D. Kiruykhin and V. A. Shkaranda, Sov. Phys. Semicond. 14, 1294 (1980).

31. D. A. Aronov, I. Z. Karimova and P. I. Knigin, Sov. Phys. Semicond. 10, 596 (1976).

32. G. Kuhnel, W. Siegel and H. A. Schneider, Phys. Stat. Sol.(a) 100, 283 (1987).

33. C. Jacoboni, C. Canali, G. Ottaviani and A. Alberigi-Quaranta, Solid-State Electron. 20, 77 (1977).

34. D. M. Caughey and R. E. Thomas, Proc. IEEE, 2129 (1969).

35. M. Ali Omar and L. Reggiani, Solid-State Electron. 30, 693 (1987).

36. M. Lax, Phys. Rev. 119, 1502 (1960).

37. V. V. Abakumov, V. I. Prel' and I. N. Yassievich, Sov. Phys. Semicond. 12, 1 (1978).

38. C. H. Henry and D. V. Lang, Phys. Rev. B, 15, 989 (1977).

39. W. Hayes and A. M. Stoneham, Defects and Defect Processes in Nonmetallic Solids (John Wiley & Sons, Inc., New York, 1985).

40. P. A. Martin, B. G. Streetman and K. Hess, J. Appl. Phys. 52, 7409 (1981).

41. R. Passler, J. Phys. C. 17, 5957 (1984).

42. R. Passler, Solid-state Electron. 27, 155 (1984).

43. W. Shockley and J. T. Read Jr., Phys. Rev. 87, 835 (1952). R. N. Hall, Proc. IEEE, 106B, 923 (1957).

44. G. F. Neumark and K. Kosai, Semiconductors and Semimetals 19, 1 (1981).

45. T. Azumi and K. Matsuzaki, Photochemistry and Photochemistry, 25, 315 (1977).

46. A. Yariv, Quantum Electronics (John Wiley & Sons, Inc., New York, 1975).

47. M. Lannoo and J. Bourgoin, Point Defects in Semiconductors II (Springer-Verlag, Berlin, 1981).

48. Helen M. J. Smith, Philos. Trans. A241, 105 (1949).

49. B. N. Brockhouse, Phys. Rev. Lett. 2, 256 (1959).

50. G. Lucovsky, Solid-State Commun. 3, 299 (1965).

51. L. S. Lu and C. T. Sah, J. Appl. Phys. 59, 173 (1986).

52. L. D. Yau and C. T. Sah, IEEE Trans. Electron Devices, ED-16, 170 (1969).

53. P. Lauritzen and C. T. Sah, IEEE Trans. Electron Devices, ED-10, 334 (1969).

54. C. T. Sah, Proc. IEEE, 52, 795 (1964).

55. P. Lauritzen, Solid-State Electron. 8, 41 (1965).

56. K. K. Wang, A. van der Ziel and E.R. Chenette, IEEE Trans. Electron Devices, ED-22, 591 (1975).

57. K. M. van Vliet and C. F. Hiatt, IEEE Trans. Electron Devices, ED-22, 593 (1975).

58. C. Y. Lu, N. C. C. Lu and C. S. Wang, Solid-State Electron. 27, 463 (1984).

59. H. C. de Graaff, M. Huybers and J. G. de Groot, Solid-State Electron. 25, 67 (1982).

60. C. H. Seager and T. G. Castner, J. Appl. Phys. 49, 3879 (1978).

61. M. Y. Luo, Ph. D. dissertation, University of Florida, Gainesville (1989).

62. H. C. de Graaff and M. Huybers, J. Appl. Phys. 54, 2504 (1983).

63. M. L. Tarng, J. Appl. Phys. 49, 4069 (1978).

64. S. M. Sze, Physics of Semiconductor Devices, 2nd edition. (John Wiley & Sons, New York, 1981).

65. K. M. van Vliet, IEEE Trans. Electron Devices, ED-23, 1236 (1976).

BIOGRAPHICAL SKETCH

Sheng-Lyang Jang was born in Taiwan, Republic of China, on January 5, 1959. He received the B.S. degree from National Chiao-Tung University, Hsinchu, Taiwan, R.O.C., in 1981, and the M.S. degree from National Taiwan University, Taipei, Taiwan, in 1983. He joined the Noise Research Laboratory at the University of Florida in 1986.

From July 1983 to May 1985, he served in the R.O.C. Navy Shipyard as an Engineer Officer. In late 1985, he became an IC designer at Syntek Design Technology Limited, Taipei, Taiwan. In early 1986, he worked as an IC designer at United Microelectronics Corporation, Hsinchu, Taiwan. His areas of interest include defect characterization in solid-state devices and device modeling.

I certify that I have read this study and that in my opinion it conforms to acceptable standards of scholarly presentation and is fully adequate, in scope and quality, as a dissertation for the degree of Doctor of Philosophy.

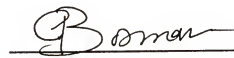

G. Bosman, Chairman
Associate Professor of Electrical Engineering

I certify that I have read this study and that in my opinion it conforms to acceptable standards of scholarly presentation and is fully adequate, in scope and quality, as a dissertation for the degree of Doctor of Philosophy.

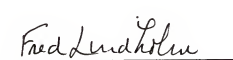

F. A. Lindholm
Professor of Electrical Engineering

I certify that I have read this study and that in my opinion it conforms to acceptable standards of scholarly presentation and is fully adequate, in scope and quality, as a dissertation for the degree of Doctor of Philosophy.

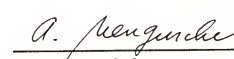

A. Neugroschel
Professor of Electrical Engineering

I certify that I have read this study and that in my opinion it conforms to acceptable standards of scholarly presentation and is fully adequate, in scope and quality, as a dissertation for the degree of Doctor of Philosophy.

S. S. Li
Professor of Electrical Engineering

I certify that I have read this study and that in my opinion it conforms to acceptable standards of scholarly presentation and is fully adequate, in scope and quality, as a dissertation for the degree of Doctor of Philosophy.

U. H. Kurzweg
Professor of Engineering Science

This thesis was submitted to the Graduate Faculty of the College of Engineering and to the Graduate School and was accepted as partial fulfillment of the requirements for the degree of Doctor of Philosophy.

December 1989

Dean, College of Engineering

Dean, Graduate School